CONSTRUCTION MATERIALS CONSULTANTS, INC.

Delamination and Potential Surface Alteration Of An Indoor Concrete Slab-on-Grade – A Comprehensive Study From Two Concrete Cores & An Incinerator Ash As A Potential Surface Contaminant

Inashco North America, Inc.
Metals Recovery Facility
3049 River Rd, Conestoga, PA 17516

October 8, 2021
CMC 0921159

TABLE OF CONTENTS

EXECUTIVE SUMMARY

The present investigation centers around an indoor concrete slab-on-grade at a metal recovery facility, placed during August/September of 2018. The slab has reportedly suffered premature delamination of hard trowel-finished surface of the floor at various areas, especially the areas subjected to heavy construction traffic including rubber tired front-end loaders and steel tracked equipment. Delamination reportedly occurred almost immediately once heavy equipment was on the slab. In addition, trash burnt at the incinerator was reportedly transported to the facility by a loader and dumped on the floor. Floors with a surface hardener at other facilities where this same procedure was performed reportedly have no surface wearing issues.

Field photos show rough and almost scarified natures of slab surface, some even with exposed near-surface reinforcing steel in the distressed areas as opposed to smooth, dense, hard shiny trowel-finished surfaces in the sound areas. The purposes of the investigation are to determine (a) the causes for premature delamination of the slab surface, and (b) whether or not dumping of incinerated ash on the floor surface has caused chemical erosion and deterioration of the slab surface.

Reported mix design of concrete contains (in a cubic yard): (a) 600 pounds of Lehigh Type I Portland cement, (b) 120 pounds of fly ash, (c) 1820 pounds of coarse aggregate, (d) 1055 pounds of sand, (e) 35 gallons of water, (f) 10 ounces of air-entraining admixture, (g) 9 ounces of water-reducing admixture, and (h) 30 ounces of mid-range water reducing admixture. Reported design air content is 6 percent, design water-cementitious materials ratio is 0.41, unit weight is 143.8 lb/ft^3, and 28-day design compressive strength is 4500 psi.

From the observed smooth, dense, shiny trowel-finished surface of the slab at the sound areas, and its reported indoor placement during the months of August and September of 2018, the above-mentioned mix for an air-entrained concrete having 6 percent design air is judged to be inconsistent for many reasons. First, according to the common industry specifications, a concrete slab intended to receive a dense hard trowel-finish should not be air entrained, and the total air content should not exceed 3 percent by volume. Second, both cores showed incorporation of polypropylene-type synthetic fibers, which is not mentioned in the mix. Even a mix containing both fibers and entrained air is not suitable for a slab receiving a hard trowel finish. Entrained air and fibers along with fly ash can affect the early age properties of concrete. Third, the slab was reportedly placed in an indoor environment during the summer/fall of 2018, which was not exposed to subfreezing temperatures, so air entrainment was unnecessary let alone to increase its potential to delaminate when subjected to trowel-finishing.

Two full-depth hardened concrete cores marked as C1 and C4 were retrieved from two different areas of distressed slab, which are 3^1/$_4$ in. (82 mm) in diameters, and 7^7/$_8$ to 8^1/$_4$ in. (2000 to 210 mm) in lengths. Both cores show a rough surface at the top and adhered subbase at the bottom indicating full-depth recovery from the slab at their respective locations. Concrete in both cores are dark gray in color tone, dense, well-consolidated, and show no apparent visual distress through the depth of recovery. Additionally, four bottles of a moist ash sample were provided for detailed compositional analysis, which emitted a strong ammonia odor after removing the bottle caps.

Both cores were examined by detailed petrographic examinations according to the procedures of ASTM C 856, "Standard Practice for Petrographic Examination of Hardened Concrete". Additionally, scanning electron microscopy and energy-dispersive X-ray microanalyses (SEM-EDS) were done on the surface deposits detected at the top exposed surface in Core C1 according to the procedures of ASTM C 1723 "Standard Guide for Examination of Hardened Concrete Using Scanning Electron Microscopy".

The ash sample was examined in further detail starting with determination of pH (alkalinity) of as-received and water-digested sample of ash, followed by determination of any potentially deleterious water-soluble anions in the filtrate from deionized water-digested ash by ion chromatography, which were followed by oven-drying of ash to do optical microscopy, SEM-EDS, X-ray diffraction (XRD), X-ray fluorescence (XRF), and thermal analysis for detailed chemical, mineralogical, microstructural analyses of ash. Remains of ash detected on the top surfaces of

Cores C1 and C4 were also examined, along with the near-surface regions of concrete to investigate any potential chemical deterioration of concrete surface from the alleged accidental disposal of ash on the concrete floor.

Based on detailed petrographic examinations, concrete in both cores are found to be compositionally similar in terms of having crushed limestone coarse aggregates, natural sand fine aggregates, and binary (Portland cement plus fly ash) cementitious paste having similar estimated cementitious materials contents that are equivalent to 7½ to 8 bags of Portland cement per cubic yard of which 15 to 20 percent is estimated to be fly ash, and similar water-cementitious materials ratios in the interior bodies estimated to be 0.40 to 0.44 (except the top 5 mm of finishing-induced densified surface region in Core C1 where *w/cm* is estimated to be 0.35 to 0.40), but the main difference occurred in their air contents and air-void systems, which are enough to indicate their derivation from actually two very different batches having very different dosages of air-entraining chemicals.

The batch delivered at the location of Core C1 was excessively air-entrained in having as high as 7 to 8 percent estimated total air, which consists of numerus very fine to fine (less than 100 microns to 1 mm size) discrete spherical and near-spherical intentionally introduced entrained air bubbles that are well-distributed throughout the paste, and sometimes occurred as clustered masses along aggregate-paste interfaces to deleteriously affect the compressive strength of concrete.

By contrast, the batch delivered at the location of Core C4 was almost non-air-entrained to marginally air-entrained in having noticeably lower air content than the previous batch. In Core C4, air occurs as a meager amount of very coarse spherical voids that are indicative of potential addition of an air-entraining agent, but the agent did not generate enough air bubbles to adequately protect the paste during freezing at critically saturated conditions. Concrete in Core C4 is marginally air-entrained having an estimated air content of 3 to 4 percent, which are mostly present in the interior body and contributed mostly from the coarse air bubbles. Dosages of air entraining chemicals in the pours at the locations of Cores C1 and C4 are clearly very different, which are judged to be due to the variations created during their mixing at the batch plant rather than from subsequent transportation and placement since such later processes of construction cannot remove air from the concrete to bring down from 7 to 8 percent air as found in Core C1 to a near non-air-entrained appearance with only 3 to 4 percent air in Core C4.

Lapped cross section of Core C1 showed spectacular development of so-called *near-surface incipient delamination* at a depth of 5 to 10 mm from the very top surface, which consist of a series of discontinuous, elongated separations or 'tears' as 'incipient delamination' situated beneath the trowel-densified surface region of concrete, beyond which concrete showed a noticeable increase in air content from dense no or low-air trowel-densified surface region of top 5 to 10 mm to excessively air-entrained body in the interior. This line of incipient delamination demarcates the boundary between the extent of trowel-densified surface region of low to no air and very low *w/cm* where finishing operations have removed mix water and air out of the surface and the interior body. Prolonged troweling operations would create a shearing action between these densified surface skin and interior less dense body to eventually join all discontinuous isolated separations to a long continuous one as delamination, which would eventually remove the trowel-densified surface under traffic load. Reported exposure of heavy traffic and occurrence of delamination immediately after such exposure justifies this observation.

In the lapped cross section of Core C4 no such incipient delamination was found since the original finished surface was already lost leaving only the delaminated surface of the slab. Nevertheless, air content shows a clear decrease at the delaminated surface region compared to the body indicating effect of hard troweling operations in reduction of air.

Therefore, *use of air entrainment in an indoor slab intended to receive a dense hard trowel-finish was found to be the main reason for the reported delamination of slab*.

The next part of the investigation centered on detailed investigation of the incinerated ash sample and its potential deleterious reactions to the Portland cement concrete. The investigation started with first detailed examinations of remains of such ash deposits on the slab surface detected on the top surfaces of both cores as thin layers less than 0.4 mm in maximum thickness. Optical and scanning electron microscopy of these deposits on the thin sections of cores showed the presence of: (a) very fine-grained deposits of organic matter, (b) ferruginous materials, (c) ultrafine

crushed quartz, (d) limestone dusts, (e) spherical fly ash, (f) porous, ultrafine-grained carbonated lime, (g) shrinkage microcracks and overall porous nature of deposit, (h) occasional synthetic fibers, and (i) angular shard-like glassy particles of slag. None of these constituents on the surface deposit are potentially harmful to concrete, hence the concrete surface region immediately beneath the deposit shows no surface alteration (leaching, erosion, carbonation, etc.). For most cases, a sharp boundary is present between the porous fragile surface deposit and the underlying dense concrete surface. The strong ammonia odor of ash, apparently, did not create any noticeable chemical alterations on the surface of concrete at least in the two examined Cores C1 and C4.

Next the bulk incinerated ash sample was examined. The ash, as mentioned, was (a) damp with abundant moisture, (b) emitted a strong ammonia odor, and (c) dark gray in color. Insertion of a pH strip immediately turned the strip to dark blue color indicating a strong alkaline nature. A portion of the ash sample as received was digested in deionized water, first at near-boiling condition for 15 minutes followed by continuous digestion for 48 hours by stirring with a magnetic stir bar to remove all leachable constituents to the water. A significant amount of fine acicular magnetite grains were found adhered to the N and S poles of magnetic bar. A second pH test on the water-digested ash with a pH meter showed 9.48 pH confirming its alkaline nature. The digested mass was then filtered to remove the filtrate for further examinations for water-soluble anions by ion chromatography. Results show detectable levels of chloride (0.715 weight percent) and sulfate (0.136 percent) ions in the filtrate. An oven-dried mass of the ash was pulverized to finer than 45 micron particle size for chemical and mineralogical analyses of ash by XRF and XRD, respectively. Results showed more or less similar silica-alumina-lime compositions all within 15 to 25 percent, subordinate magnesia-sodium-iron oxide compositions within 3 to 12 percent, 5.45 percent sulfate, and 7.2 percent balance. XRD results show quartz from its ubiquitous presence in the concrete sand, melilite from slag, phlogopite and montmorillonite clay, halite (source of chloride in IC result), brucite, titanomagnetite (which showed magnetic adherence to the stirring bar), and an amorphous phase which did not produce any diffraction peak but indicated its presence from a low angle hump in the diffraction pattern. Glass is positively detected in optical microscopy and its sodium-lime-silicate composition was subsequently confirmed from SEM-EDS studies. Optical microscopy showed (a) dark opaque metal and metal oxide particles, (b) spherical fly ash particles some of which are circled, (c) medium to dark brown and clear shard-like glassy fragments of slag, (d) fine angular quartz particles, (e) ultrafine-grained carbonated lime, (f) occasional synthetic fibers, (g) dark organic matter, (h) shale fragments, and (i) miscellaneous undetectable ultrafine particles that are too fine to be detected at the magnification of optical microscope. SEM-EDS studies of ash showed sodium-lime-silicate glass, slag, fly ash, quartz, dolomite, and miscellaneous other silicate grains none of which are potentially deleterious to the concrete surface. Results of thermal analysis of ash were consistent with those obtained from optical microscopy and XRD.

Based on detailed laboratory examinations the two most important conclusions derived are: (1) the deleterious role of incorporation of air entrainment in the mix for causing delamination of the indoor slab-on-grade after hard trowel finishing operations, and, (2) no deleterious reaction of the incinerator ash with concrete surface at least at the top surfaces of two cores where remains of such deposits are detected, which are compositionally not very different from the concrete *per se* and present as soft, porous, fragile mass mostly in sharp contact to the concrete. Detailed optical and scanning electron microscopy of the very top surface regions of both cores show no evidence of any chemical alteration or leaching of paste from the alleged exposure of the ash contaminant. Apparently, the strong ammonia odor detected in the moist ash sample caused no detectable deleterious chemical effect on the concrete surfaces of the examined two cores. The very top surface regions of both cores show dense paste with no indication of any alteration, leaching, carbonation, loss of calcium hydroxide component of cement hydration, or other chemical erosions from the alleged exposure to surface contaminants having such an odor.

Based on these observations, the main body of the slab can still be perfectly serviceable after the necessary repair of the distressed/delaminated/ash-contaminated surface regions. Any ‘sound’ areas may potentially cause future delamination, if the areas have air entrained concrete, and received hard-troweling. After delamination, however, the interior slab should still be serviceable since, after all, there is no evidence of any chemical or physical deterioration of concrete detected in the main bodies of the cores where the concrete is dense, well-consolidated, and present in sound conditions.

INTRODUCTION

Reported herein are the results of detailed investigation of delamination and surface erosion of an indoor concrete slab-on-grade at a metal recovery facility, placed during August/September of 2018, which has suffered from premature delamination of hard trowel-finished surface of the floor at various areas, especially the areas subjected to heavy construction traffic including rubber tired front-end loaders and steel tracked equipment. Delamination reportedly occurred almost immediately once heavy equipment was on the slab. Trash burnt at the incinerator was reportedly transported to the facility by a loader and dumped on the floor. Floors with a surface hardener at other facilities where this same procedure was performed reportedly have no surface wearing issues.

BACKGROUND INFORMATION

Reported mix design of concrete contains (in a cubic yard): (a) 600 pounds of Lehigh Type I Portland cement, (b) 120 pounds of fly ash, (c) 1820 pounds of coarse aggregate, (d) 1055 pounds of sand, (e) 35 gallons of water, (f) 10 ounces of air-entraining admixture, (g) 9 ounces of water-reducing admixture, and (h) 30 ounces of mid-range water reducing admixture. Reported design air content is 6 percent, design water-cementitious materials ratio is 0.41, unit weight is 143.8 lb/ft^3, and 28-day design compressive strength is 4500 psi.

PURPOSE OF PRESENT INVESTIGATION

Field photos in Figures 1 to 3 show rough and almost scarified nature of slab surface, some even with exposed near-surface reinforcing steel in the distressed areas as opposed to smooth, dense, hard shiny trowel-finished surfaces in the sound areas. The purposes of the investigation are to determine (a) the causes for premature delamination of the slab surface, and (b) whether or not dumping of incinerated ash on the floor surface has caused chemical erosion and deterioration of the slab surface.

SAMPLES

Table 1 summarizes preliminary descriptions of the cores as received. Figures 4 to 7 show the cores, as received as well as the ash sample.

Core ID	Core Diameter (in.)	Core Length (in.)	Exposed Surface	Bottom Surface	Major Cracking	Reinforcing Steel	Condition
C1	3 1/4 in. (82 mm)	8 1/4 in. (210 mm)	Rough, top 10 mm has darker gray damp appearance	Adhered subbase materials	No visible cracking	None	Intact, Ring-sounded, Dry
C4	3 1/4 in. (82 mm)	7 7/8 in. (200 mm)	Rough, delaminated	Adhered subbase materials	No visible cracking	1/4 in. diameter mesh at 7 1/4 in. depth	Intact, Ring-sounded, Dry

Table 1: Description of the cores, as received.

FIELD PHOTOS

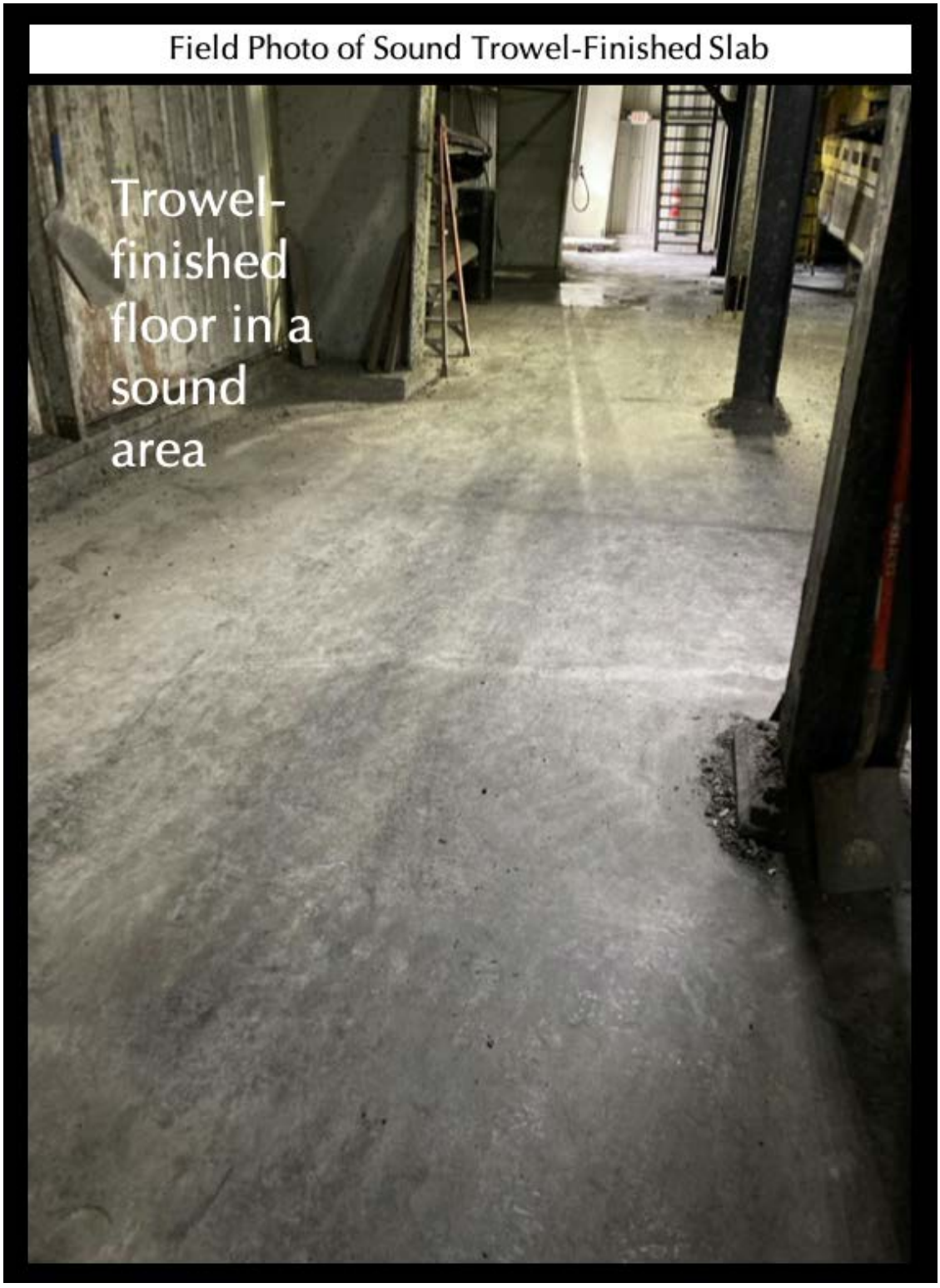

Figure 1: Field photo of the shiny, dense, smooth, flat trowel-finished concrete surface in the sound area, which is free from any delamination or surface contamination.

Figure 2: Field photos of rough distressed area in the top and scarified surface in the bottom photos that were subjected to delamination from loss of the original densified trowel-finished surface.

Figure 3: Field photo of the distressed concrete slab surface showing rough surface with exposed reinforcing steel at the surface where the original trowel-finished surface has, reportedly, delaminated.

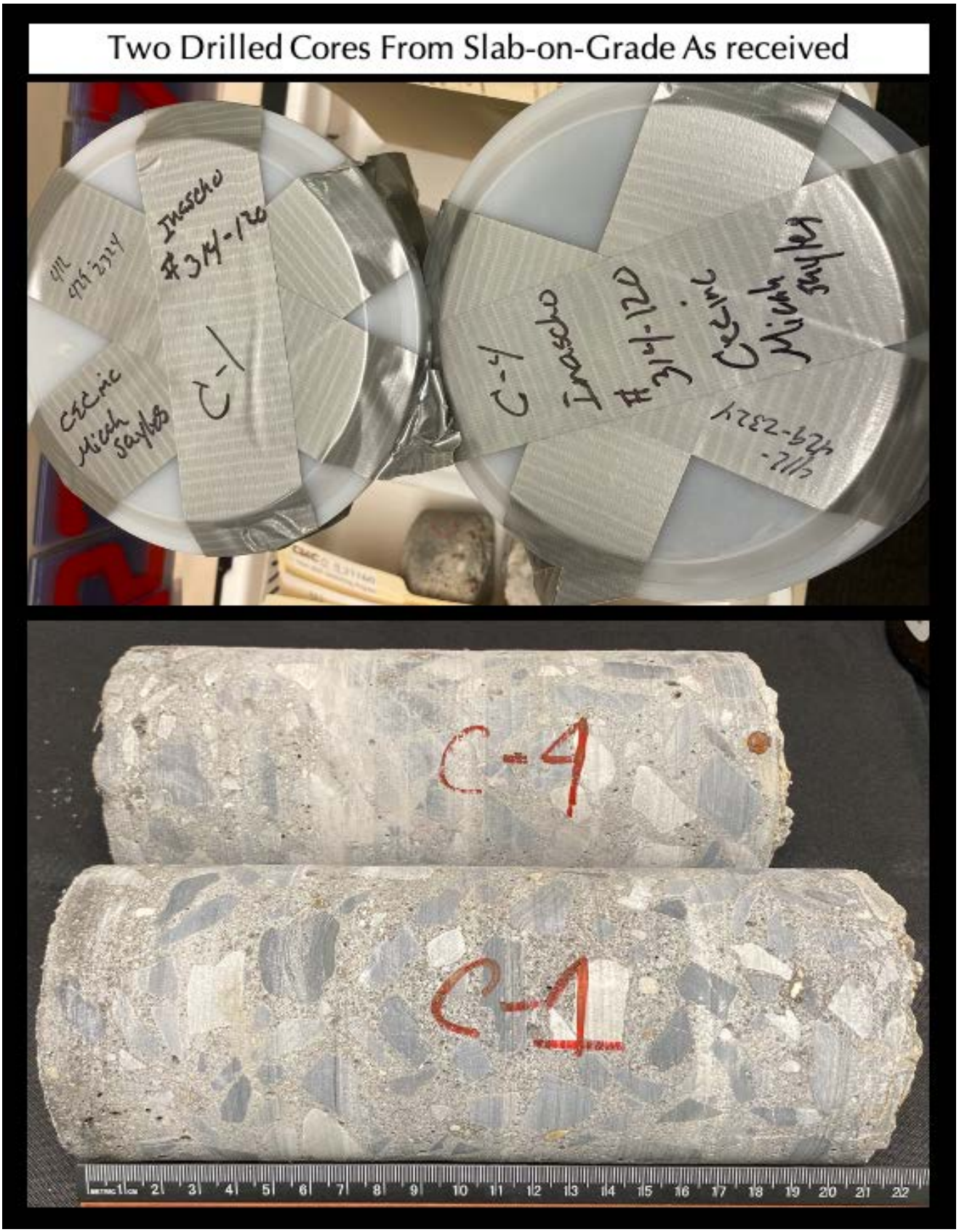

Figure 4: Two concrete cores, C1 and C4, as received in plastic molds, that were drilled through the entire depth of slab at their respective locations.

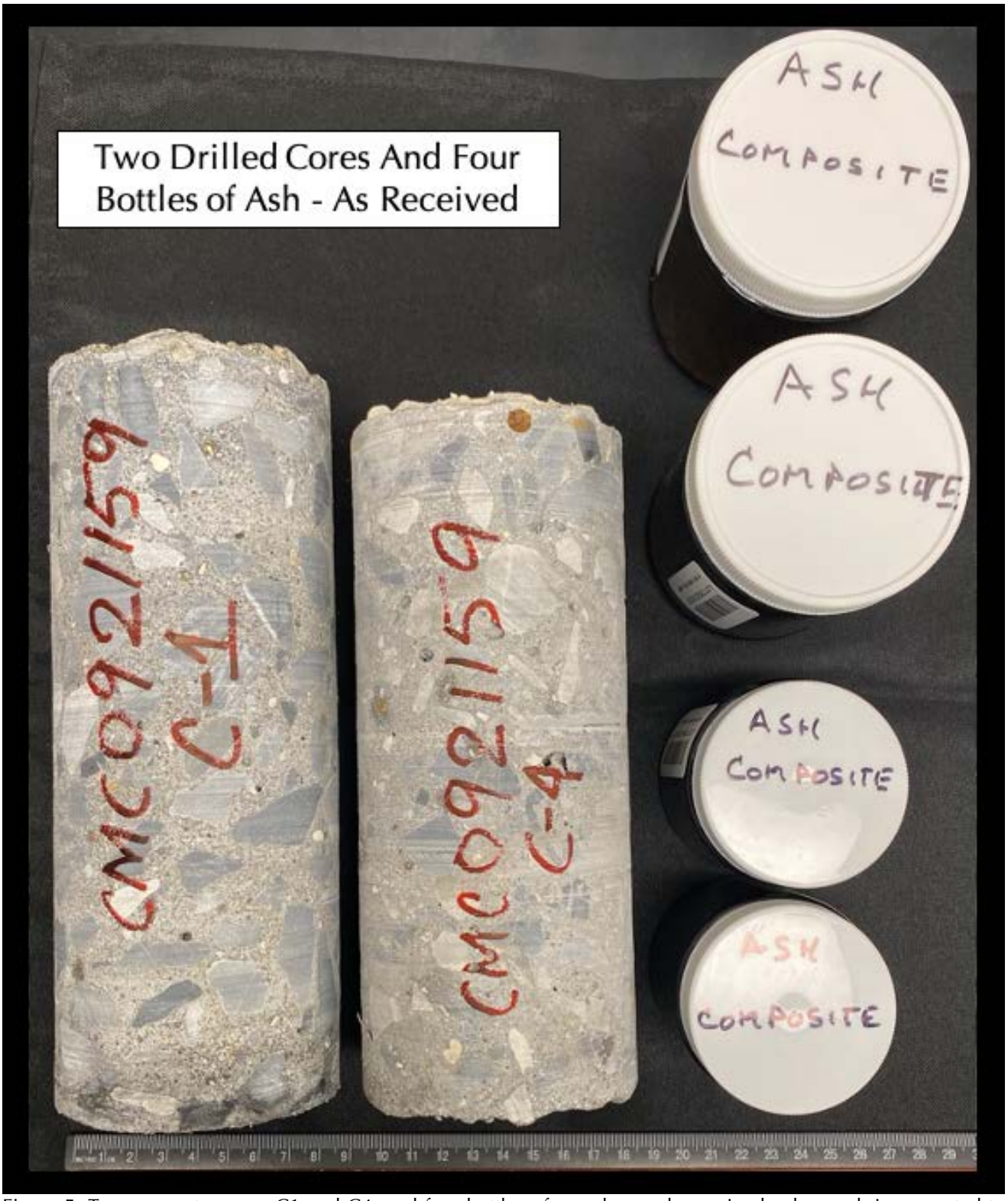

Figure 5: Two concrete cores, C1 and C4, and four bottles of an ash sample received, where ash is suspected to have contaminated the concrete surface.

Figure 6: End surface (exposed ends) of Cores C1 and C4, as received, showing rough surfaces where Core C1 has a near-surface 'incipient delamination' present as elongated separations or 'tears,' whereas C4 has no such near-surface separations, but the entire exposed surface is rough.

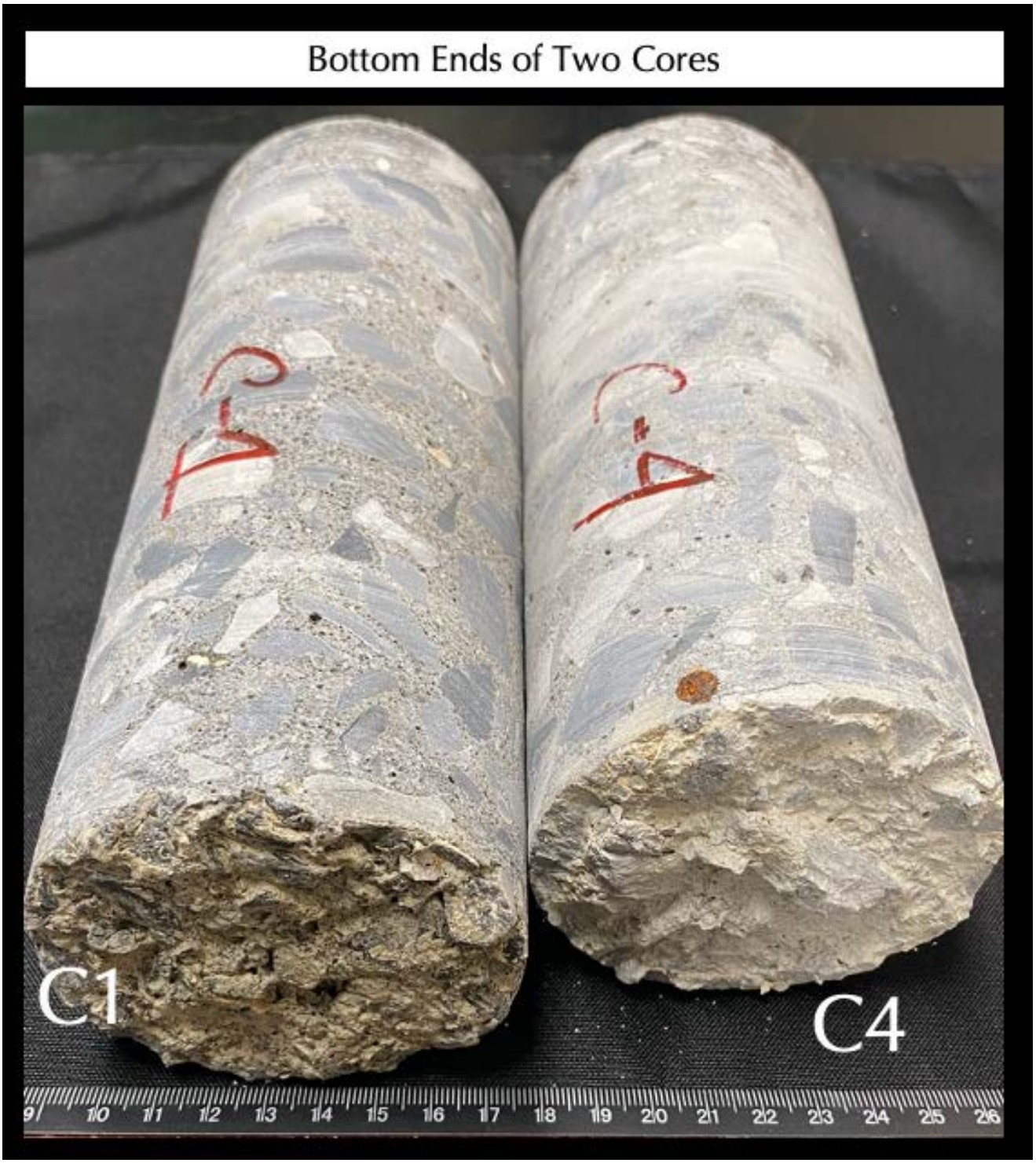

Figure 7: Opposite bottom ends of the cores, as received, showing the subbase materials indicating full-depth retrieval of cores at their respective locations.

METHODOLOGIES

PETROGRAPHIC EXAMINATIONS OF CONCRETE AND INCINERATOR ASH

Both concrete cores and the ash sample were examined by using the methods of ASTM C 856 "Standard Practice for Petrographic Examination of Hardened Concrete." Details of petrographic examinations and sample preparation are described in Jana (1997, 2001, 2004, 2005, 2006, 2007). The steps of petrographic examinations include (Jana 2006):

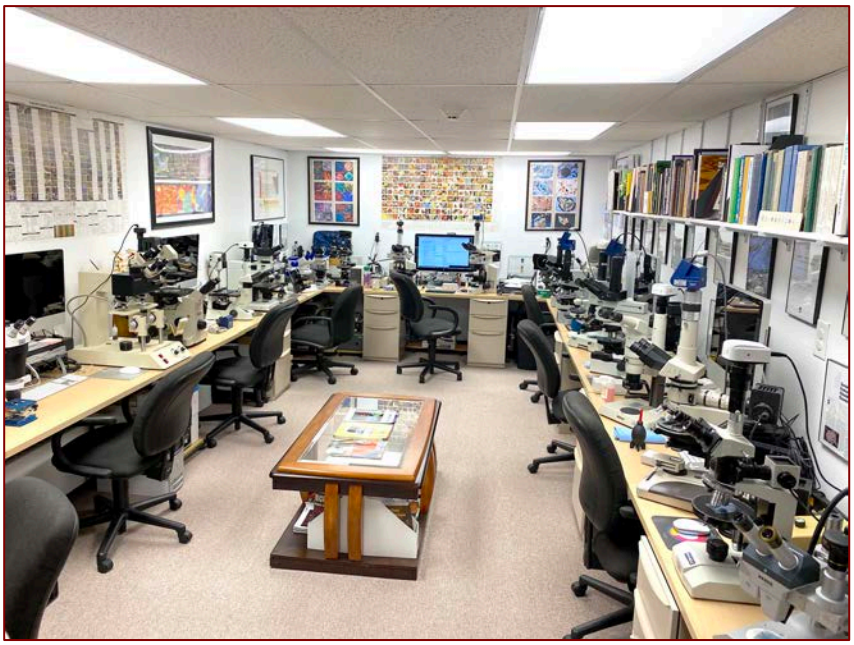

Figure 8: The optical microscopy laboratory at CMC which houses many microscopes used for this project.

i. Visual examinations of samples, as received;
ii. Low-power stereo microscopical examinations of as-received, saw-cut and freshly fractured sections, and lapped cross sections of cores for evaluation of textures, and composition;
iii. Low-power stereo microscopical examinations of air contents and air-void systems of concretes in the cores;
iv. Examinations of oil immersion mounts in a petrographic microscope for mineralogical compositions of specific areas of interest;
v. Examinations of blue dye-mixed (to highlight open spaces, cracks, etc.) epoxy-impregnated large area (50 mm × 75 mm) thin sections of concretes and ash sample in a petrographic microscope for detailed compositional and microstructural analyses;
vi. Photographing samples, as received and at various stages of preparation with a digital camera and a flatbed scanner;
vii. Micrographs of lapped cross sections and thin sections of samples taken with stereomicroscope and petrographic microscope, respectively, to provide detailed compositional and mineralogical information of concretes;
viii. Figure 8 shows various microscopes in the optical microscopy lab that were used during petrographic examinations of concrete and ash samples.

SCANNING ELECTRON MICROSCOPY AND ENERGY-DISPERSIVE X-RAY SPECTROSCOPY (SEM-EDS)

Surface deposits on concrete cores as well as a representative portion of oven-dried mass of the ash sample were examined from their respective thin sections already prepared and used in optical microscopy for further determinations of compositions and identity by Cambridge CamScan Series II scanning electron microscope equipped with a backscatter detector, a secondary electron detector, and energy-dispersive X-ray fluorescence.

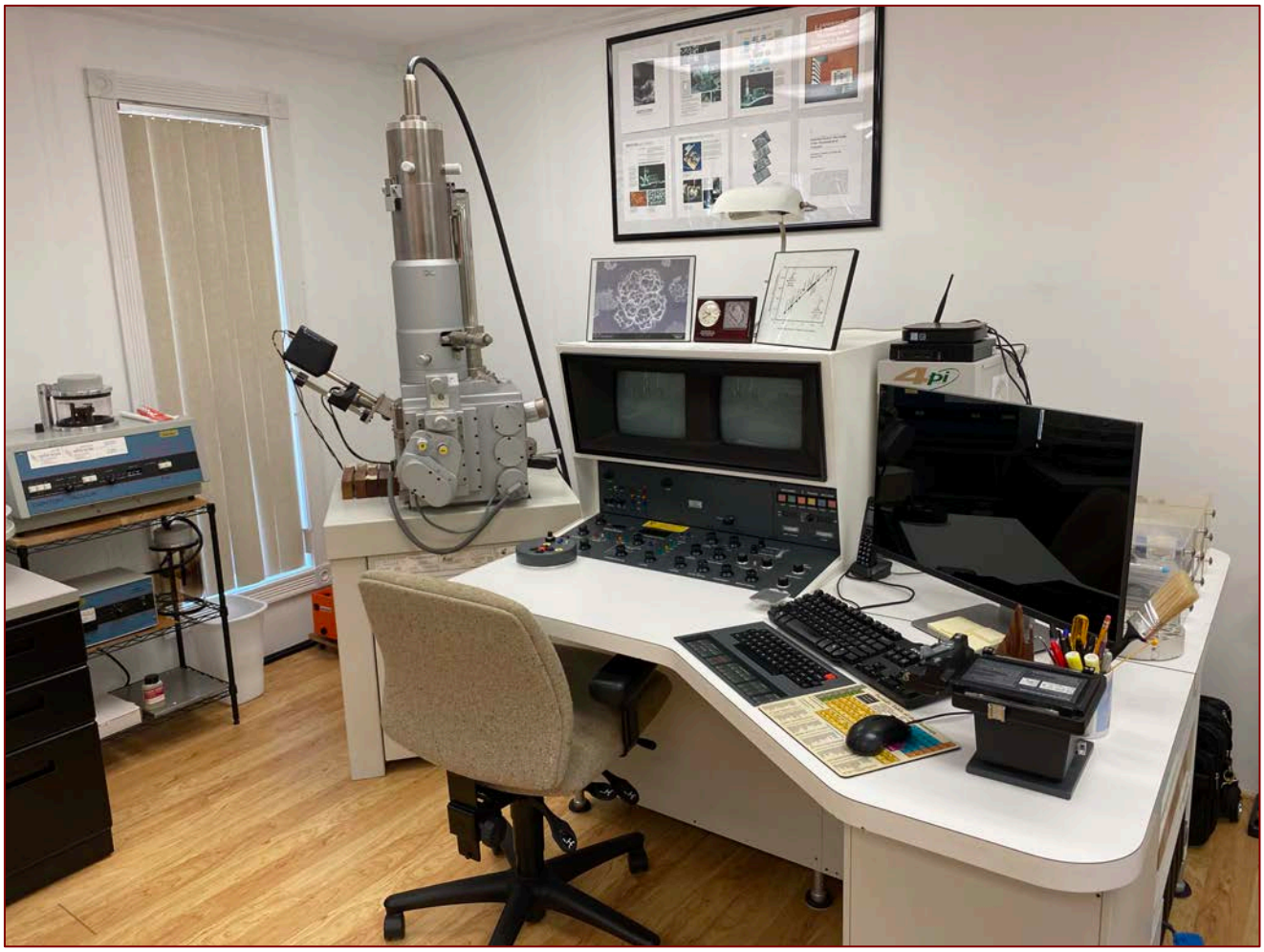

Figure 9: SEM-EDS: Cambridge CamScan Series II Scanning Electron Microscope and 4Pi Revolution software, backscatter detector, secondary electron detector, and energy-dispersive X-ray fluorescence spectrometer used for microstructural and microchemical analyses of surface deposits in Core C1 as well as of the ash sample.

X-RAY DIFFRACTION OF INCINERATOR ASH

Representative pieces of oven-dried mass of the ash sample were pulverized to finer than 44-micron (US 325 sieve) particle size for X-ray diffraction studies. The purpose of this study is to detect: (a) the major and minor minerals in the ash sample, and, (b) the presence of any potentially deleterious minerals in the ash, which could cause surface erosion of the concrete slab.

X-ray diffraction was carried out in a Bruker D2 Phaser (2nd Generation) benchtop Powder diffractometer Bragg-Brentano geometry) employing a Cu X-ray tube (Cu k-alpha radiation of 1.54 angstroms), a primary slit of 1 mm, a receiving slit of 3 mm, a position sensitive 1D Lynxeye XE-T detector. Generator settings used are 30 kV and 10mA (300 watt). Sample was placed in a zero background sample holder which is an optically polished 111 plane of silicon wafer attached to a stainless steel sample holder for use in the 6-position sample stage of D2 Phaser. Tests were scanned at 2θ from 8° to 64° with a step of 0.05° 2θ integrated at 0.05 sec. step^{-1} dwell time.

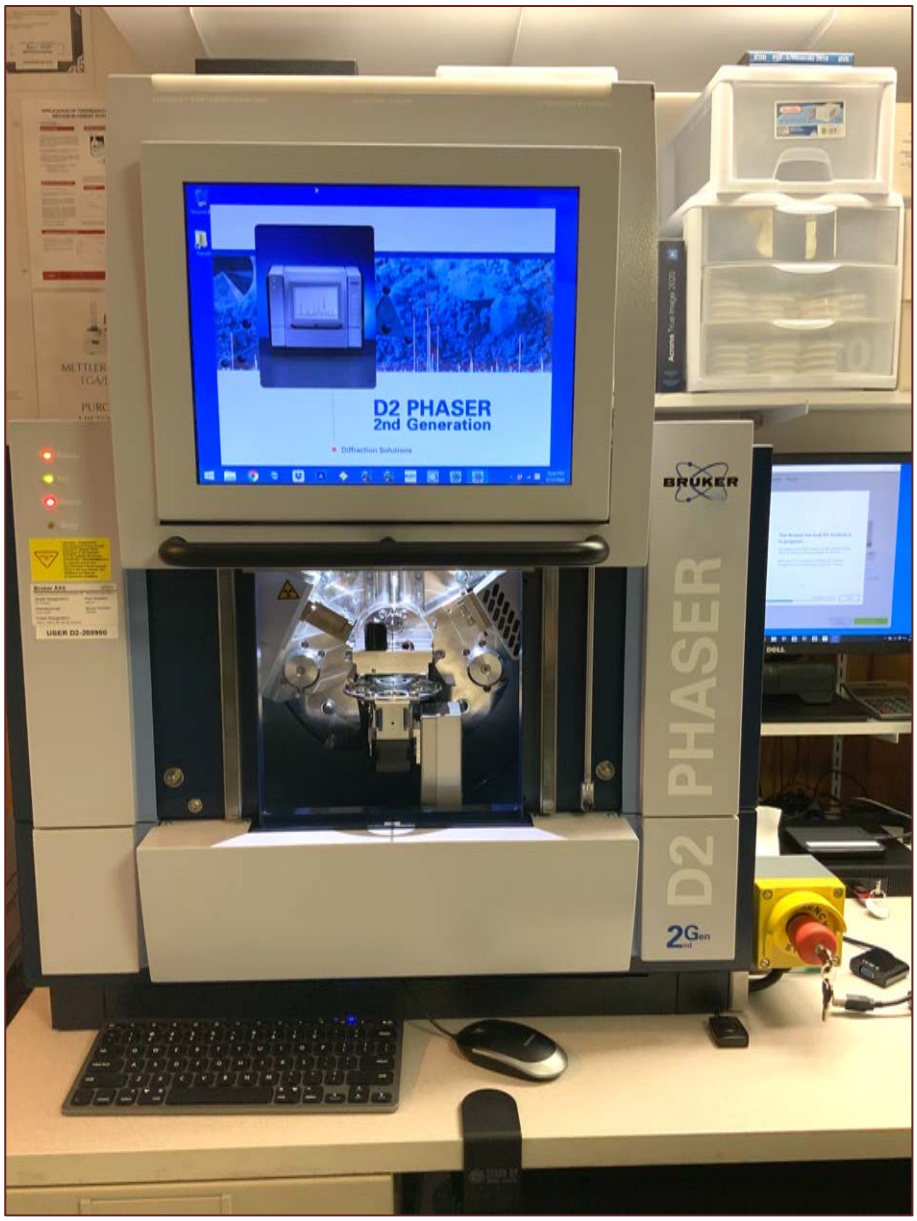

Figure 10: Bruker's D2 Phaser (2nd generation) benchtop X-ray powder diffractometer with Lynxeye 1D position sensitive detector used in X-ray diffraction studies of ash sample.

The resulting diffraction patterns were collected by Bruker's Diffrac.Measurement software. Phase identification was done with Bruker's Diffrac.EVA software with the search-match database from Crystallographic Open Database (COD). Additional phase identification, and Rietveld quantitative analyses were carried out with Match! software.

X-RAY FLUORESCENCE SPECTROSCOPY OF INCINERATOR ASH

X-ray fluorescence (XRF) was used for determining major element oxide compositions of ash sample, which provide clues about the presence of any potentially deleterious components in ash that could be detrimental to the concrete surface.

A series of standards from Portland cements, lime, gypsum to various rocks, and masonry mortars of certified compositions (e.g., from USGS, GSA, NIST, CCRL, Brammer, or measured by ICP) are used to calibrate the instrument for various oxides and empirical calculations are done from such calibrations to determine oxide compositions of concretes.

Figure 11: Rigaku NEX-CG in CMC, which can perform analyses of 9 pressed pellet or fused bead of sample. Samples are prepared either as pressed pellet (usually the one already prepared for XRD) or can also accommodate fused bead with proper calibration of standard beads.

An energy-dispersive bench-top X-ray fluorescence unit from Rigaku Americas Corporation (NEX-CG) was used (Figure 11). Rigaku NEX CG delivers rapid qualitative and quantitative determination of major and minor atomic elements in a wide variety of sample types with minimal standards. Unlike conventional EDXRF analyzers, the NEX CG was engineered with a unique close-coupled Cartesian Geometry (CG) optical kernel that dramatically increases signal-to-noise. By using monochromatic secondary target excitation, instead of conventional direct excitation, sensitivity is further improved. The resulting dramatic reduction in background noise, and simultaneous increase in element peaks, result in a spectrometer capable of routine trace element analysis even in difficult sample types. The instrument is calibrated by using various certified (CCRL, NIST, GSA, and Brammer) reference standards of cements and rocks.

IN SEARCH OF POTENTIALLY DELETERIOUS WATER-SOLUBLE ANIONS IN INCINERATOR ASH AND pH

A portion of the original damp ash sample, as received, was digested in deionized water first in near-boiling condition for 15 minutes, followed by room temperature digestion for 48 hours. The purpose of this test is to determine the potential presence of any water-soluble anions in the ash (e.g., chloride, sulfate), which could cause chemical corrosion of the concrete surface.

The digested sample solution was then filtered under vacuum, first through two 2.5-micron filter papers, followed by another filtration through two 0.2-micron filter papers to collect the filtrate. The filtrate thus obtained was diluted to a final volume of 500 ml in a volumetric flask. The filtrates thus prepared were used for ion chromatography by following the methods of ASTM C 4327 using Metrohm 881 Compact IC Professional with 858 professional sample processor (Figure 12). The instrument was calibrated with standard anion solutions of known concentrations.

Figure 12: Set-ups for chloride and sulfate analysis by ion chromatography and pH of ash sample.

In addition, alkalinity of the deionized water-digested ash sample was measured in a Metrohm 744 pH meter as well as from a pH strip.

Due to the strong ammonia odor of the ash sample when received, the sample was first digested in deionized water before insertion of the pH probe. A pH strip inserted in the original damp sample immediately turned the strip color to dark blue indicating high alkalinity of the ash sample.

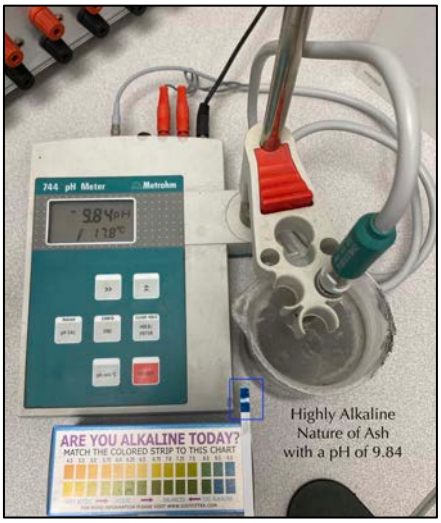

PETROGRAPHIC EXAMINATIONS

CROSS SECTIONS OF CONCRETE CORES

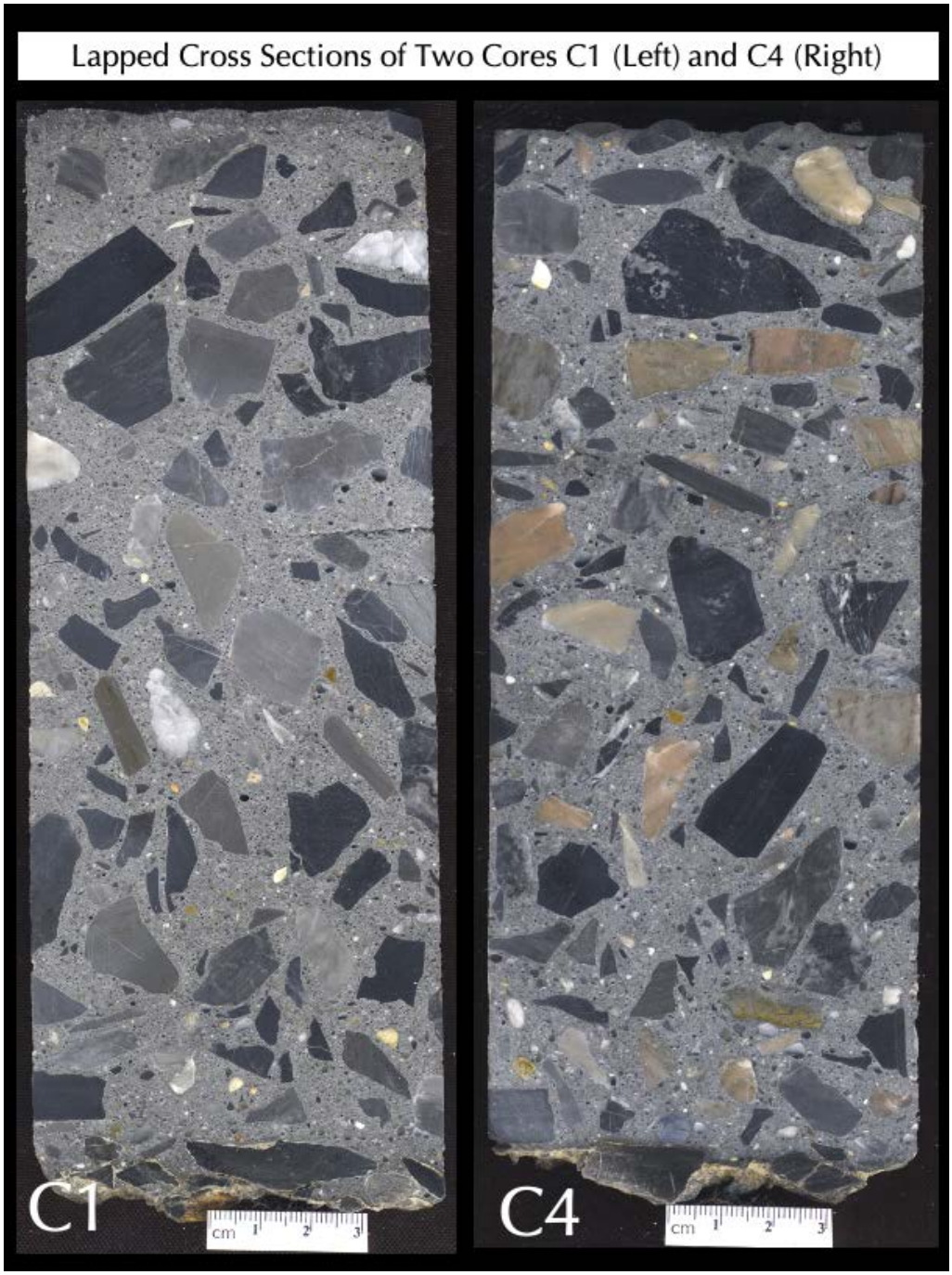

Figure 13: Lapped cross sections of Cores C1 and C4 showing overall densified concrete containing compositionally similar, medium to dark gray, angular, equidimensional to a few elongated, well-graded, well-distributed, crushed limestone coarse aggregates, dark gray paste due to the incorporation of fly ash along with Portland cement, rough exposed surface ends at top, and, adhered subbase material at the bottom ends indicating full-depth recovery of cores from the slab. Notice the overall good consolidation of concrete at both core locations as well as sound, visually crack-free natures, and free of any discolorations at the surface regions from any surface contaminants.

Figure 14: Saw-cut cross sections of Cores C1 and C4 showing overall densified concrete containing compositionally similar, medium to dark gray, angular, equidimensional to a few elongated, well-graded, well-distributed, crushed limestone coarse aggregates, dark gray paste due to the incorporation of fly ash along with Portland cement, rough exposed surface ends at top, and adhered subbase material at the bottom ends indicating full-depth recovery of cores from the slab.

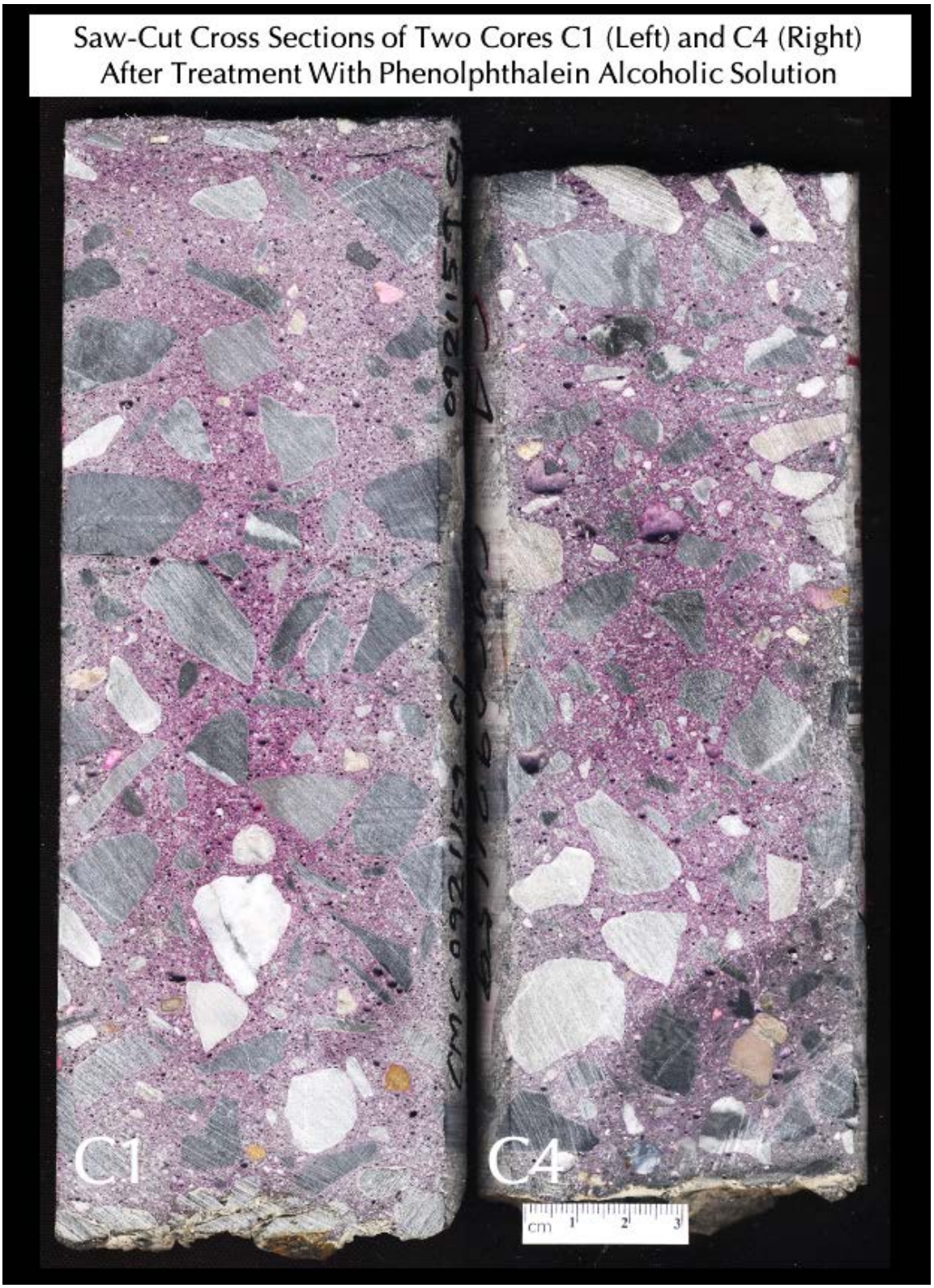

Figure 15: Saw-cut cross sections from Figure 14 after treatment with phenolphthalein alcoholic solutions showing overall dense non-carbonated nature of concrete except only minimal patchy carbonation at the surface that are only detected from thin sections.

MICROGRAPHS OF LAPPED CROSS SECTIONS OF CONCRETE CORES

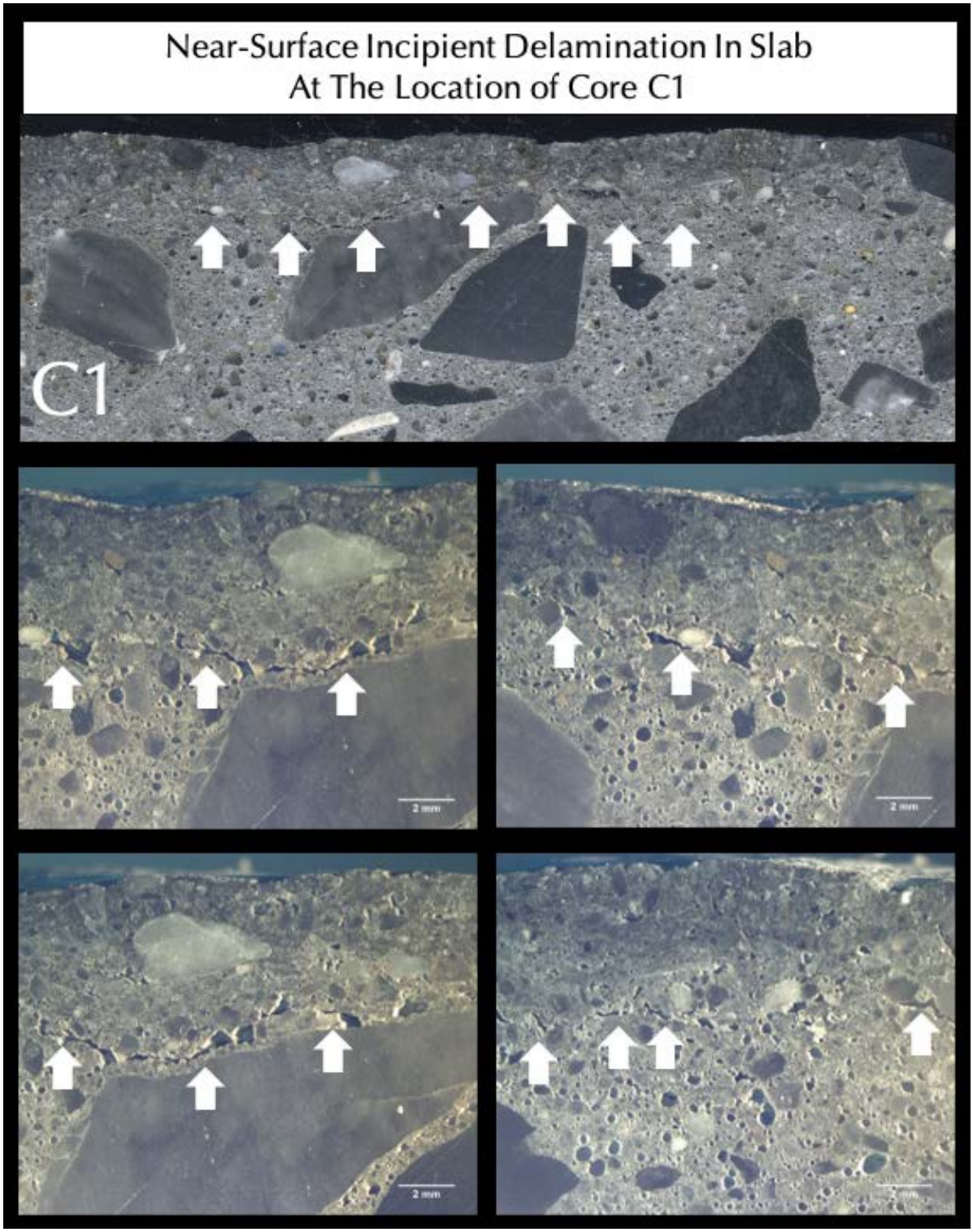

Figure 16: Micrographs of lapped cross section of Core C1 showing elongated near-surface incipient delamination (marked with arrows) as elongated tears or separations between the trowel-densified low to no-air very low *w/cm* surface region, and, interior excessively air-entrained concrete. This incipient delamination can cause eventual removal of the finished surface under traffic load.

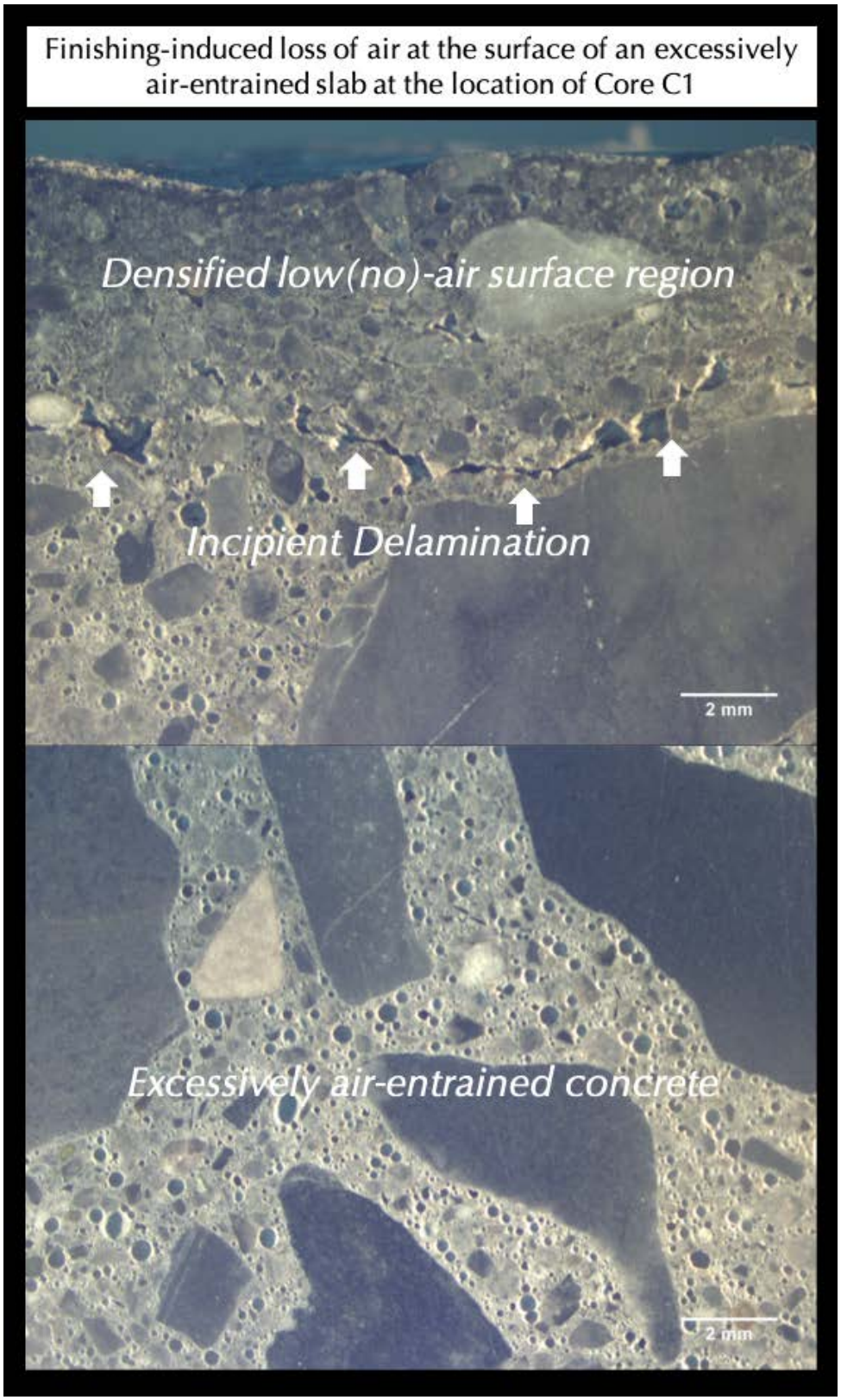

Figure 17: Micrographs of lapped cross section of Core C1 showing elongated near-surface incipient delamination (marked with arrows) as elongated tears or separations between the trowel-densified low to no-air very low *w/cm* surface region and interior excessively air-entrained concrete. This incipient delamination can cause eventual removal of the finished surface under traffic load.

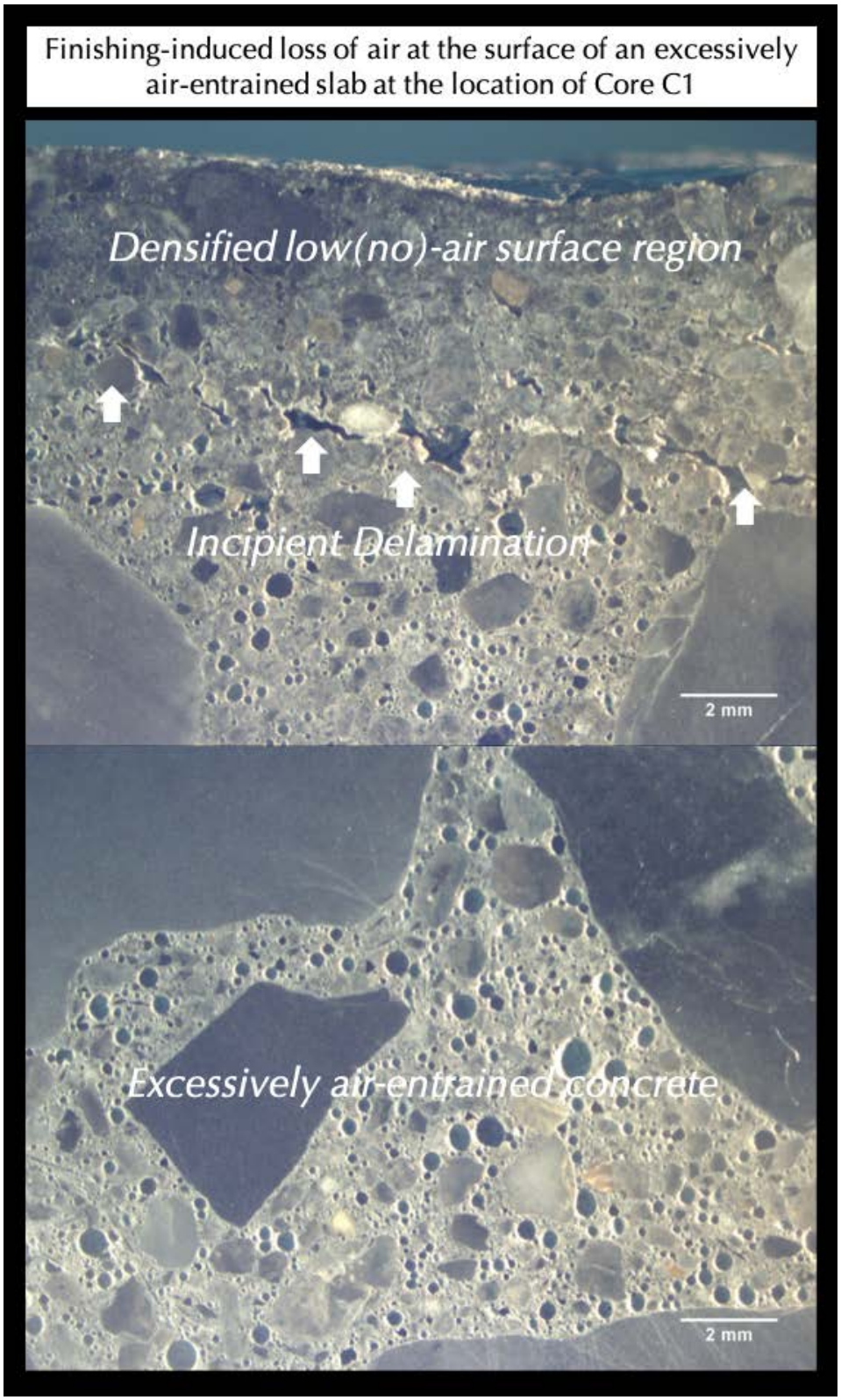

Figure 18: Micrographs of lapped cross section of Core C1 showing elongated near-surface incipient delamination (marked with arrows) as elongated tears or separations between the trowel-densified low to no-air very low *w/cm* surface region and interior excessively air-entrained concrete. This incipient delamination can cause eventual removal of the finished surface under traffic load.

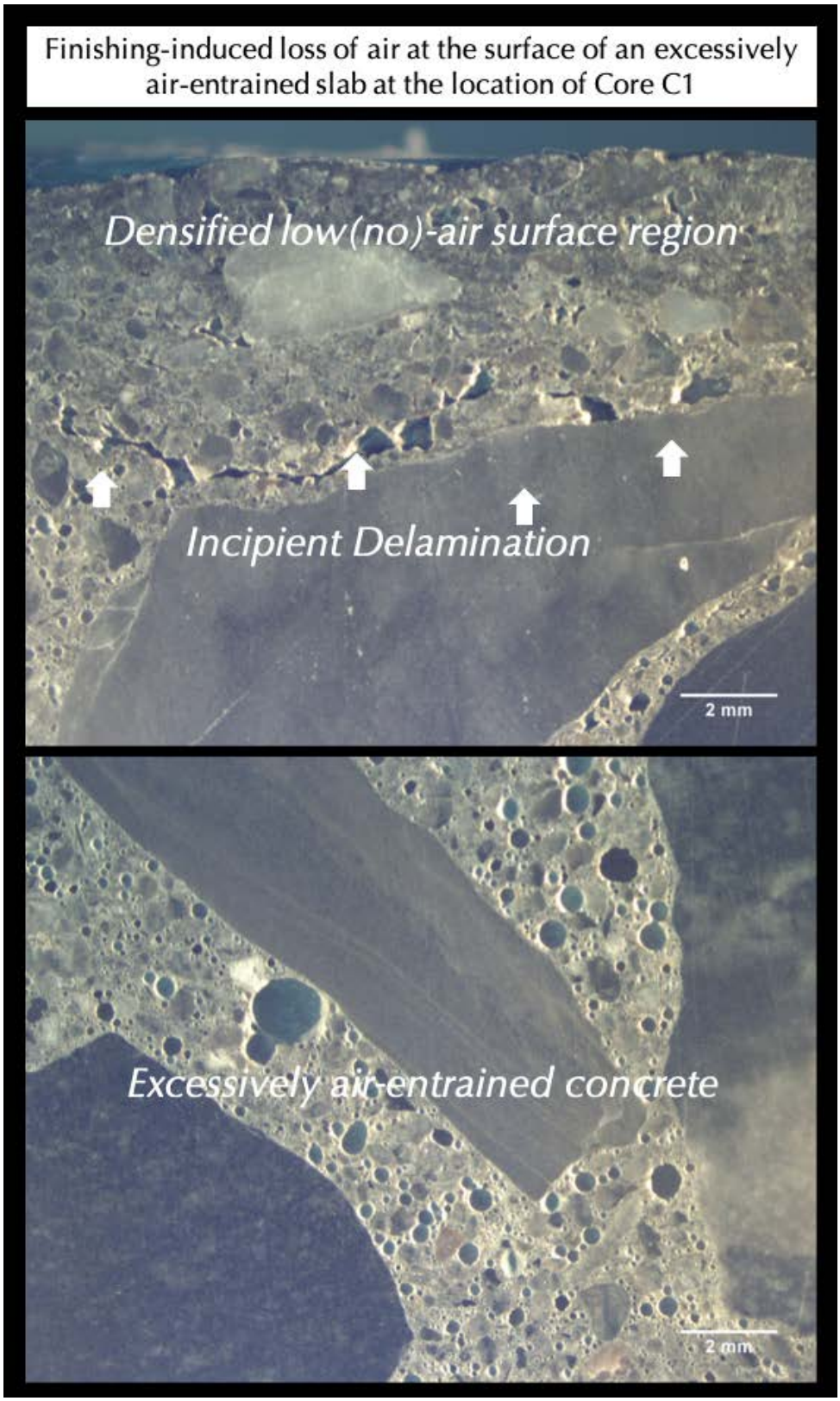

Figure 19: Micrographs of lapped cross section of Core C1 showing elongated near-surface incipient delamination (marked with arrows) as elongated tears or separations between the trowel-densified low to no-air very low *w/cm* surface region and interior excessively air-entrained concrete. This incipient delamination can cause eventual removal of the finished surface under traffic load.

Figure 20: Micrographs of lapped cross section of Core C1 showing elongated near-surface incipient delamination (marked with arrows) as elongated tears or separations between the trowel-densified low to no-air very low *w/cm* surface region and interior excessively air-entrained concrete. This incipient delamination can cause eventual removal of the finished surface under traffic load.

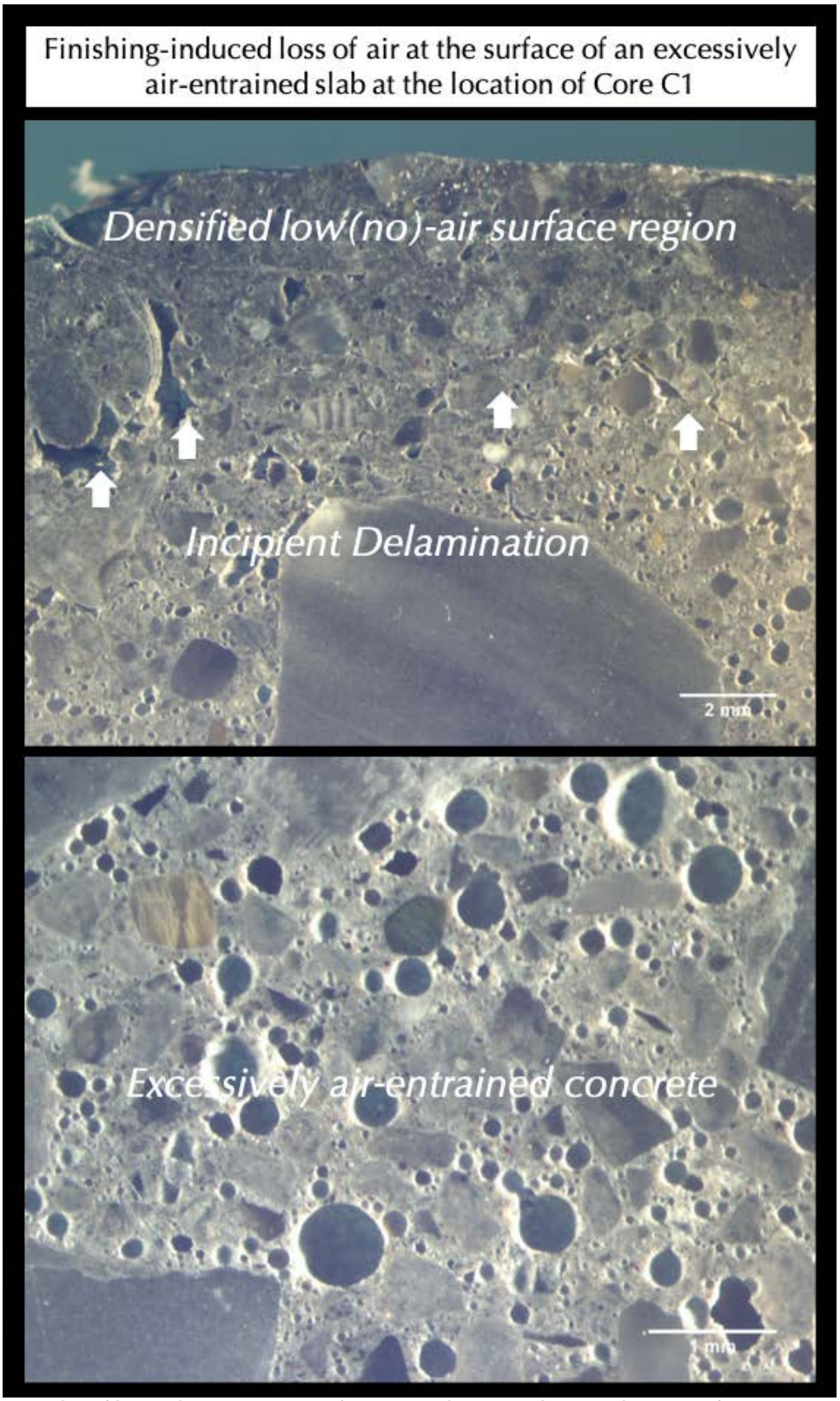

Figure 21: Micrographs of lapped cross section of Core C1 showing elongated near-surface incipient delamination (marked with arrows) as elongated tears or separations between the trowel-densified low to no-air very low *w/cm* surface region and interior excessively air-entrained concrete. This incipient delamination can cause eventual removal of the finished surface under traffic load.

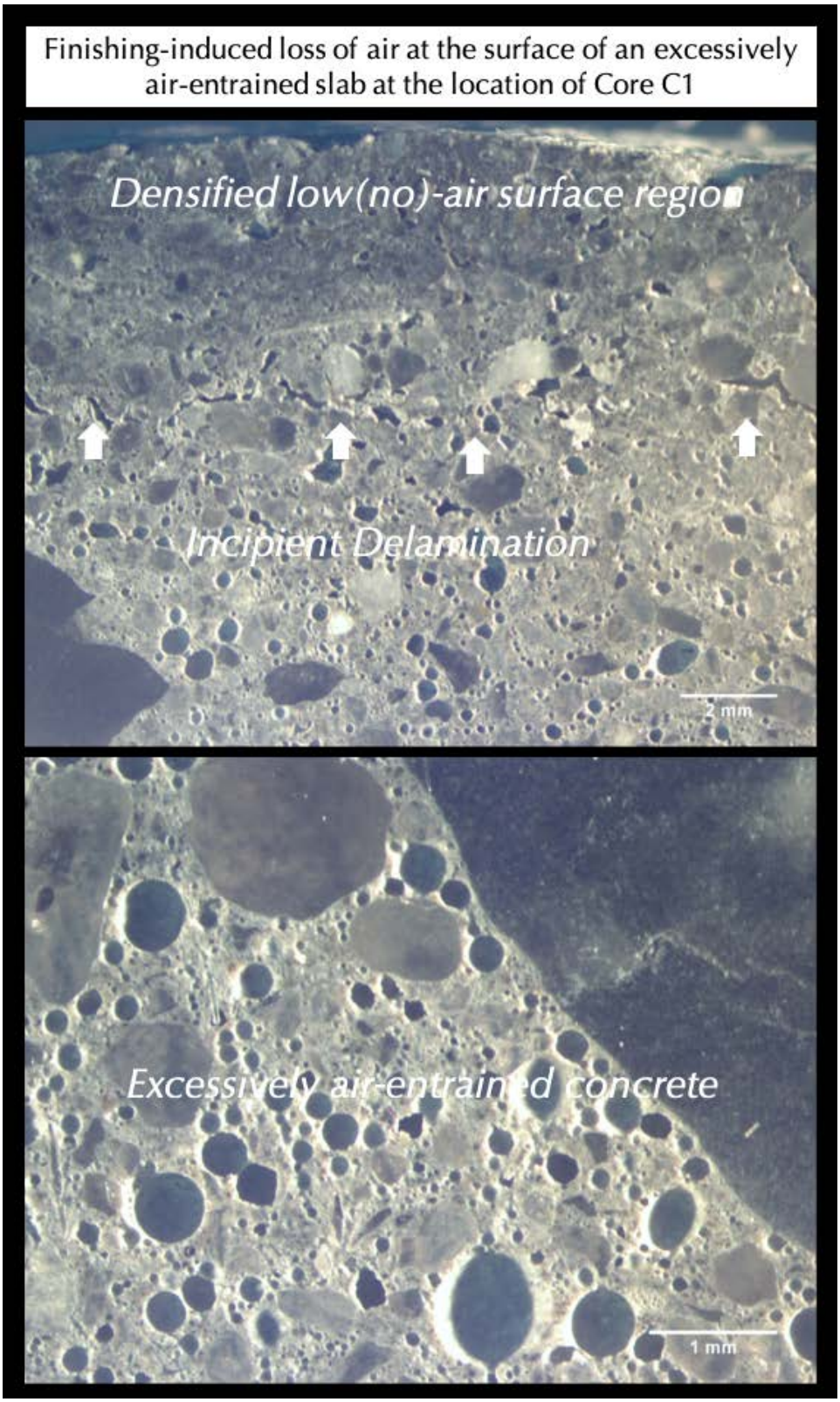

Figure 22: Micrographs of lapped cross section of Core C1 showing elongated near-surface incipient delamination (marked with arrows) as elongated tears or separations between the trowel-densified low to no-air very low *w/cm* surface region and interior excessively air-entrained concrete. This incipient delamination can cause eventual removal of the finished surface under traffic load.

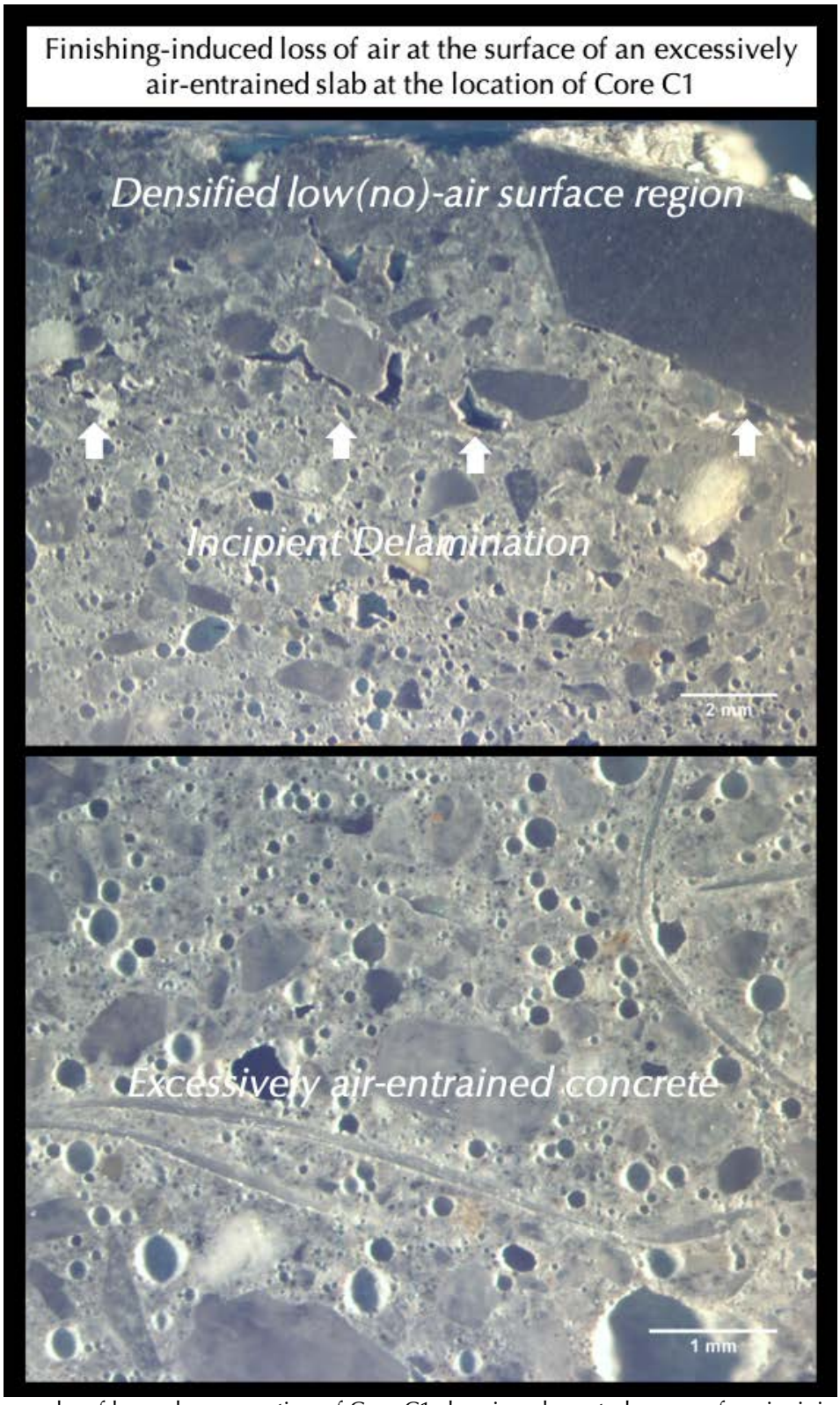

Figure 23: Micrographs of lapped cross section of Core C1 showing elongated near-surface incipient delamination (marked with arrows) as elongated tears or separations between the trowel-densified low to no-air very low *w/cm* surface region and interior excessively air-entrained concrete. Notice some synthetic fibers in concrete. This incipient delamination can cause eventual removal of the finished surface under traffic load.

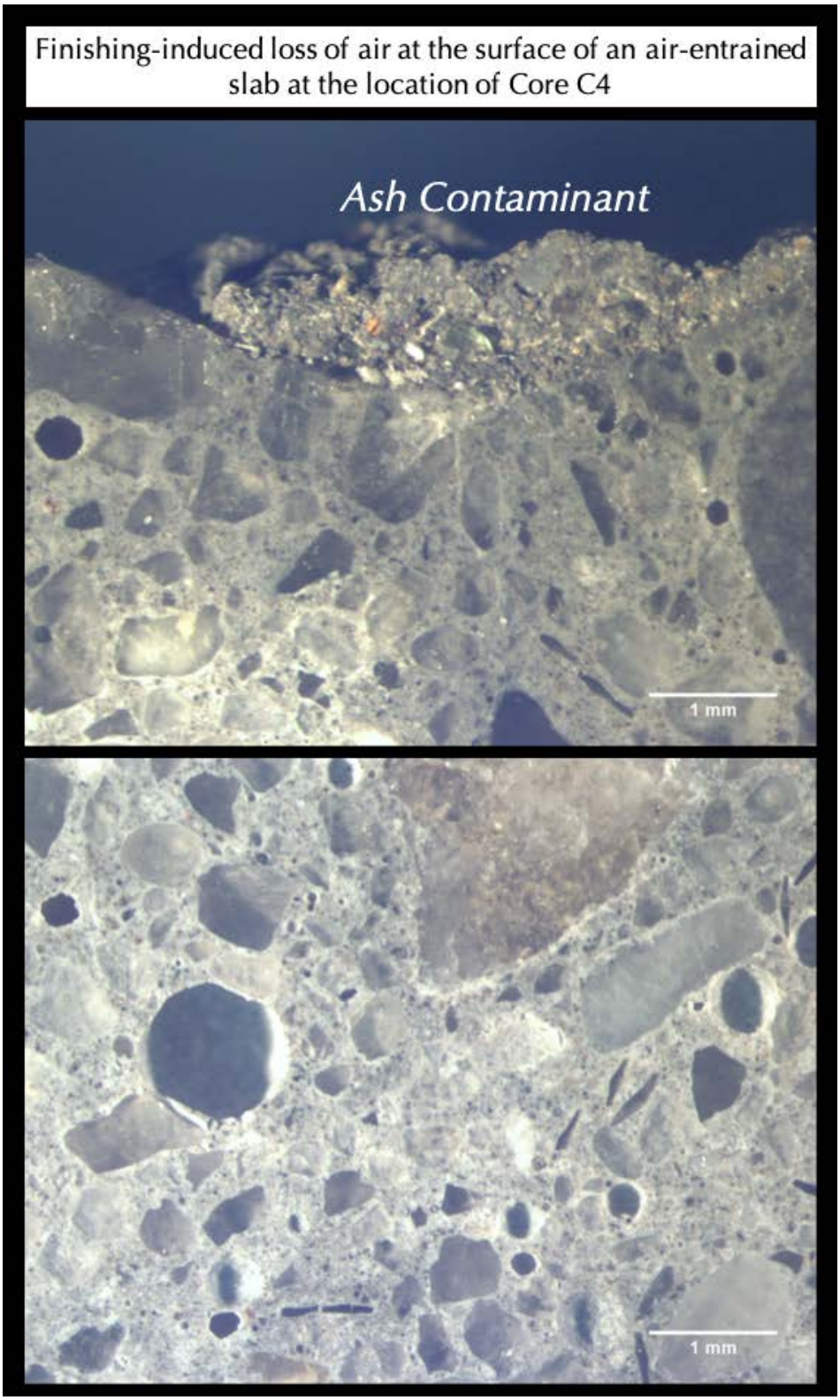

Figure 24: Micrographs of lapped cross section of Core C4 showing the absence of trowel-densified surface prior due to already delamination of the finished surface, leaving only the underlying concrete body on which a thin layer of incinerator ash deposits are present. Notice the marginally air-entrained nature of concrete having mostly coarse air voids at moderate amounts, as opposed to excessive air-entrainment of many very fine air voids as seen in Core C1.

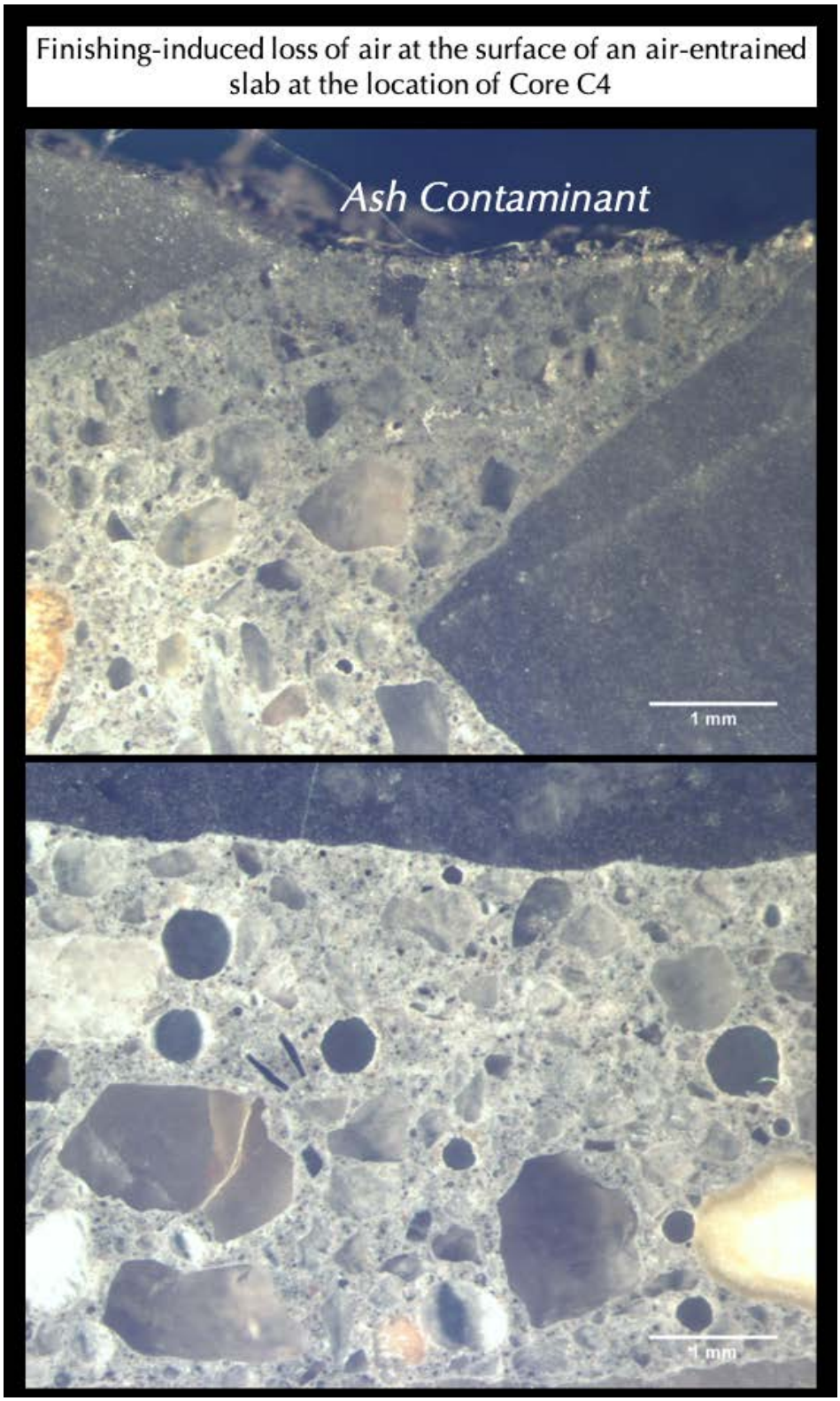

Figure 25: Micrographs of lapped cross section of Core C4 showing the absence of trowel-densified surface region due to prior delamination of the finished surface, leaving only the underlying concrete body on which a thin layer of incinerator ash deposits are present. Notice the marginally air-entrained nature of concrete having mostly coarse air voids at moderate amounts, as opposed to excessive air-entrainment of many very fine air voids as seen in Core C1.

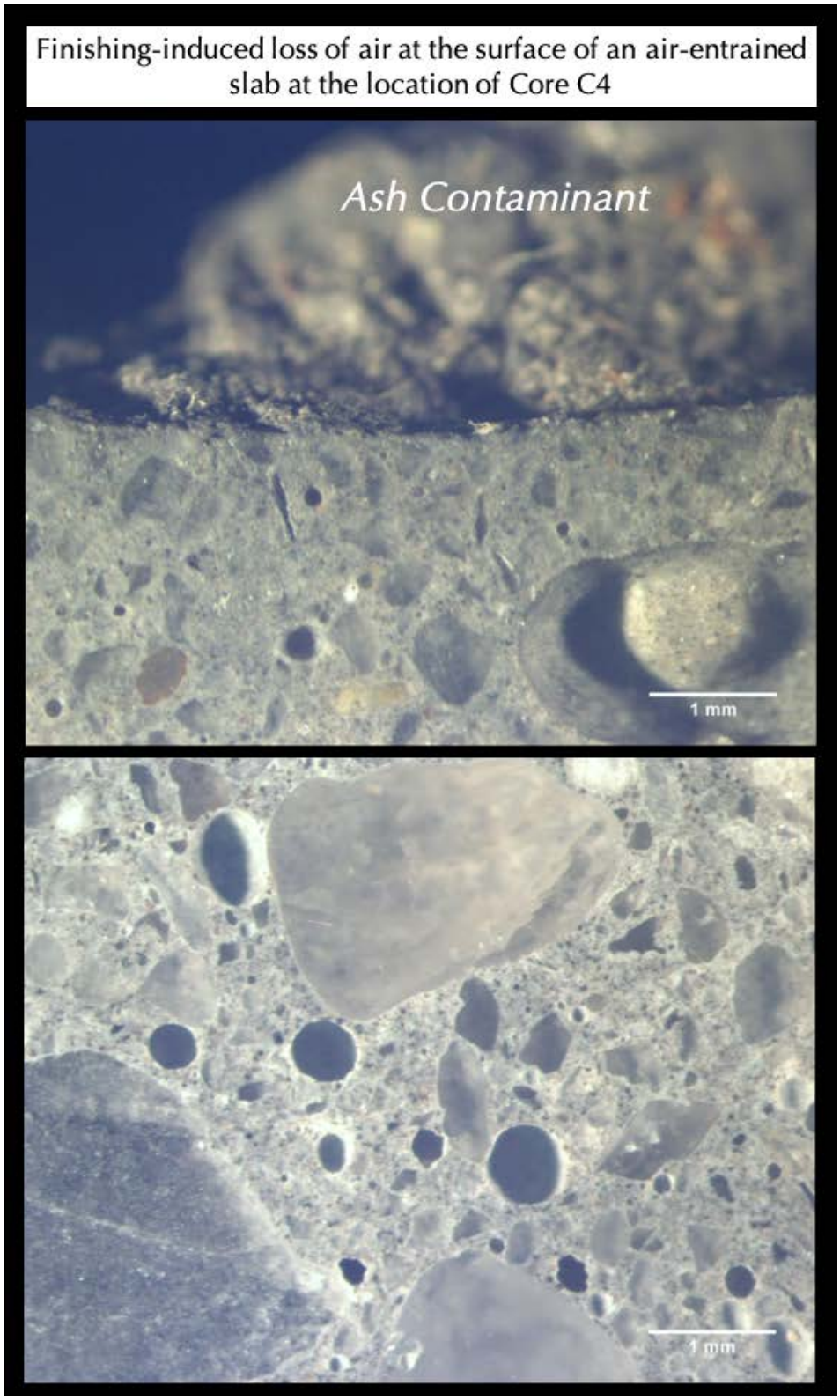

Figure 26: Micrographs of lapped cross section of Core C4 showing the absence of trowel-densified surface region due to prior delamination of the finished surface leaving only the underlying concrete body on which a thin layer of incinerator ash deposits are present. Notice the marginally air-entrained nature of concrete having mostly coarse air voids at moderate amounts, as opposed to excessive air-entrainment of many very fine air voids as seen in Core C1.

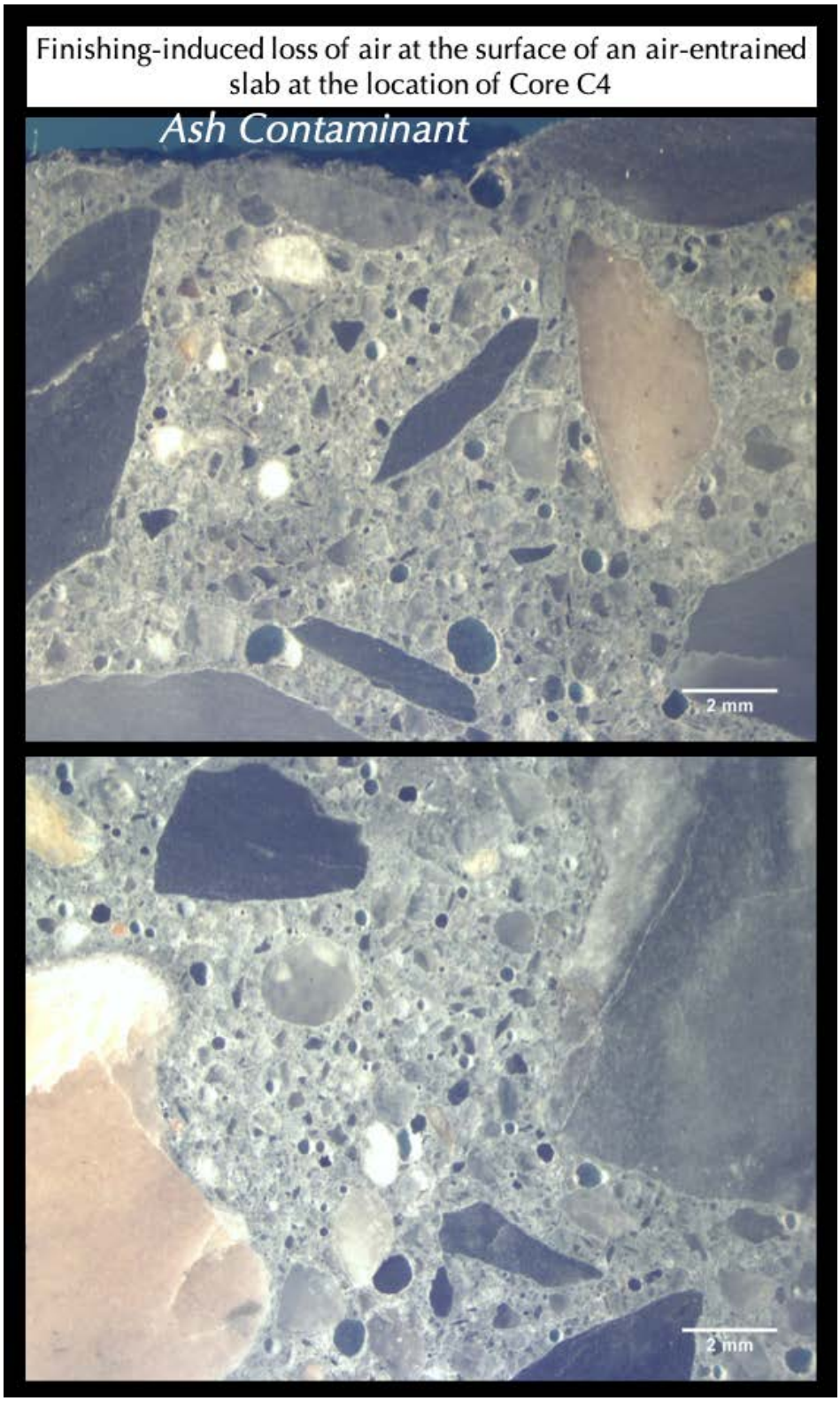

Figure 27: Micrographs of lapped cross section of Core C4 showing the absence of trowel-densified surface region due to prior delamination of the finished surface leaving only the underlying concrete body on which a thin layer of incinerator ash deposits are present. Notice the marginally air-entrained nature of concrete having mostly coarse air voids at moderate amounts, as opposed to excessive air-entrainment of many very fine air voids as seen in Core C1.

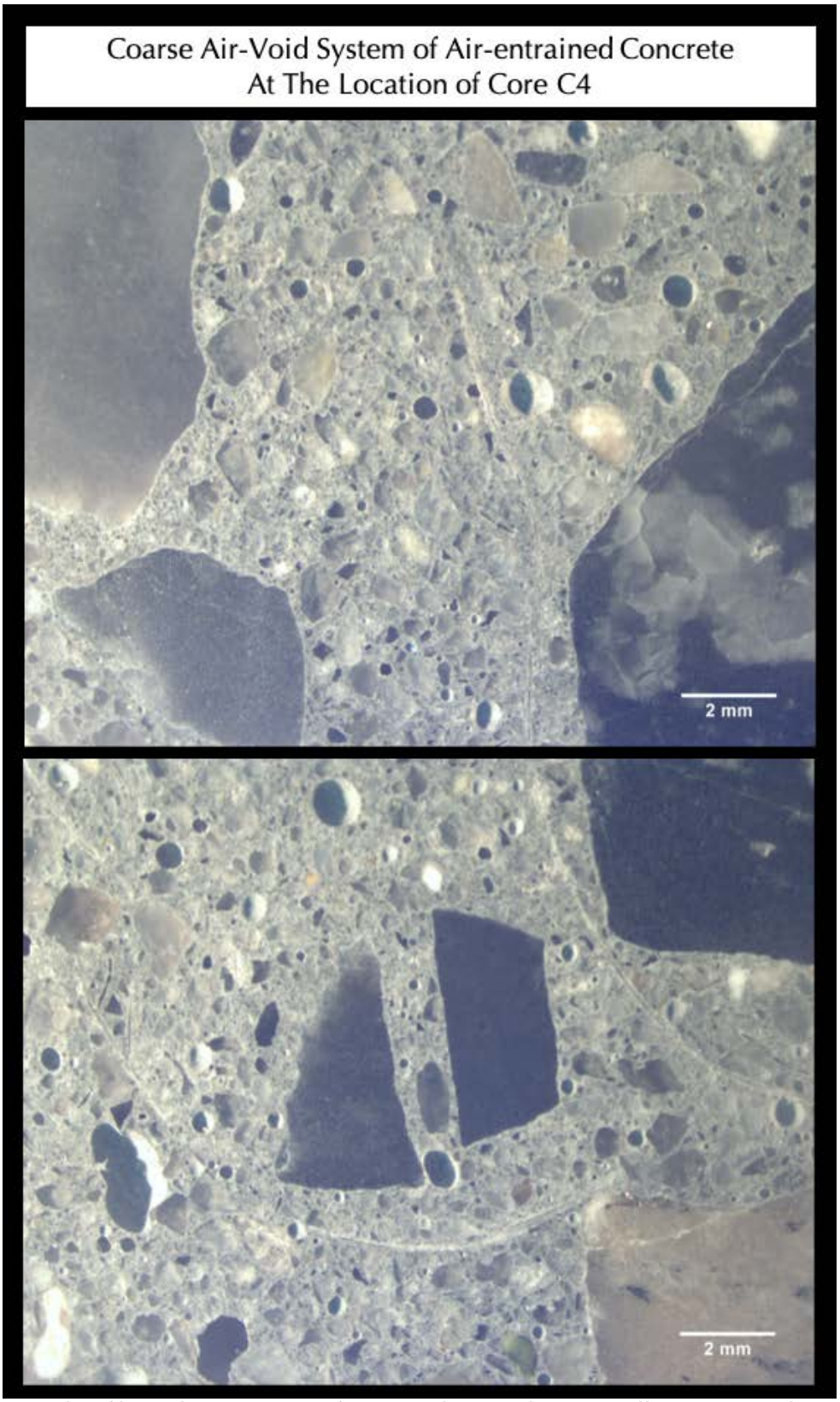

Figure 28: Micrographs of lapped cross section of Core C4 showing the marginally air-entrained nature of concrete having mostly coarse air voids at moderate amounts, as opposed to excessive air-entrainment of many very fine air voids as seen in Core C1. Notice some synthetic fibers in the bottom photo.

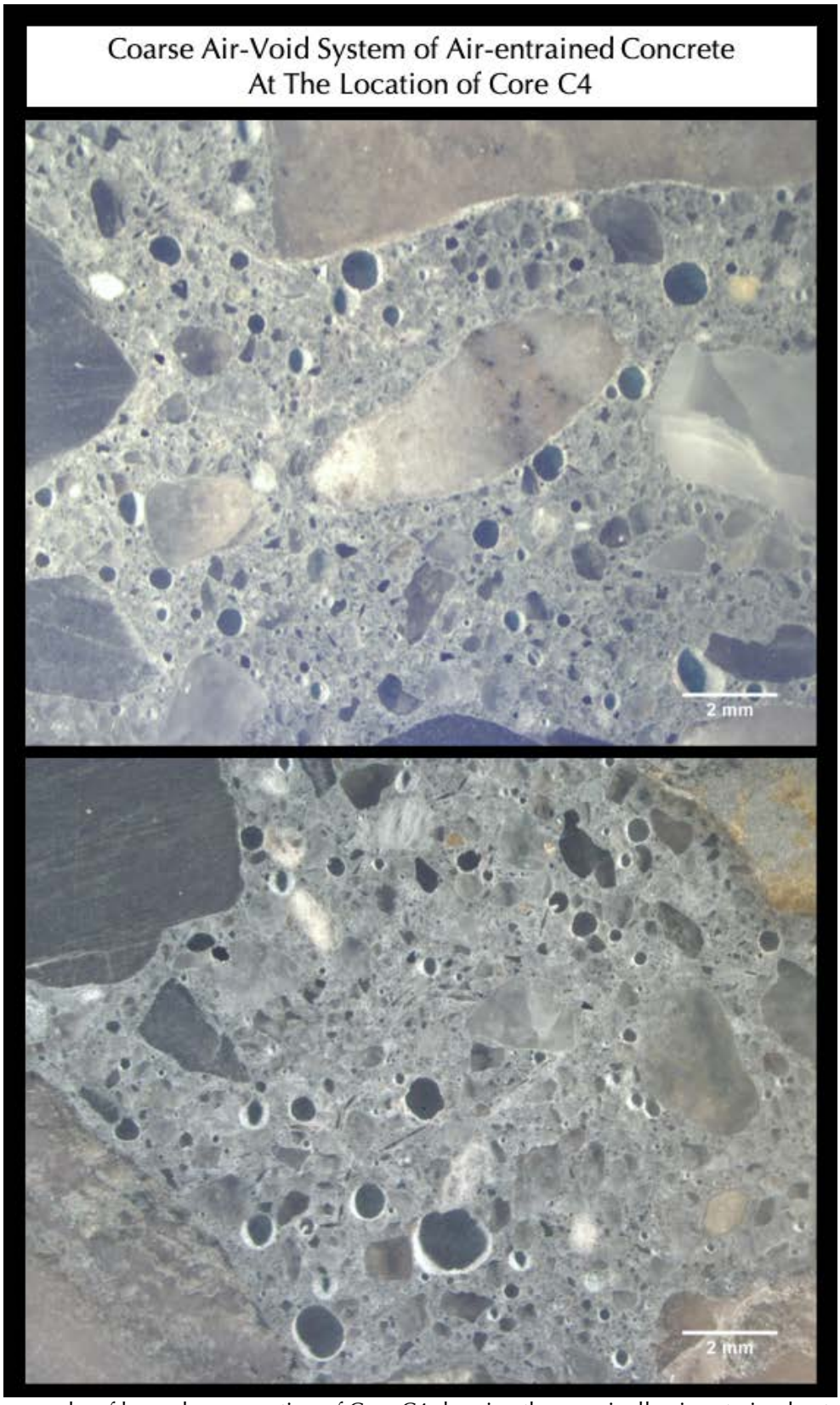

Figure 29: Micrographs of lapped cross section of Core C4 showing the marginally air-entrained nature of concrete having mostly coarse air voids at moderate amounts, as opposed to excessive air-entrainment of many very fine air voids as seen in Core C1.

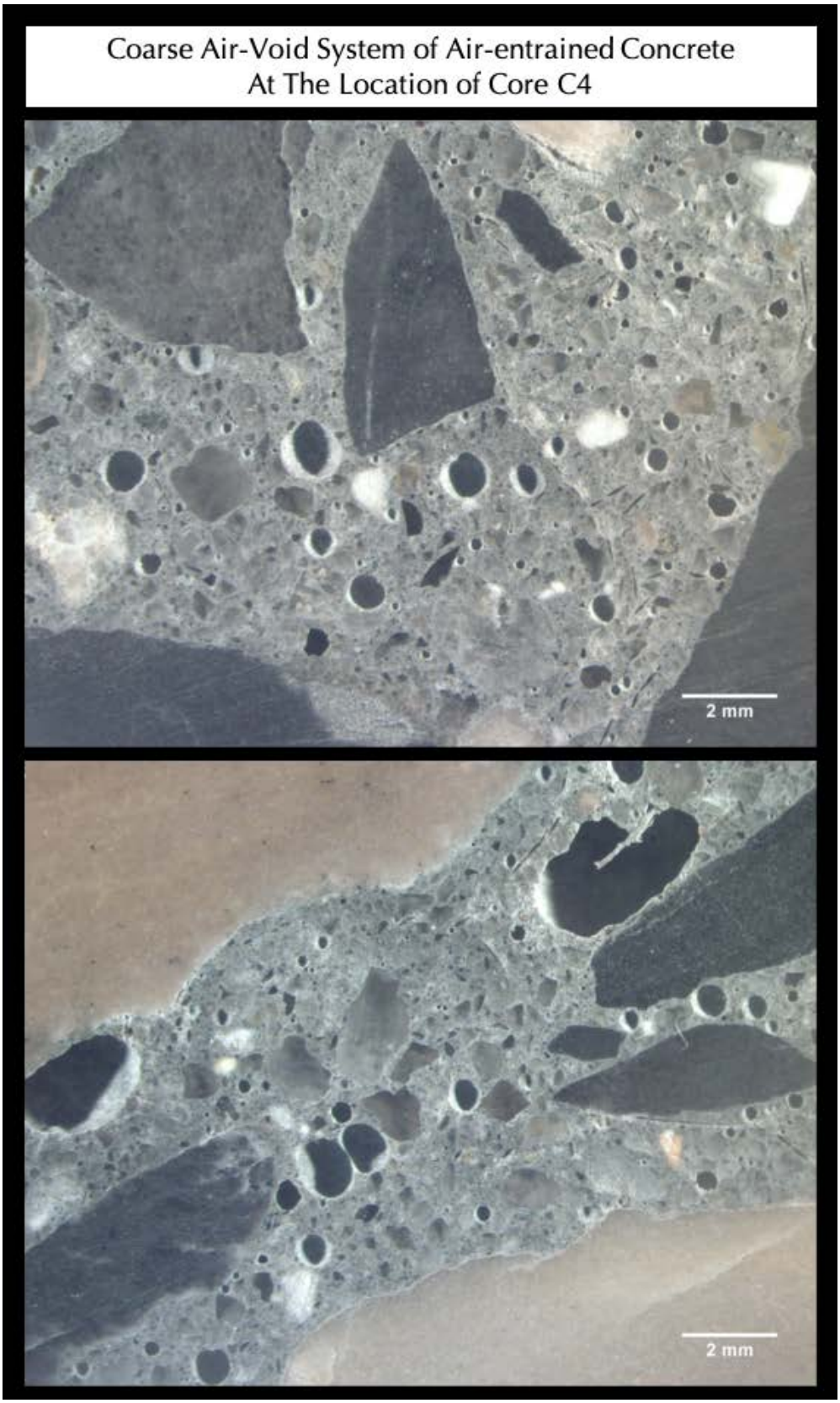

Figure 30: Micrographs of lapped cross section of Core C4 showing the marginally air-entrained nature of concrete having mostly coarse air voids at moderate amounts, as opposed to excessive air-entrainment of many very fine air voids as seen in Core C1.

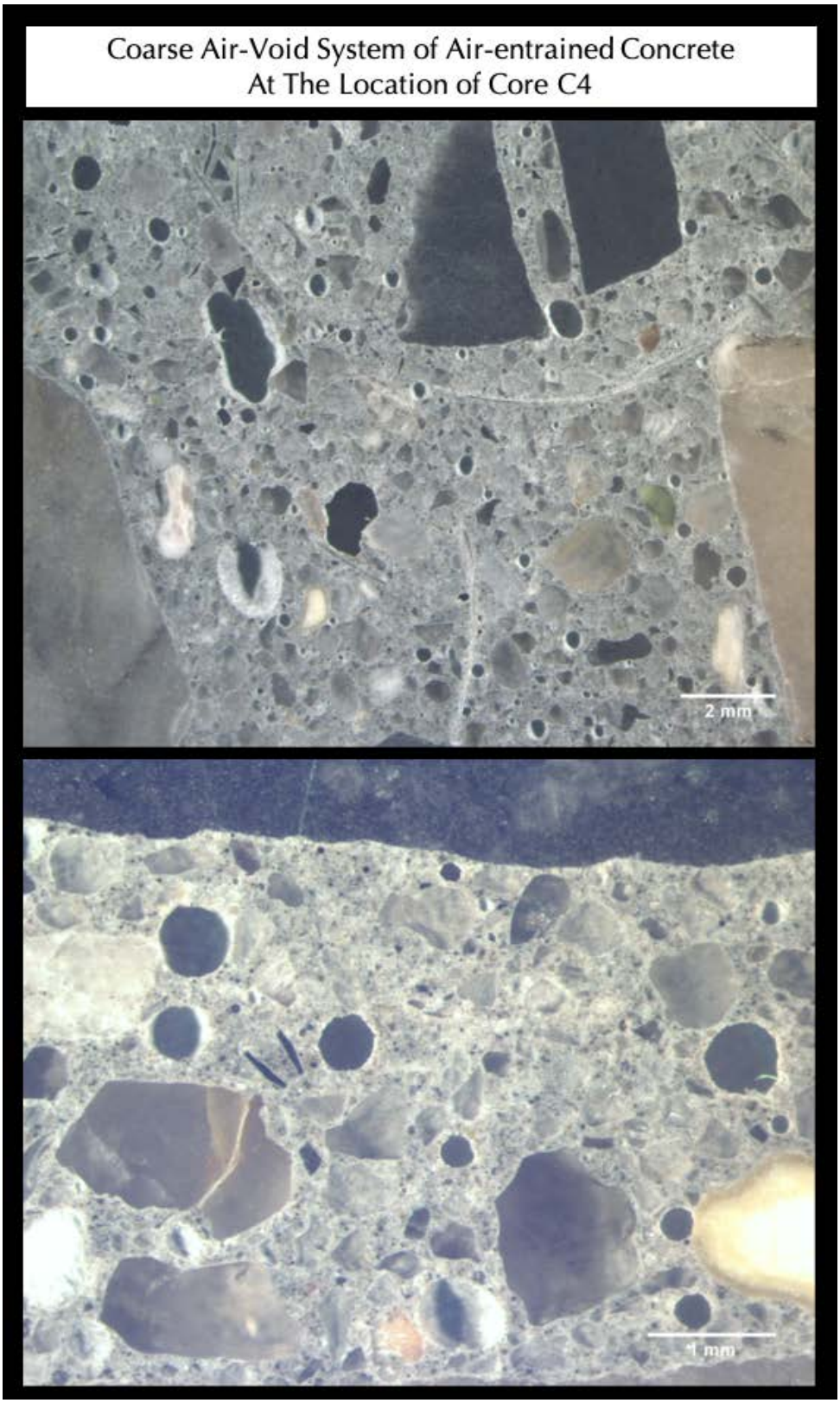

Figure 31: Micrographs of lapped cross section of Core C4 showing the marginally air-entrained nature of concrete having mostly coarse air voids at moderate amounts, as opposed to excessive air-entrainment of many very fine air voids in Core C1. Notice some synthetic fibers in the top photo.

THIN SECTIONS OF CONCRETE CORES

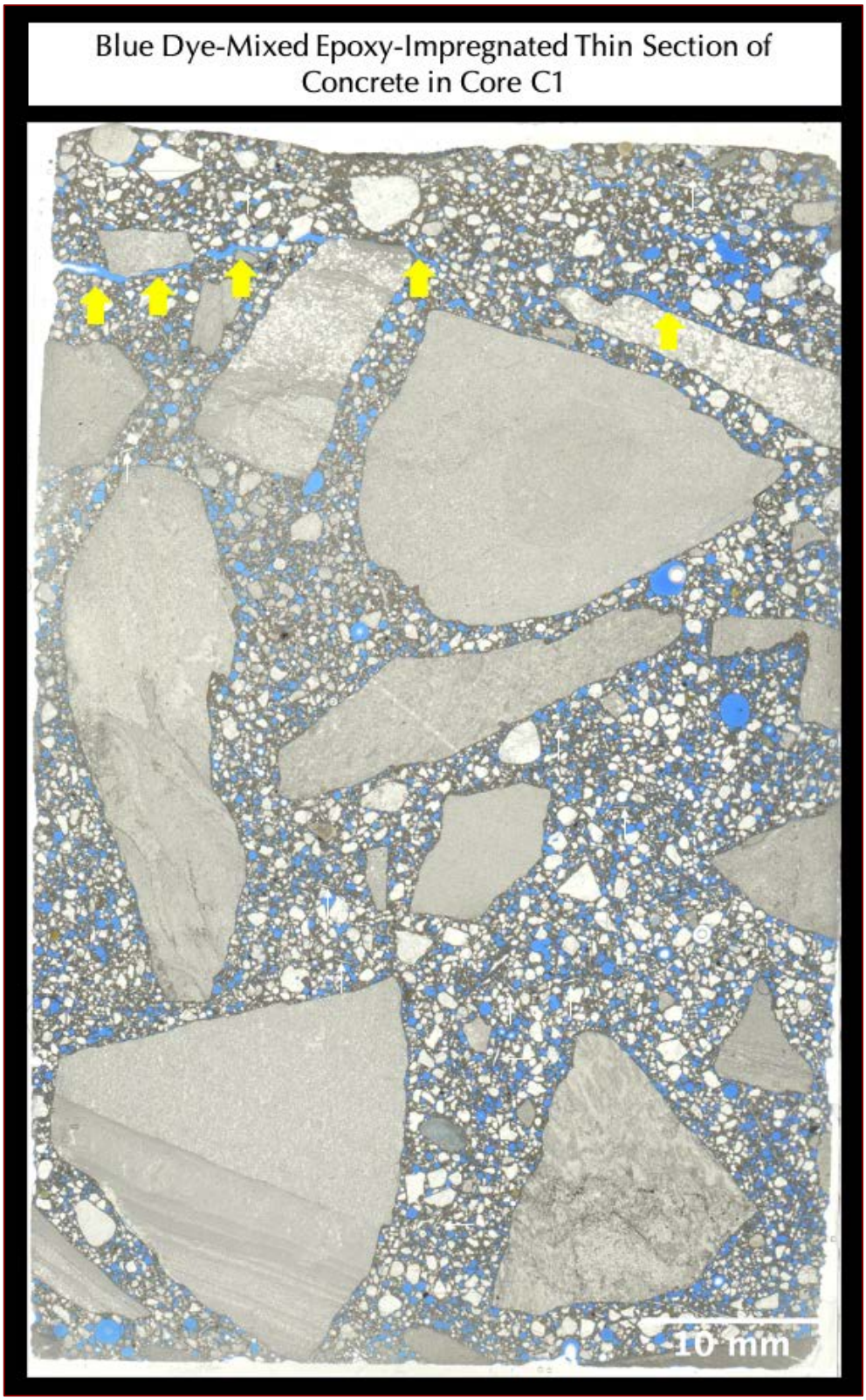

Figure 32: Blue dye-mixed epoxy-encapsulated thin section of Core C1 taken by using a flatbed film scanner, where thin section was scanned with a polarizing filter to recreate plane polarized light view of sample to show:

(a) The densified trowel-finished surface region, incipient delamination as isolated elongated tears that are highlighted by the blue epoxy and arrows,

(b) Excessively air-entrained nature of concrete where air voids are highlighted by blue epoxy,

(c) Size, shape, angularity, gradation, and distribution of crushed limestone coarse aggregate and natural siliceous sand fine aggregates, and,

(d) Distribution of fine, hair-like polypropylene type synthetic fibers throughout the depth of core, some of which are marked with thin white arrows.

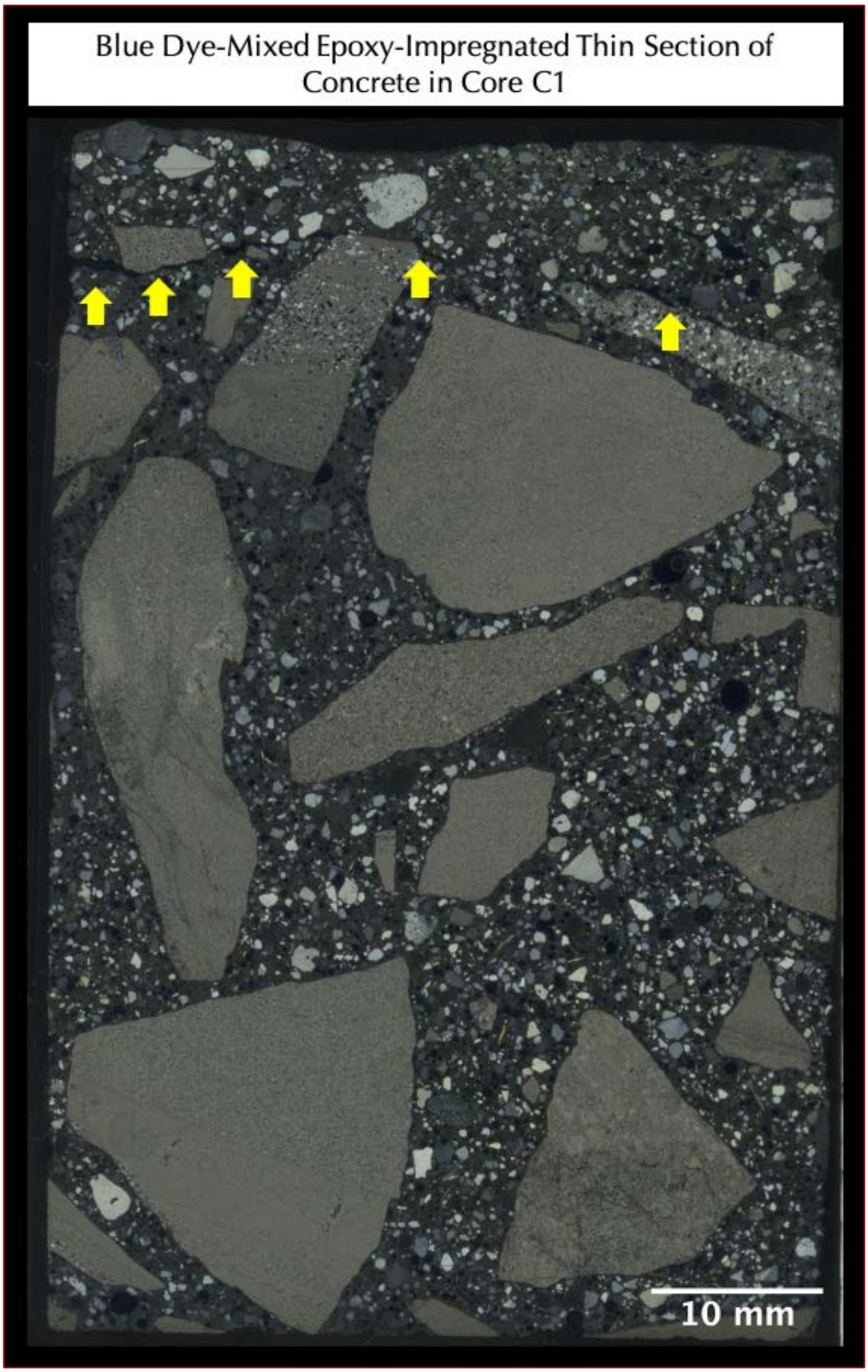

Figure 33: Blue dye-mixed epoxy-encapsulated thin section of Core C1 taken by using a flatbed film scanner, where thin section was scanned with two polarizing filters at perpendicular orientations to recreate cross polarized light view of sample where crushed limestone coarse aggregate and natural siliceous sand fine aggregates are highlighted. Arrows show near-surface incipient delamination.

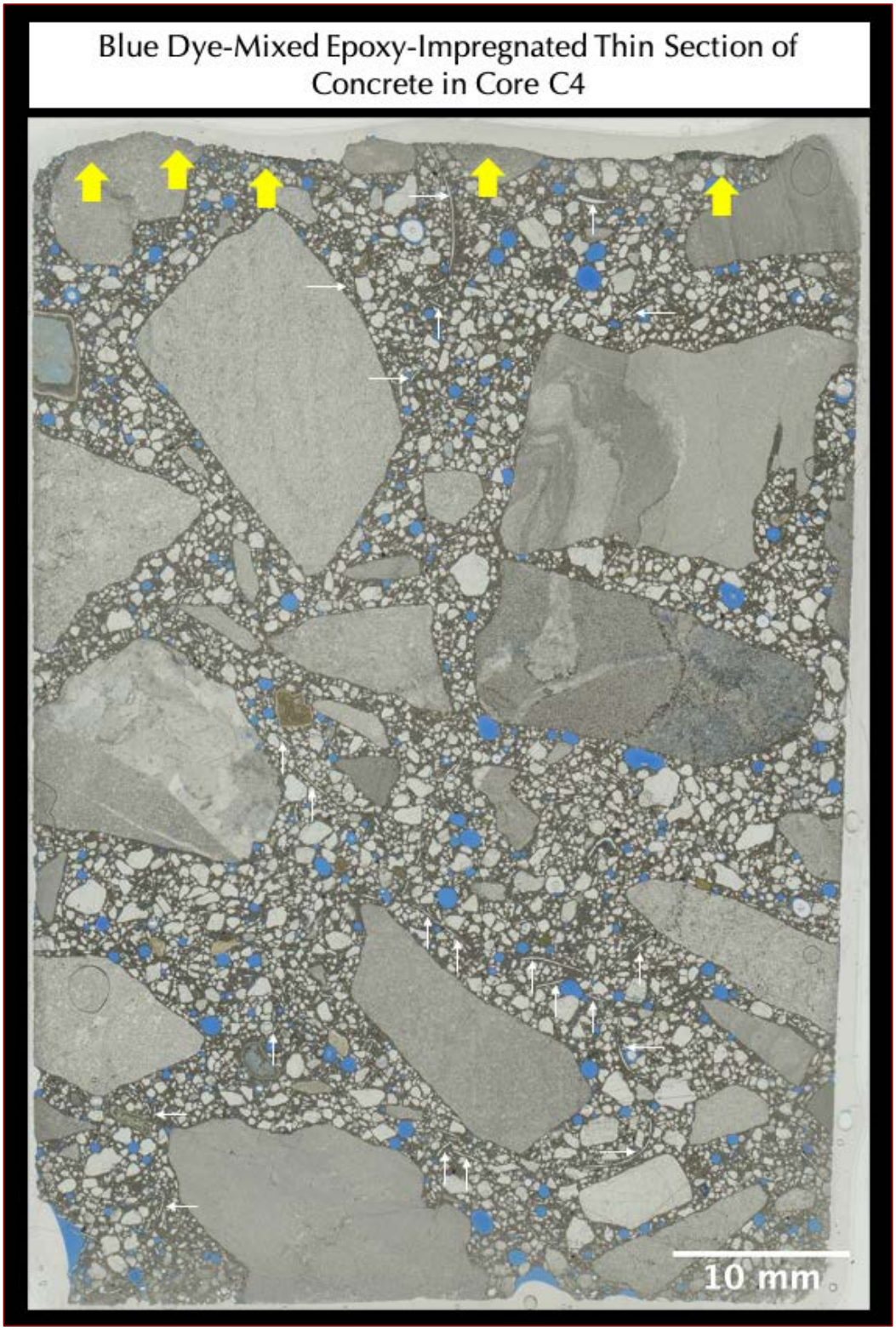

Figure 34: Blue dye-mixed epoxy-encapsulated thin section of Core C4 taken by using a flatbed film scanner, where thin section was scanned with a polarizing filter to recreate plane polarized light view of sample to show:

(a) The delaminated surface region marked by arrows,

(b) Marginally air-entrained nature of concrete where many coarse air voids are highlighted by blue epoxy,

(c) Size, shape, angularity, gradation, and distribution of crushed limestone coarse aggregate and natural siliceous sand fine aggregates, and,

(d) Distribution of fine, hair-like polypropylene type synthetic fibers throughout the depth of core, some of which are marked with thin white arrows.

Figure 35: Blue dye-mixed epoxy-encapsulated thin section of Core C4 taken by using a flatbed film scanner, where thin section was scanned with two polarizing filters at perpendicular orientations to recreate cross polarized light view of sample where crushed limestone coarse aggregate and natural siliceous sand fine aggregates are highlighted. Arrows show surface delamination.

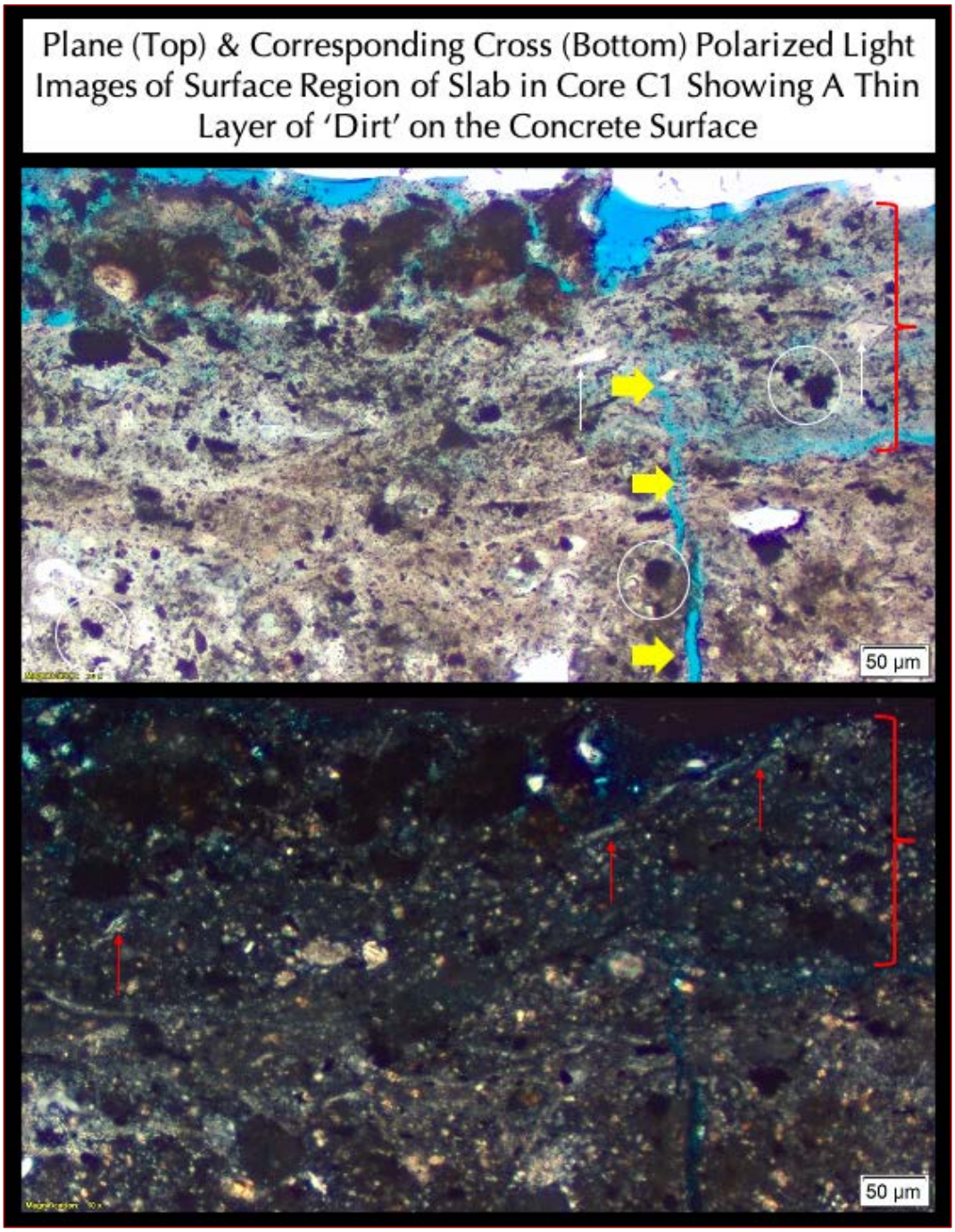

Figure 36: Micrographs of thin section of surface region of Core C1 showing the potential contaminant on the surface of concrete consisting of (a) very fine-grained deposits of organic matter, (b) ferruginous materials, (c) ultrafine crushed quartz, (d) limestone dusts, (e) spherical fly ash (some ash particles are circled), (f) porous, ultrafine-grained carbonated lime, (g) shrinkage microcracks and overall porous nature of deposit that is highlighted by blue epoxy, (h) synthetic fibers (marked with thin red arrows), and (i) angular shard-like glassy particles of slag (a few marked with thin white arrows). None of these constituents in the surface deposit are potentially harmful to concrete, hence the concrete surface region immediately beneath the deposit shows no surface alteration (leaching, erosion, carbonation, etc.). Notice the sharp boundary between porous surface deposit and underlying dense concrete surface.

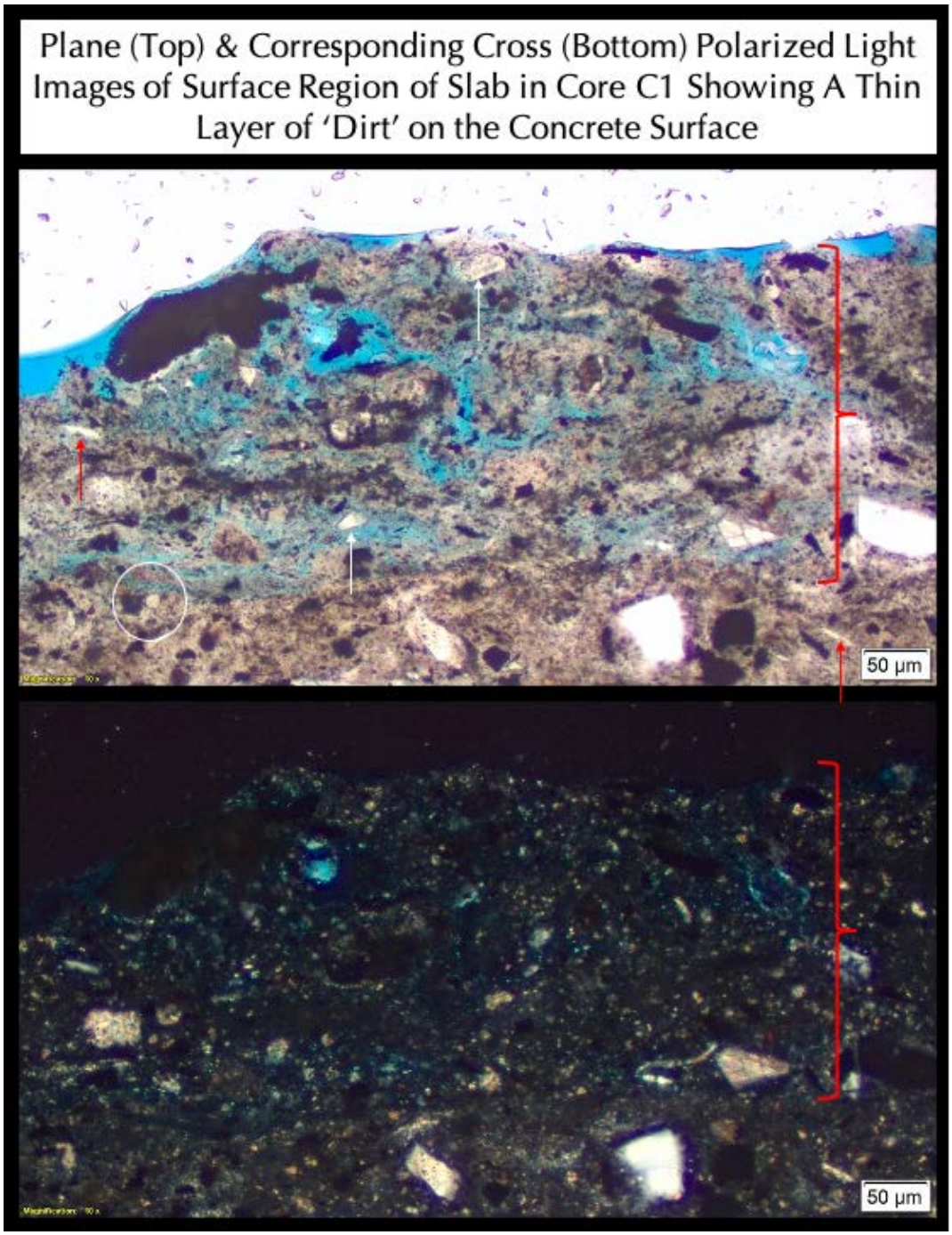

Figure 37: Micrographs of thin section of surface region of Core C1 showing the potential contaminant on the surface of concrete consisting of (a) very fine-grained deposits of organic matter, (b) ferruginous materials, (c) ultrafine crushed quartz, (d) limestone dusts, (e) spherical fly ash (some ash particles are circled), (f) porous, ultrafine-grained carbonated lime, (g) shrinkage microcracks and overall porous nature of deposit that is highlighted by blue epoxy, (h) synthetic fibers (marked with thin red arrows), and (i) angular shard-like glassy particles of slag (a few marked with thin white arrows). None of these constituents in the surface deposit are potentially harmful to concrete, hence the concrete surface region immediately beneath the deposit shows no surface alteration (leaching, erosion, carbonation, etc.). Notice the sharp boundary between porous surface deposit and underlying dense concrete surface.

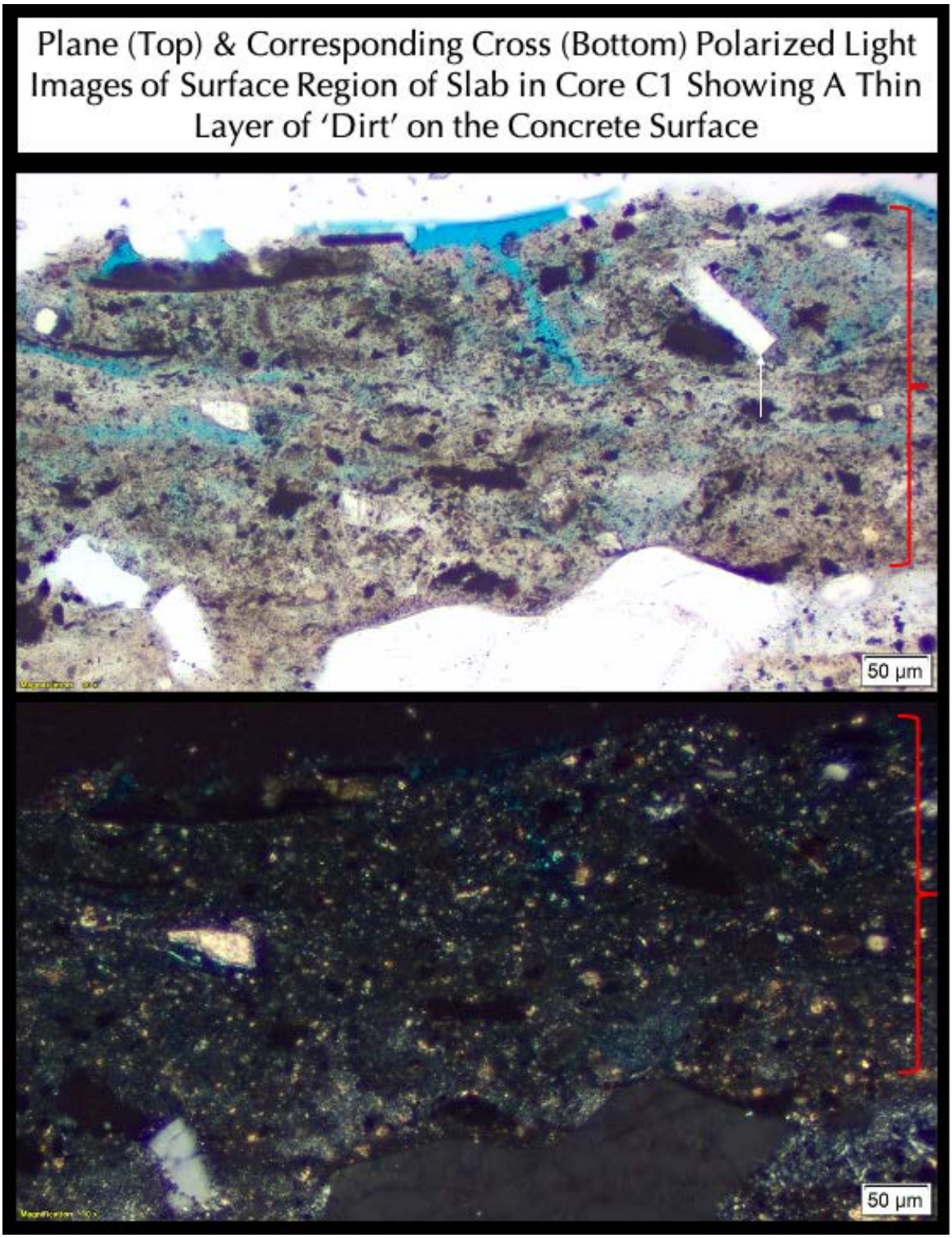

Figure 38: Micrographs of thin section of surface region of Core C1 showing the potential contaminant on the surface of concrete consisting of (a) very fine-grained deposits of organic matter, (b) ferruginous materials, (c) ultrafine crushed quartz, (d) limestone dusts, (e) spherical fly ash, (f) lime, (g) shrinkage microcrack and overall porous nature of deposit that are highlighted by blue epoxy, (h) synthetic fibers, and (i) angular shard-like glassy particles of slag (a few marked with thin white arrows). None of these constituents in the surface deposit are potentially harmful to concrete, hence the concrete surface region immediately beneath the deposit shows no surface alteration (leaching, erosion, carbonation, etc.).

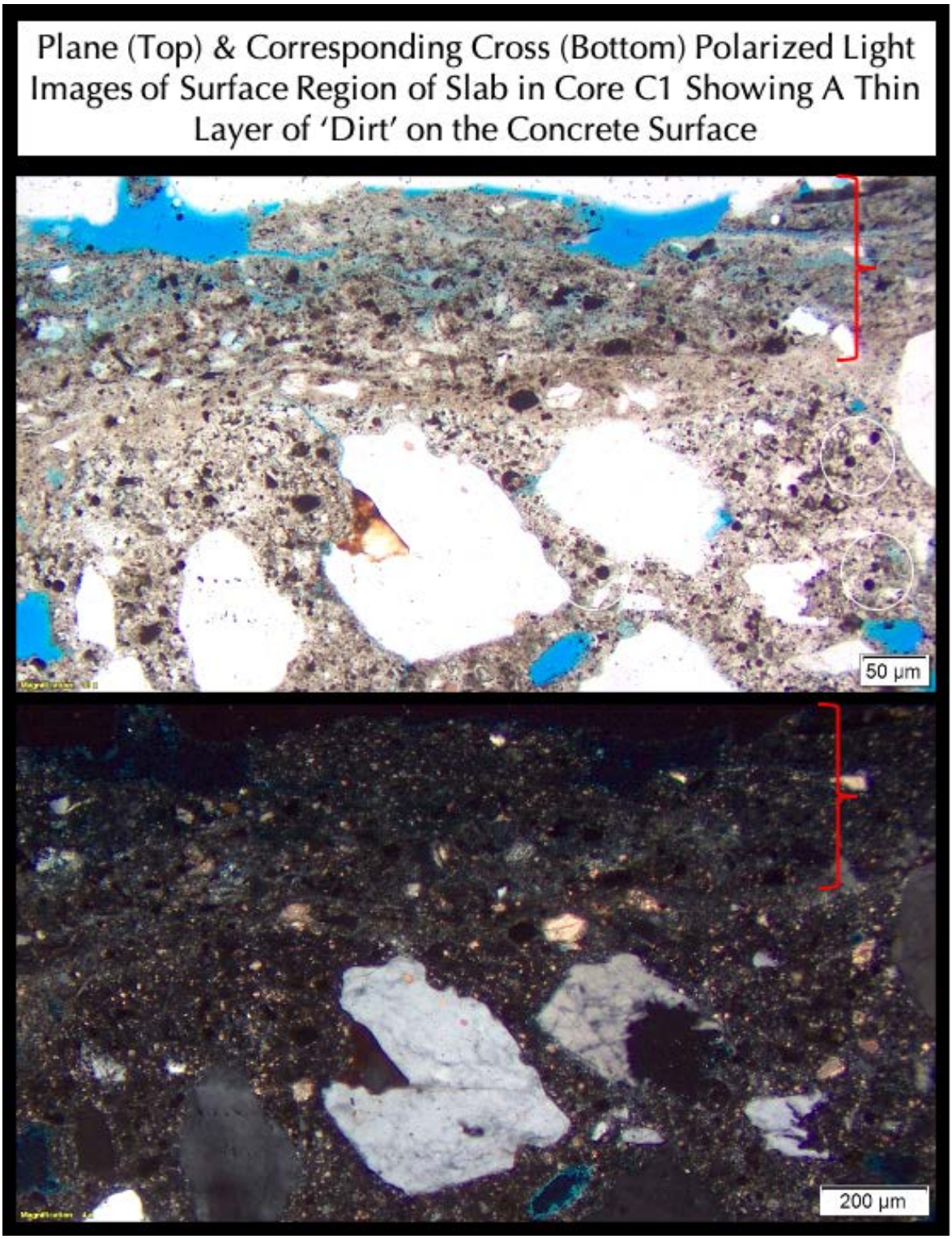

Figure 39: Micrographs of thin section of surface region of Core C1 showing the potential contaminant on the surface of concrete consisting of (a) very fine-grained deposits of organic matter, (b) ferruginous materials, (c) ultrafine crushed quartz, (d) limestone dusts, (e) spherical fly ash (some ash particles are circled), (f) porous, ultrafine-grained carbonated lime, (g) shrinkage microcracks and overall porous nature of deposit that are highlighted by blue epoxy, (h) synthetic fibers, and (i) angular shard-like glassy particles of slag (a few marked with thin white arrows). None of these constituents in the surface deposit are potentially harmful to concrete, hence the concrete surface region immediately beneath the deposit shows no surface alteration (leaching, erosion, carbonation, etc.).

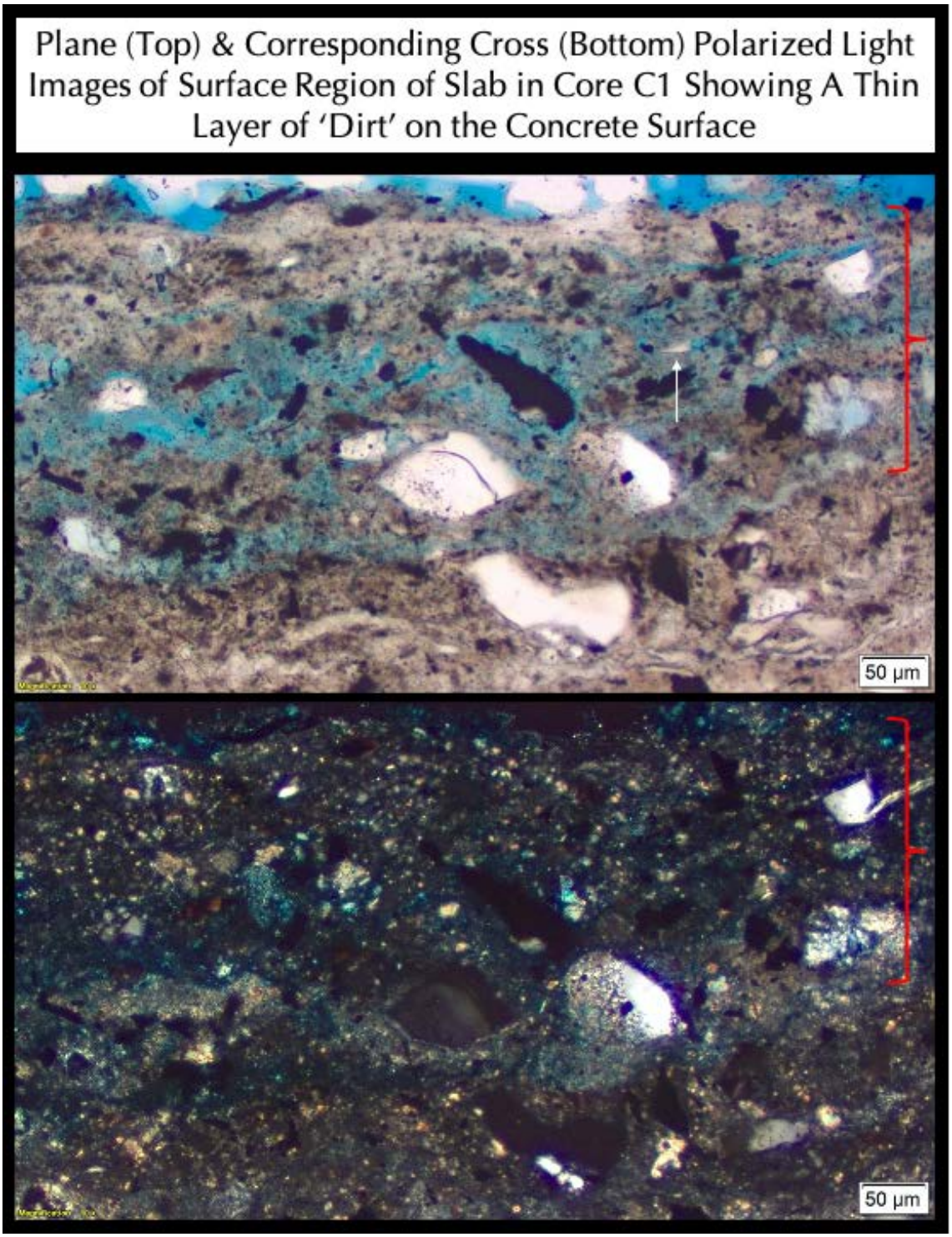

Figure 40: Micrographs of thin section of surface region of Core C1 showing the potential contaminant on the surface of concrete consisting of (a) very fine-grained deposits of organic matter, (b) ferruginous materials, (c) ultrafine crushed quartz, (d) limestone dust, (e) spherical fly ash, (f) porous, ultrafine-grained carbonated lime, (g) shrinkage microcracks and overall porous nature of deposit that are highlighted by blue epoxy, (h) synthetic fibers, and (i) angular shard-like glassy particles of slag (a few marked with thin white arrows). None of these constituents in the surface deposit are potentially harmful to concrete, hence the concrete surface region immediately beneath the deposit shows no surface alteration (leaching, erosion, carbonation, etc.). Notice the sharp boundary between porous surface deposit and underlying dense concrete surface.

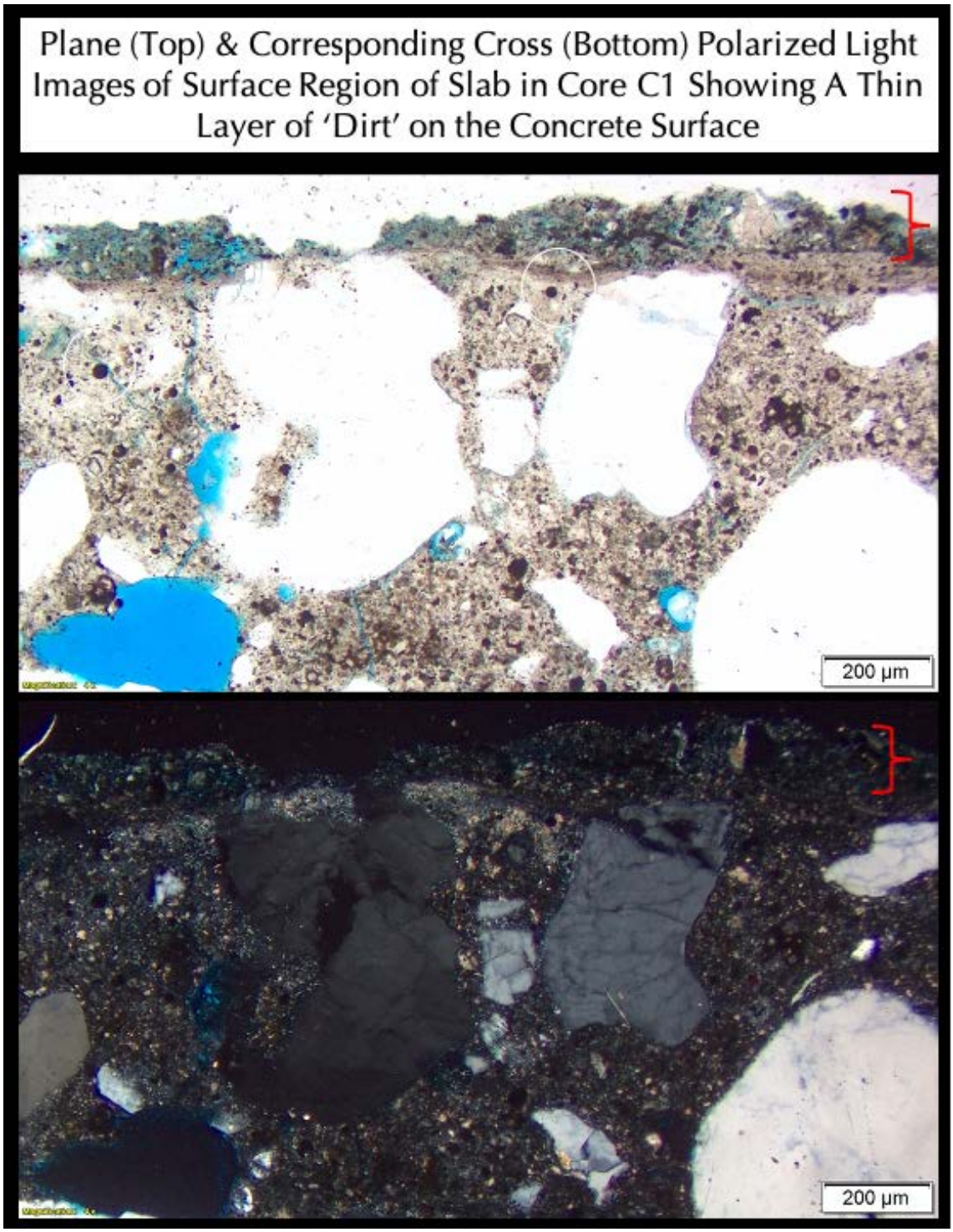

Figure 41: Micrographs of thin section of surface region of Core C1 showing the potential contaminant on the surface of concrete consisting of (a) very fine-grained deposits of organic matter, (b) ferruginous materials, (c) ultrafine crushed quartz, (d) limestone dust, (e) spherical fly ash, (f) porous, ultrafine-grained carbonated lime, (g) shrinkage microcracks and overall porous nature of deposit that are highlighted by blue epoxy, (h) synthetic fibers, and (i) angular shard-like glassy particles of slag. None of these constituents in the surface deposit are potentially harmful to concrete, hence the concrete surface region immediately beneath the deposit shows no surface alteration (leaching, erosion, carbonation, etc.). Notice the sharp boundary between porous surface deposit and underlying dense concrete surface.

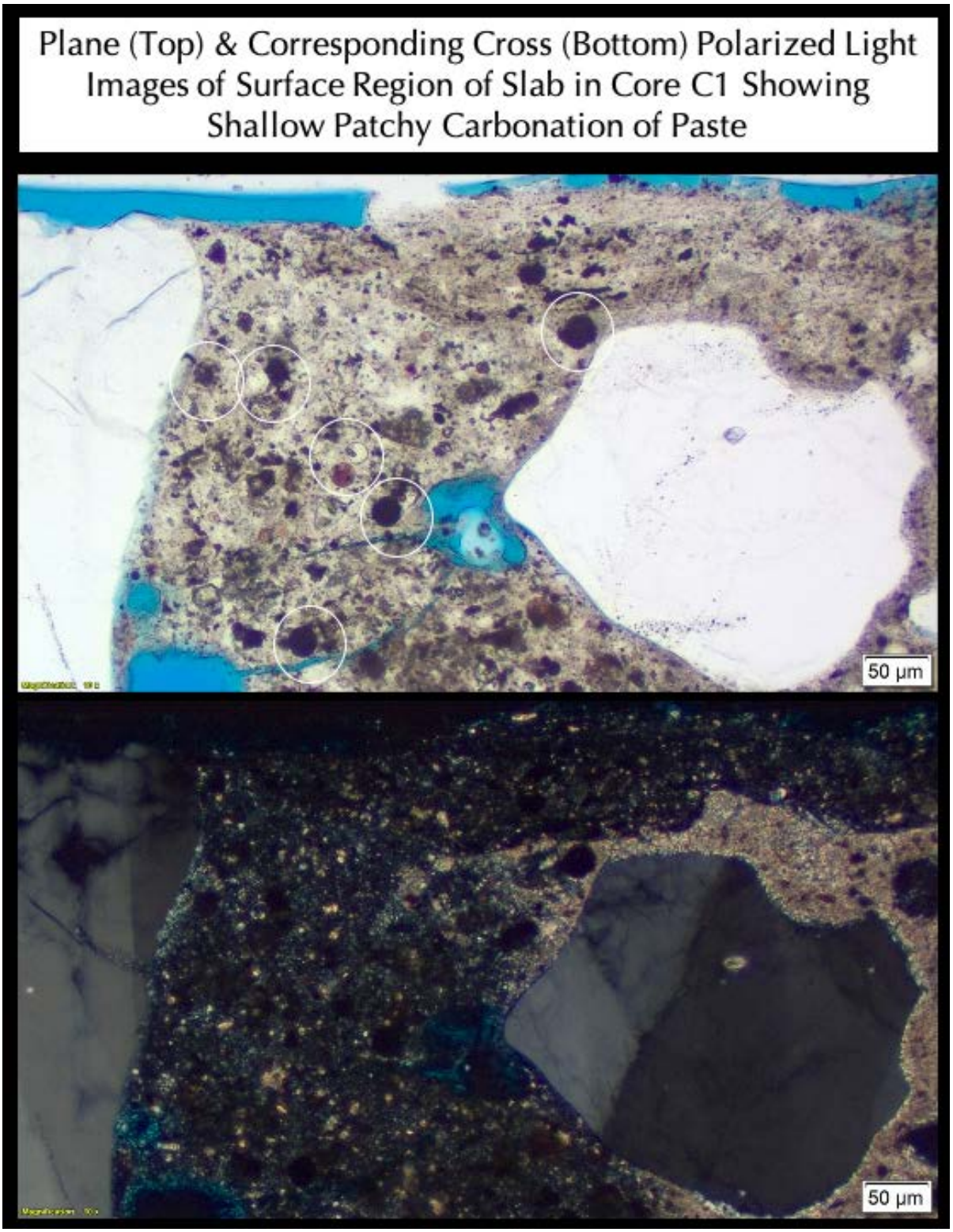

Figure 42: Micrographs of thin section of surface region of Core C1 showing the surface region of concrete consisting of (a) very dense paste of Portland cement and (b) fly ash where some spherical fly ash particles are circled, (c) quartz sand fine aggregate, and (d) patchy carbonation of paste at isolated locations of surface due to overall well-consolidated and densified surface by trowel-finishing. Scattered throughout the paste are some limestone fine particles mixed with cement hydration products that are judged to be dusts from crushed limestone coarse aggregate. Depth of carbonation is within the top 1 to 2 mm of surface.

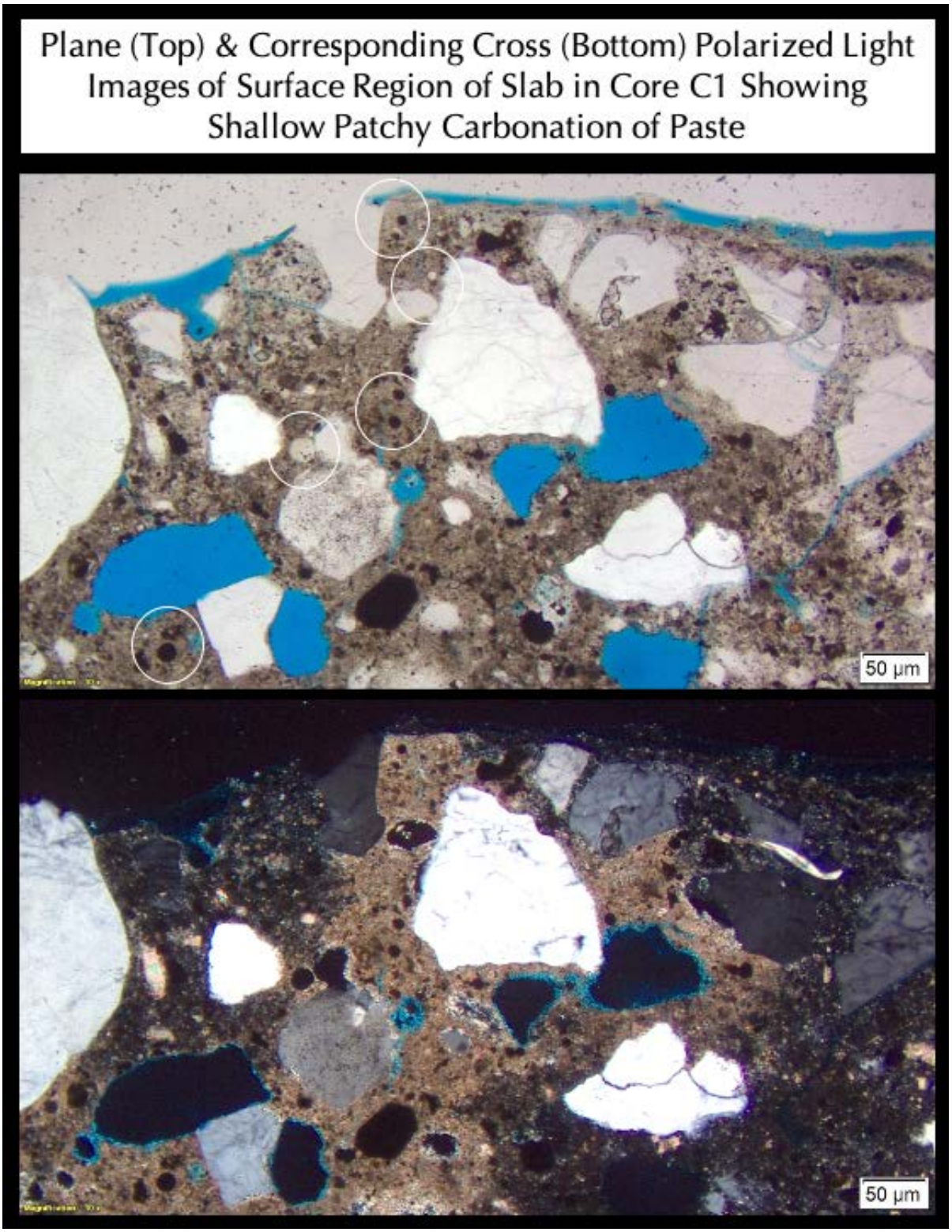

Figure 43: Micrographs of thin section of surface region of Core C1 showing the surface region of concrete consisting of (a) very dense paste of Portland cement and (b) fly ash where some spherical fly ash particles are circled, (c) quartz sand fine aggregate, and (d) patchy carbonation of paste at isolated locations of surface due to overall well-consolidated and densified surface by trowel-finishing. Scattered throughout the paste are some limestone fine particles mixed with cement hydration products that are judged to be dusts from crushed limestone coarse aggregate. Depth of carbonation is within the top 1 to 2 mm of surface.

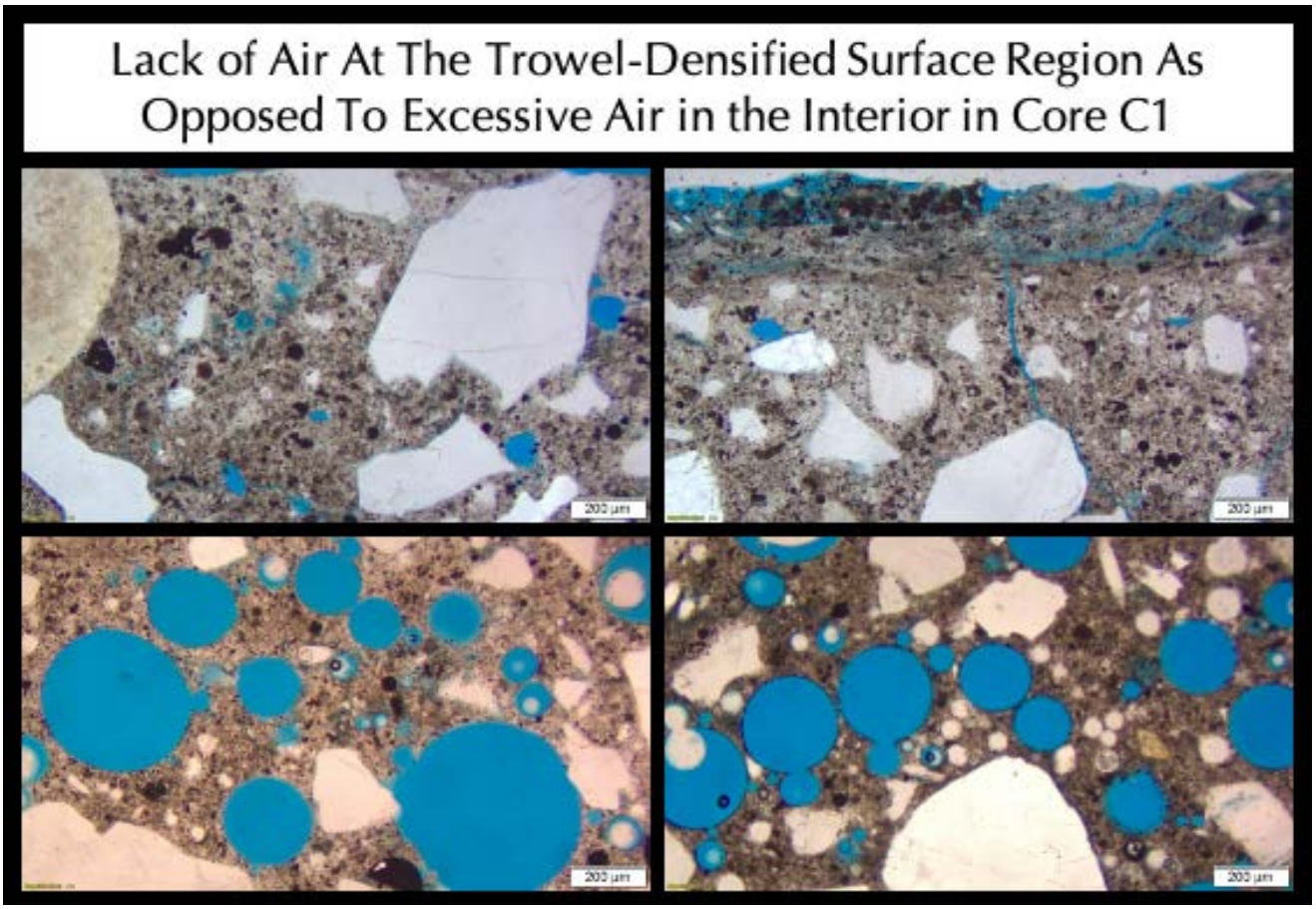

Figure 44: Micrographs of thin section of surface region of Core C1 showing the contrasting air content and air-void systems between the trowel-densified surface region that lacks air voids due to troweling operations, whereas excessively air-entrained interior where spherical entrained air voids are highlighted by blue epoxy. Many fine spherical fly ash particles are seen in paste, especially in the densified paste beneath the surface, which along with medium to dark gray crushed limestone coarse aggregate particles have imparted the overall dark gray color tone of concrete.

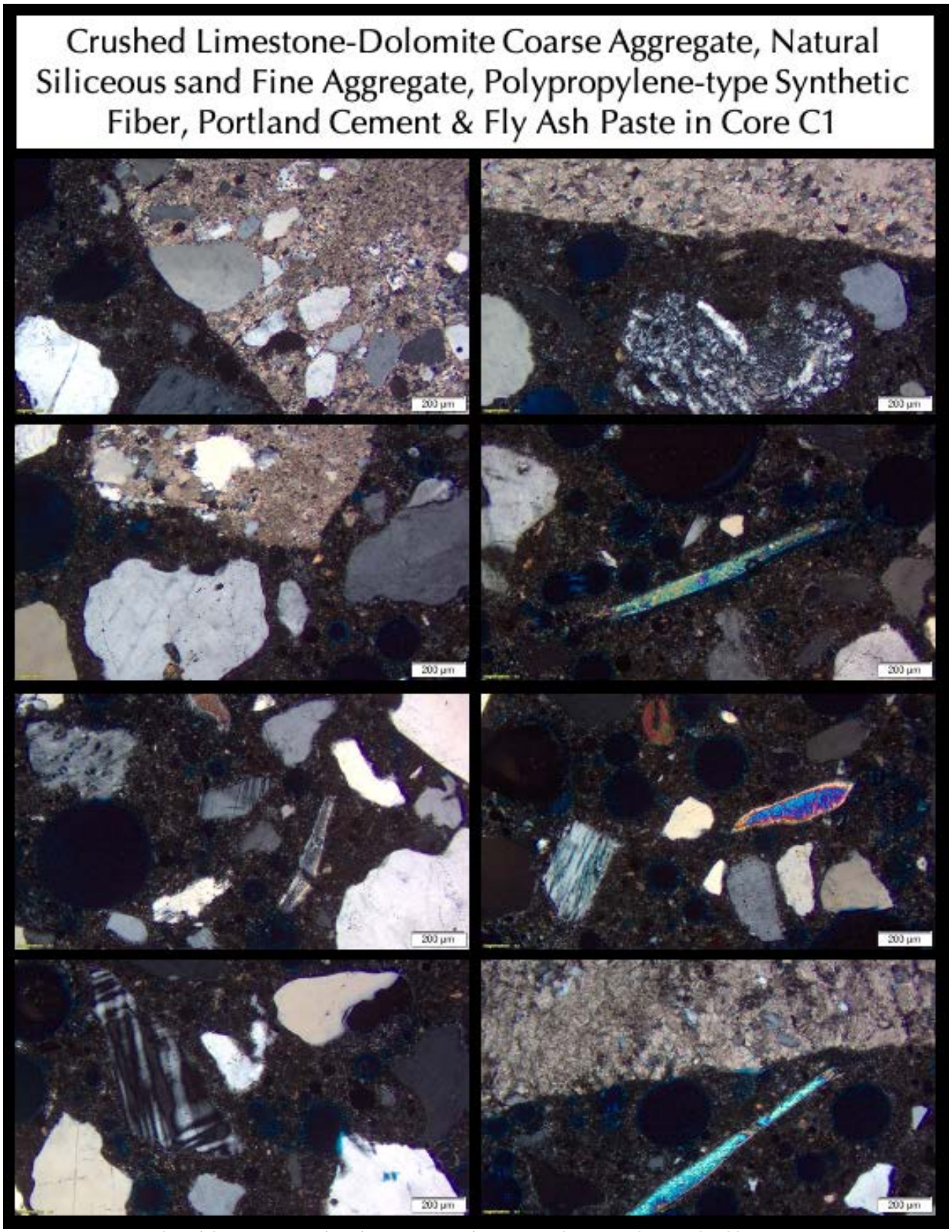

Figure 45: Micrographs of thin section of surface region of Core C1 showing the crushed limestone coarse aggregate, natural siliceous sand (quartz, quartzite, feldspar, chert, etc.) fine aggregate, and polypropylene-type synthetic fibers.

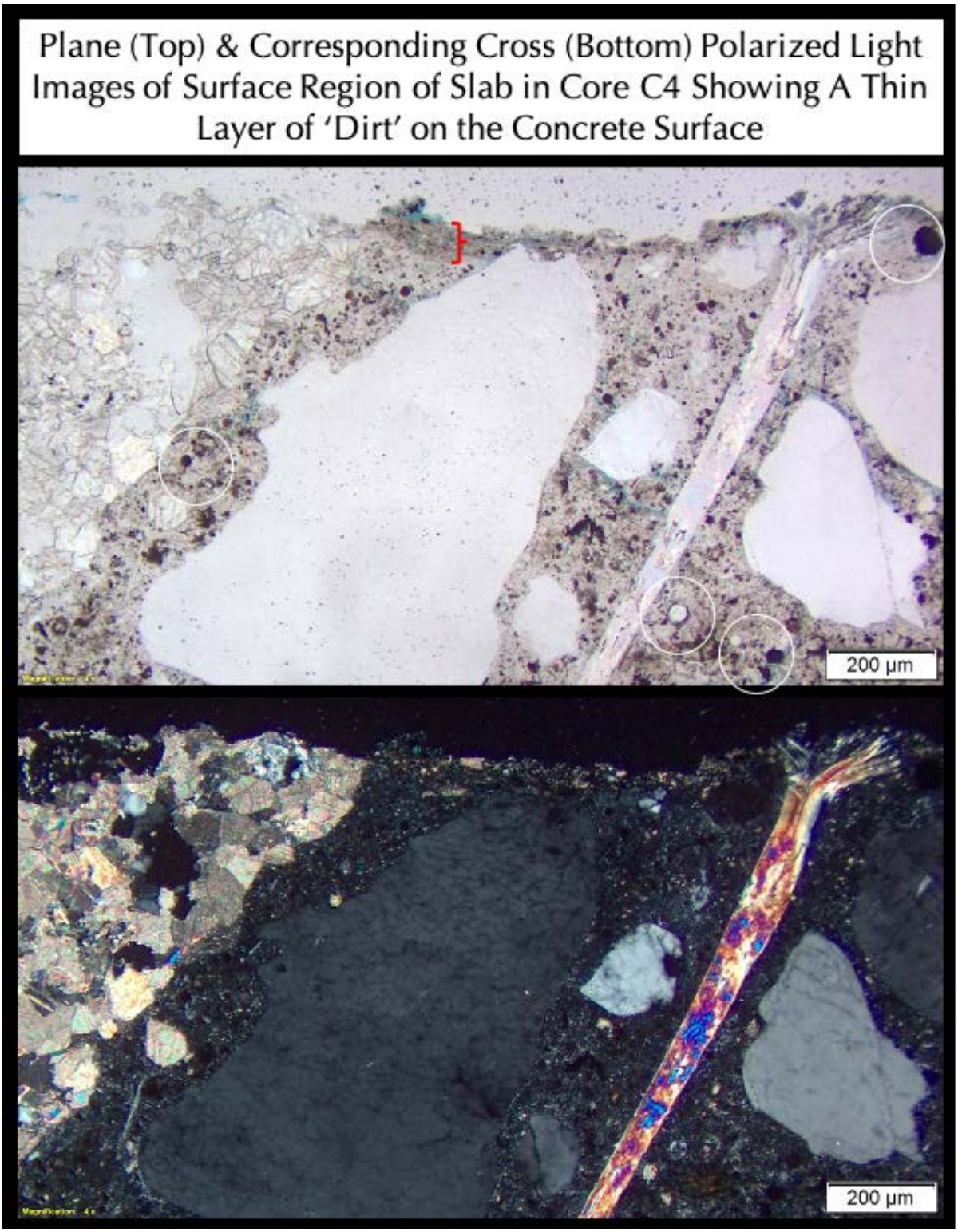

Figure 46: Micrographs of thin section of surface region of Core C4 showing the already delaminated concrete surface where the original trowel-densified surface is lost thus exposing the near-surface crushed limestone coarse aggregate and interstitial mortar fraction of concrete. Notice a long synthetic fiber, a few quartz sand fine aggregate, and a crushed marble coarse aggregate at left. Notice lack of any carbonation, leaching or alteration of surface region of paste which is very dense and made using major amount of Portland cement and subordinate amount of fly ash; a few residual fly ash particles are circled.

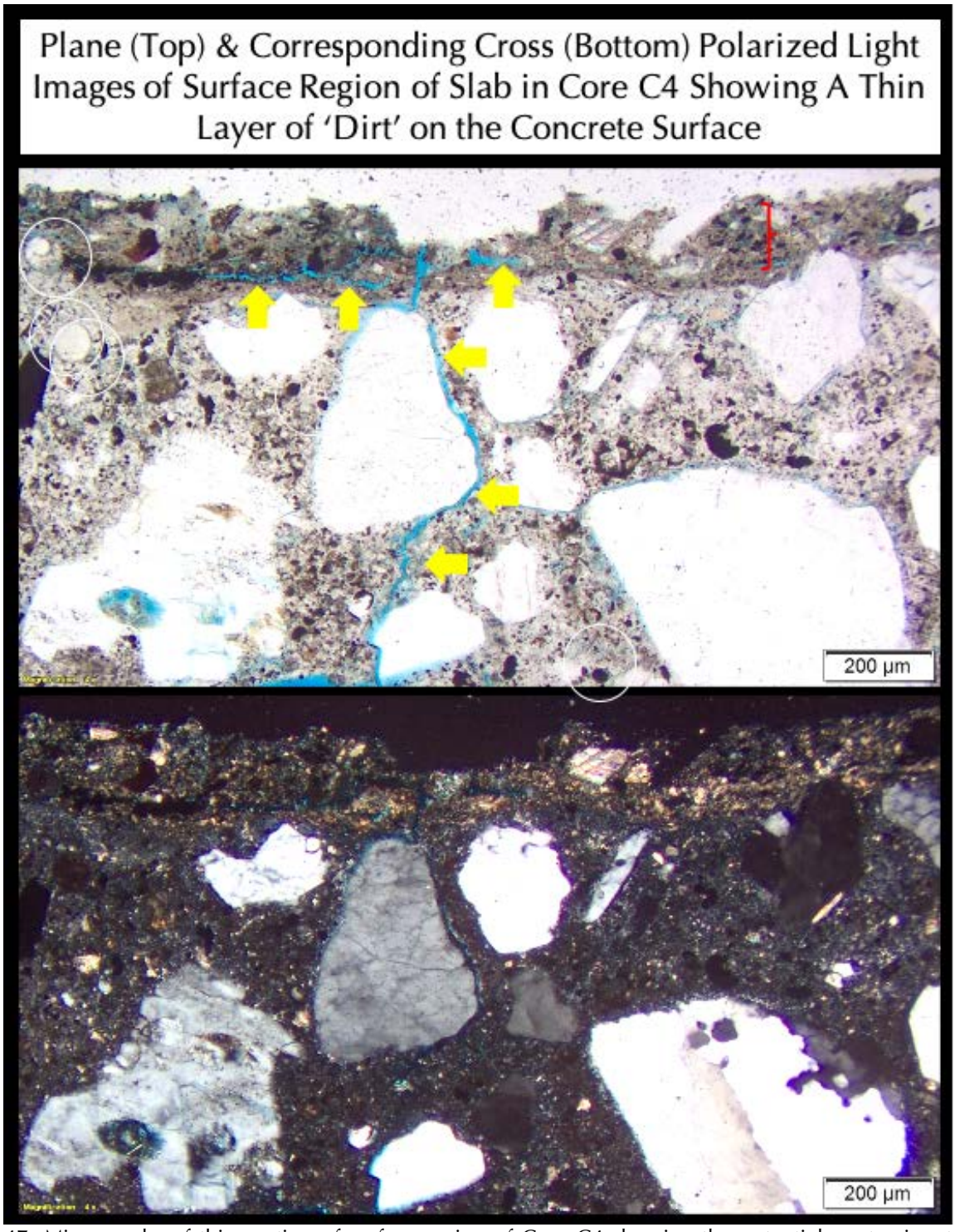

Figure 47: Micrographs of thin section of surface region of Core C4 showing the potential contaminant on the surface of concrete consisting of (a) very fine-grained deposits of organic matter, (b) ferruginous materials, (c) ultrafine crushed quartz, (d) limestone dusts, (e) spherical fly ash, (f) porous, ultrafine-grained carbonated lime, (g) shrinkage microcracks and overall porous nature of surface deposit that are highlighted by blue epoxy, (h) synthetic fibers, and (i) angular shard-like glassy particles of slag. None of these constituents in the surface deposit are potentially harmful to concrete, hence the concrete surface region immediately beneath the deposit shows no surface alteration (leaching, erosion, carbonation, etc.). Notice the sharp boundary between porous surface deposit and underlying dense concrete surface.

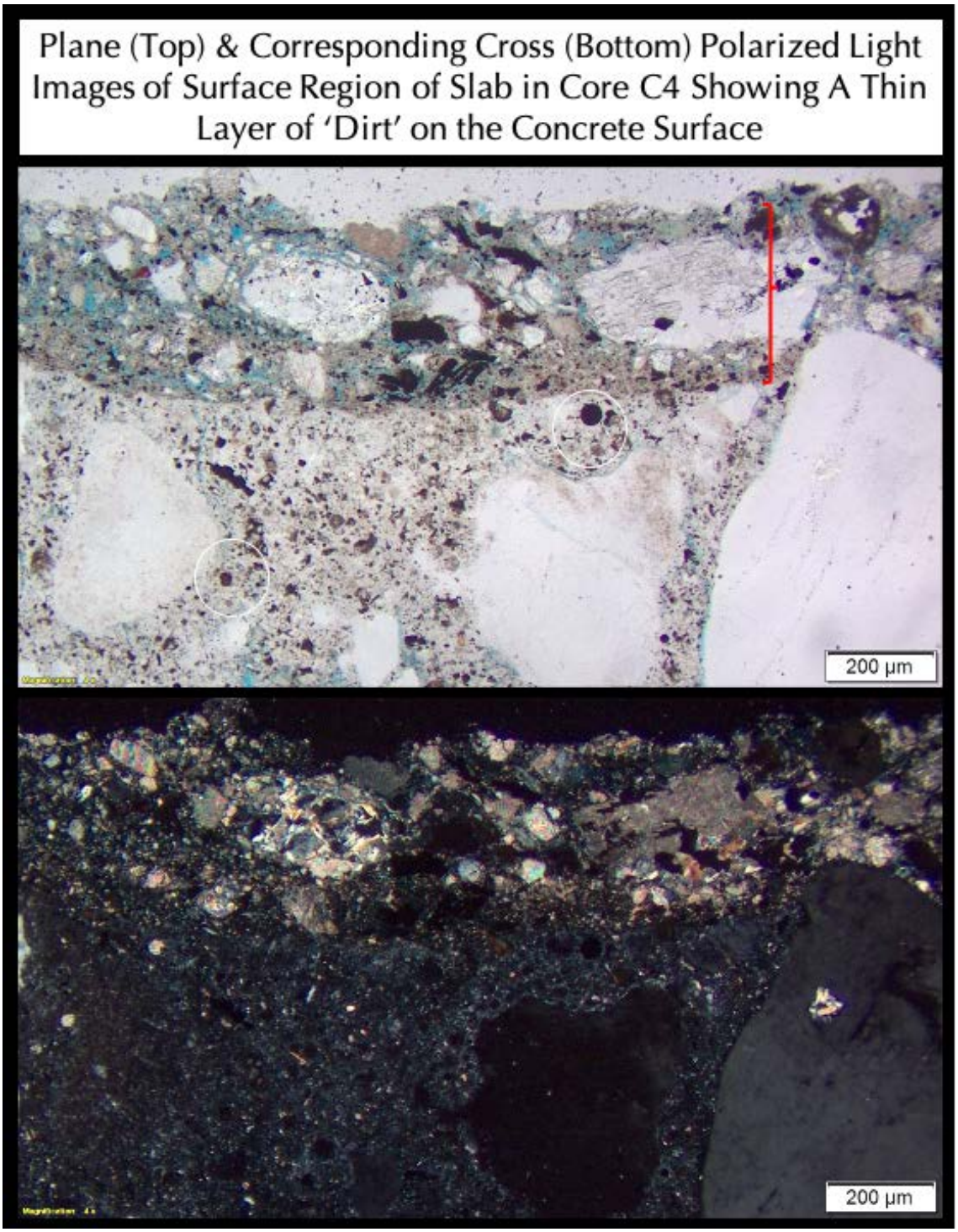

Figure 48: Micrographs of thin section of surface region of Core C4 showing the potential contaminant on the surface of concrete consisting of (a) very fine-grained deposits of organic matter, (b) ferruginous materials, (c) ultrafine crushed quartz, (d) limestone dusts, (e) spherical fly ash, (f) porous, ultrafine-grained carbonated lime, (g) shrinkage microcracks and overall porous nature of surface deposit that are highlighted by blue epoxy, (h) synthetic fibers, and (i) angular shard-like glassy particles of slag. None of these constituents in the surface deposit are potentially harmful to concrete, hence the concrete surface region immediately beneath the deposit shows no surface alteration (leaching, erosion, carbonation, etc.). Notice the sharp boundary between porous surface deposit and underlying dense concrete surface.

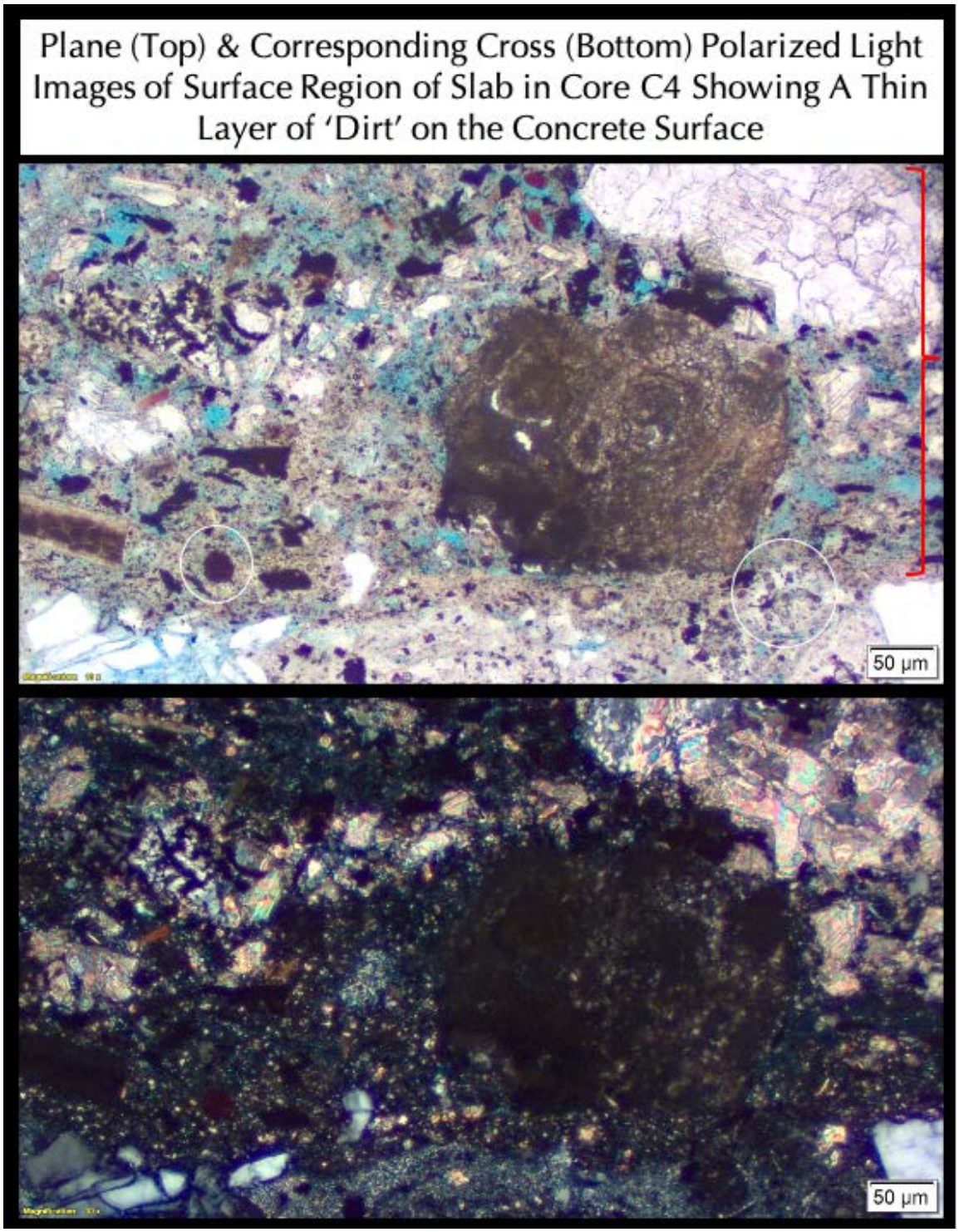

Figure 49: Micrographs of thin section of surface region of Core C4 showing the potential contaminant on the surface of concrete consisting of (a) very fine-grained deposits of organic matter, (b) ferruginous materials, (c) ultrafine crushed quartz, (d) limestone dusts, (e) spherical fly ash, (f) porous, ultrafine-grained carbonated lime, (g) shrinkage microcracks and overall porous nature of surface deposit that are highlighted by blue epoxy, (h) synthetic fibers, and (i) angular shard-like glassy particles of slag. None of these constituents in the surface deposit are potentially harmful to concrete, hence the concrete surface region immediately beneath the deposit shows no surface alteration (leaching, erosion, carbonation, etc.).

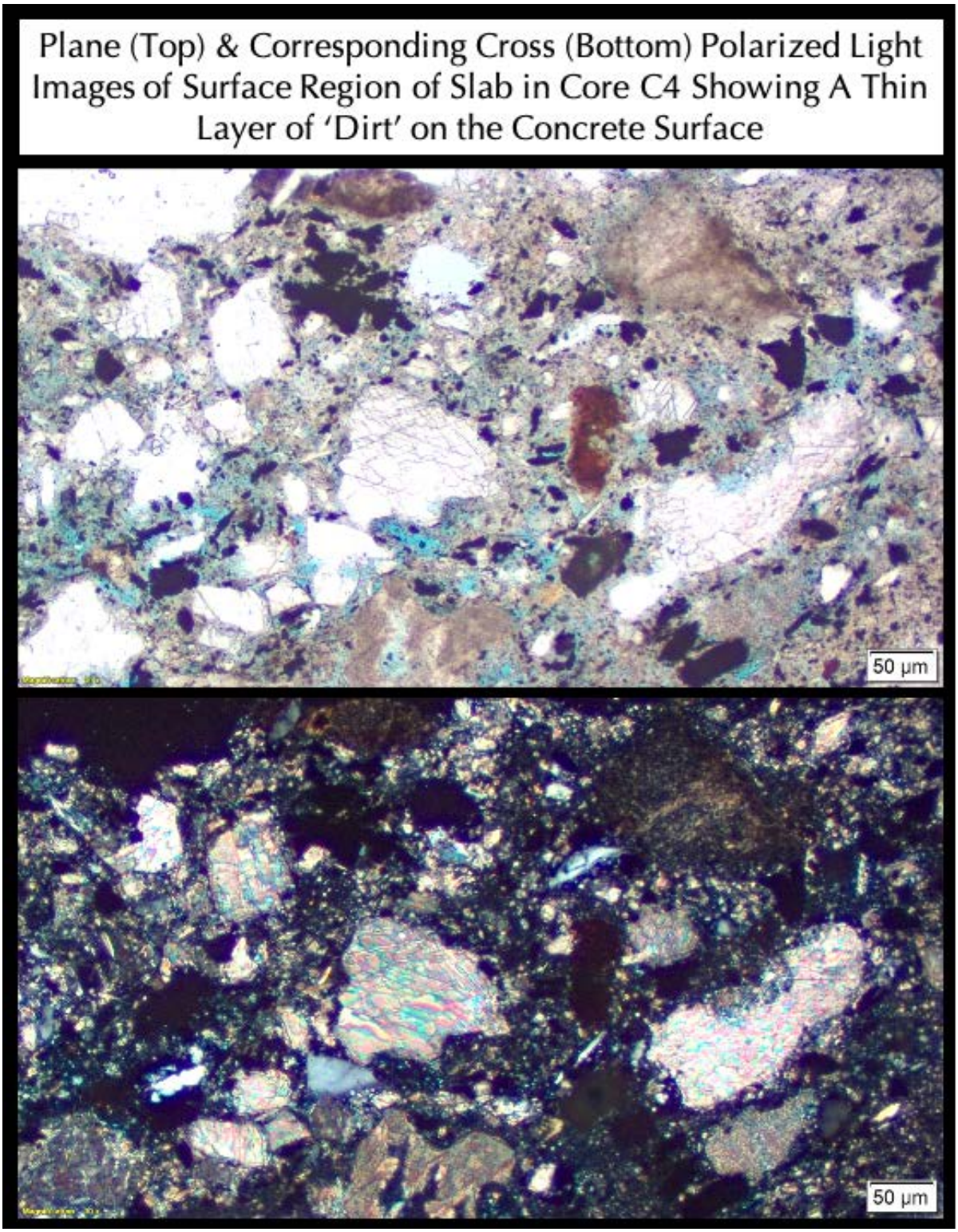

Figure 50: Micrographs of thin section of surface region of Core C4 showing the potential contaminant on the surface of concrete consisting of (a) very fine-grained deposits of organic matter, (b) ferruginous materials, (c) ultrafine crushed quartz, (d) limestone dusts, (e) spherical fly ash, (f) porous, ultrafine-grained carbonated lime, (g) shrinkage microcracks and overall porous nature of surface deposit that are highlighted by blue epoxy, (h) synthetic fibers, and (i) angular shard-like glassy particles of slag. None of these constituents in the surface deposit are potentially harmful to concrete. Notice abundant crushed marble in the surface deposit.

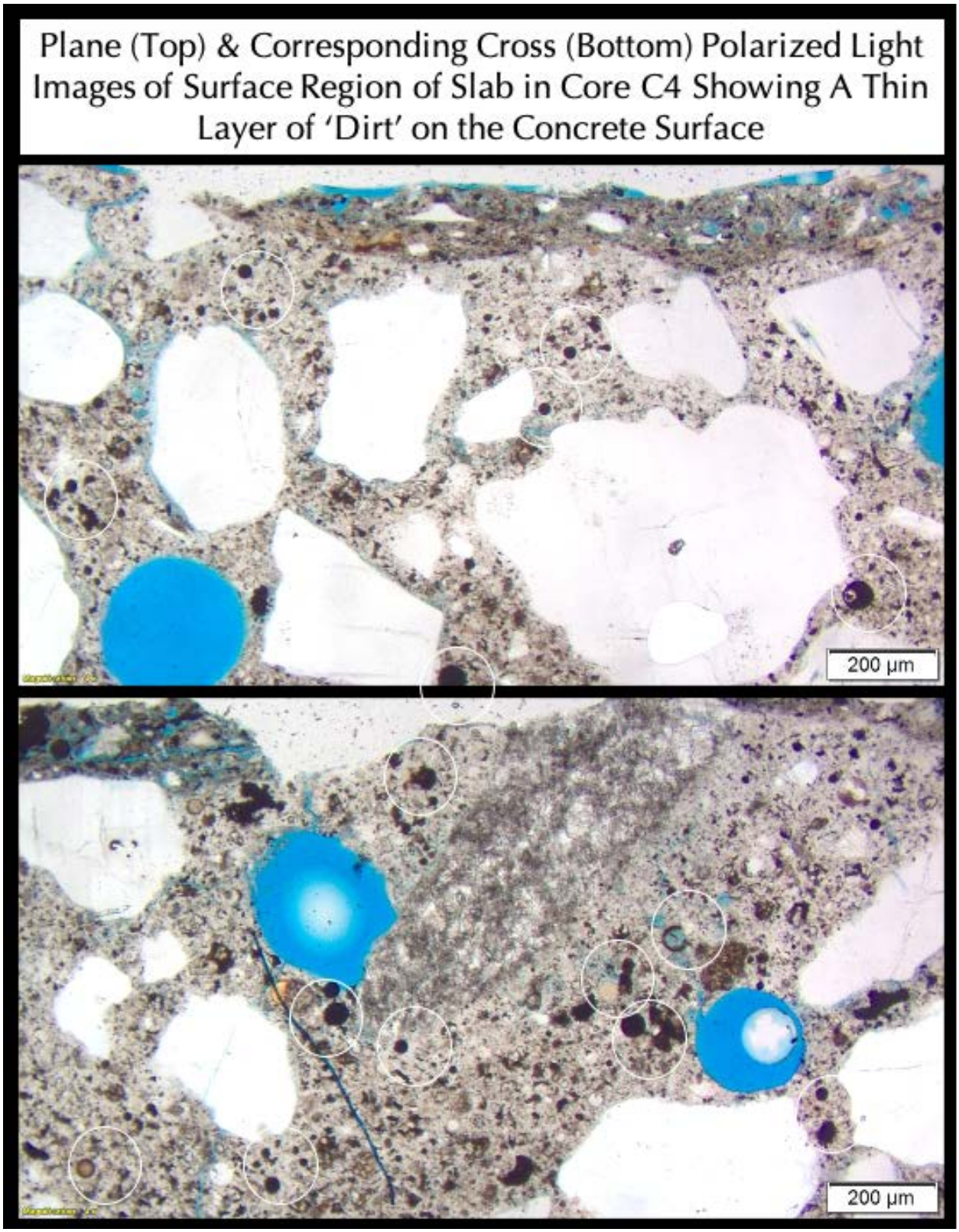

Figure 51: Micrographs of thin section of surface region of Core C4 showing the surface region of concrete consisting of (a) very dense paste of Portland cement and (b) fly ash where some spherical fly ash particles are circled, (c) quartz sand fine aggregate, and (d) overall well-consolidated and densified surface by trowel-finishing.

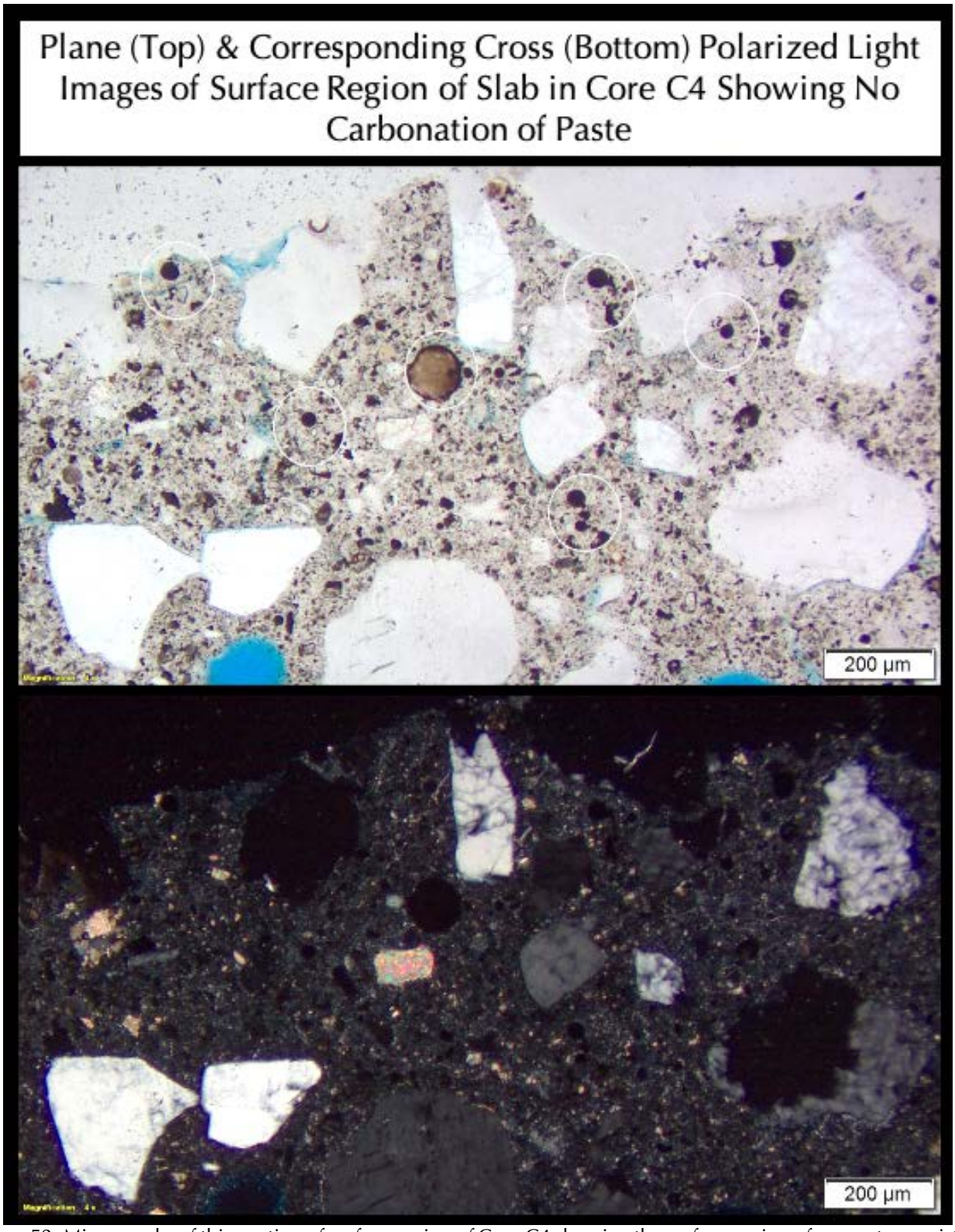

Figure 52: Micrographs of thin section of surface region of Core C4 showing the surface region of concrete consisting of (a) very dense paste of Portland cement and (b) fly ash where some spherical fly ash particles are circled, (c) quartz sand fine aggregate, and (d) lack of carbonation of paste due to overall well-consolidated and densified surface by trowel-finishing. Scattered throughout the paste are some limestone fine particles mixed with cement hydration products that are judged to be dusts from crushed limestone coarse aggregate.

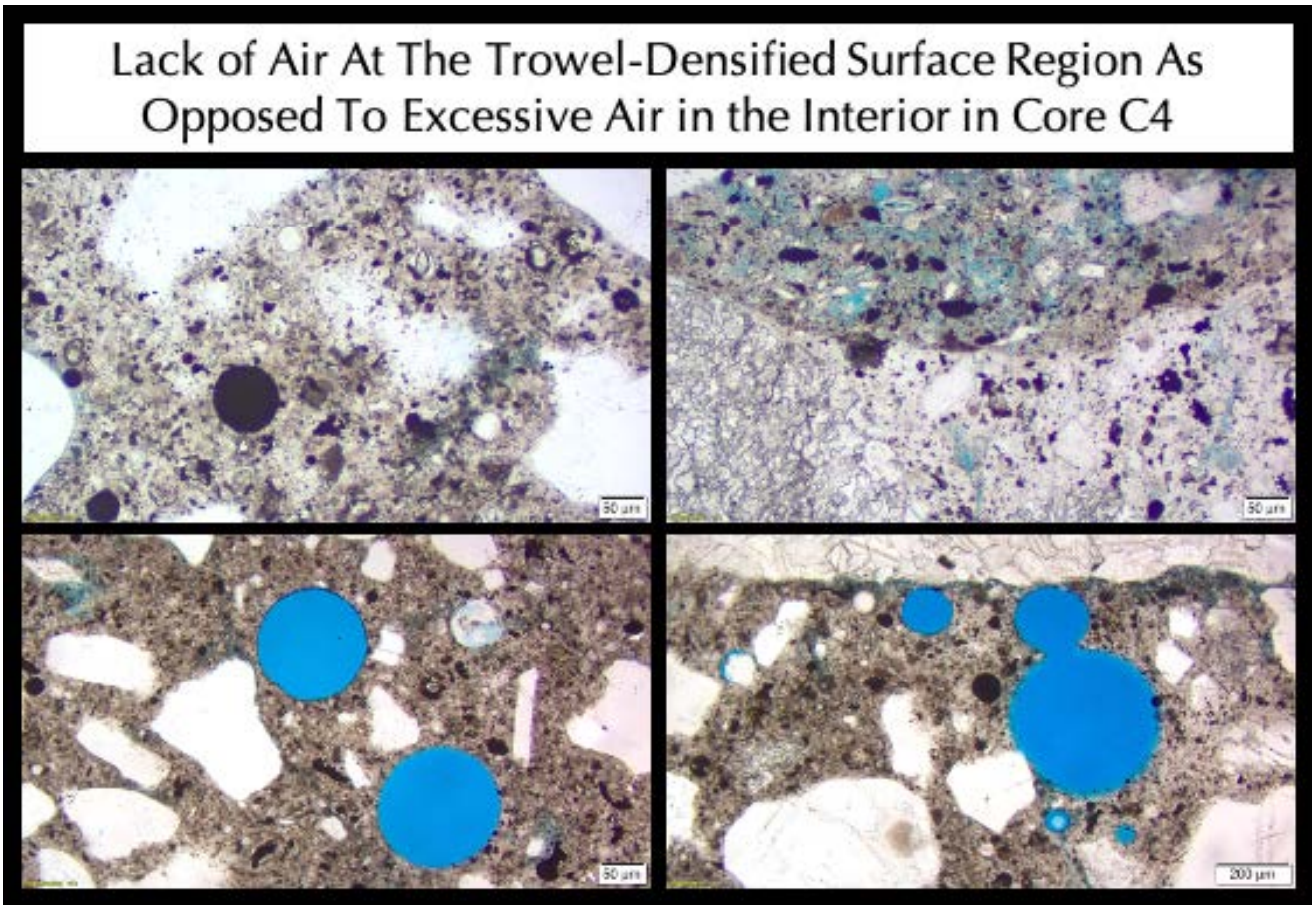

Figure 53: Micrographs of thin section of surface region of Core C4 showing the contrasting air content and air-void systems between the trowel-densified surface region that lacks air voids due to troweling operations, whereas marginally air-entrained interior where a few coarse spherical entrained air voids are highlighted by blue epoxy. Many fine spherical fly ash particles are seen in paste especially in the densified paste beneath the surface, which along with medium to dark gray crushed limestone coarse aggregate particles have imparted the overall dark gray color tone of concrete.

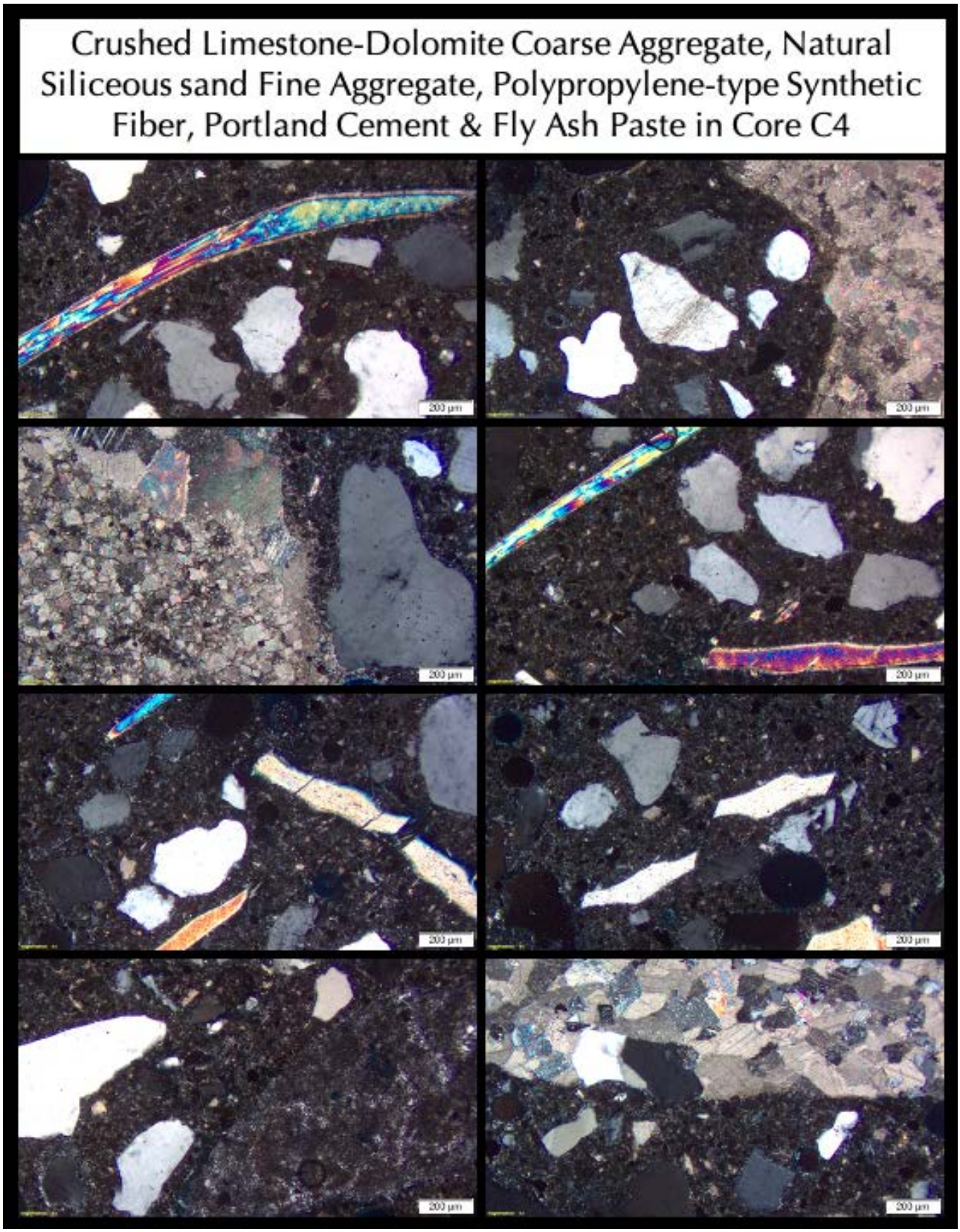

Figure 54: Micrographs of thin section of surface region of Core C4 showing the crushed limestone coarse aggregate, natural siliceous sand (quartz, quartzite, feldspar, chert, etc.) fine aggregate, and polypropylene-type synthetic fibers.

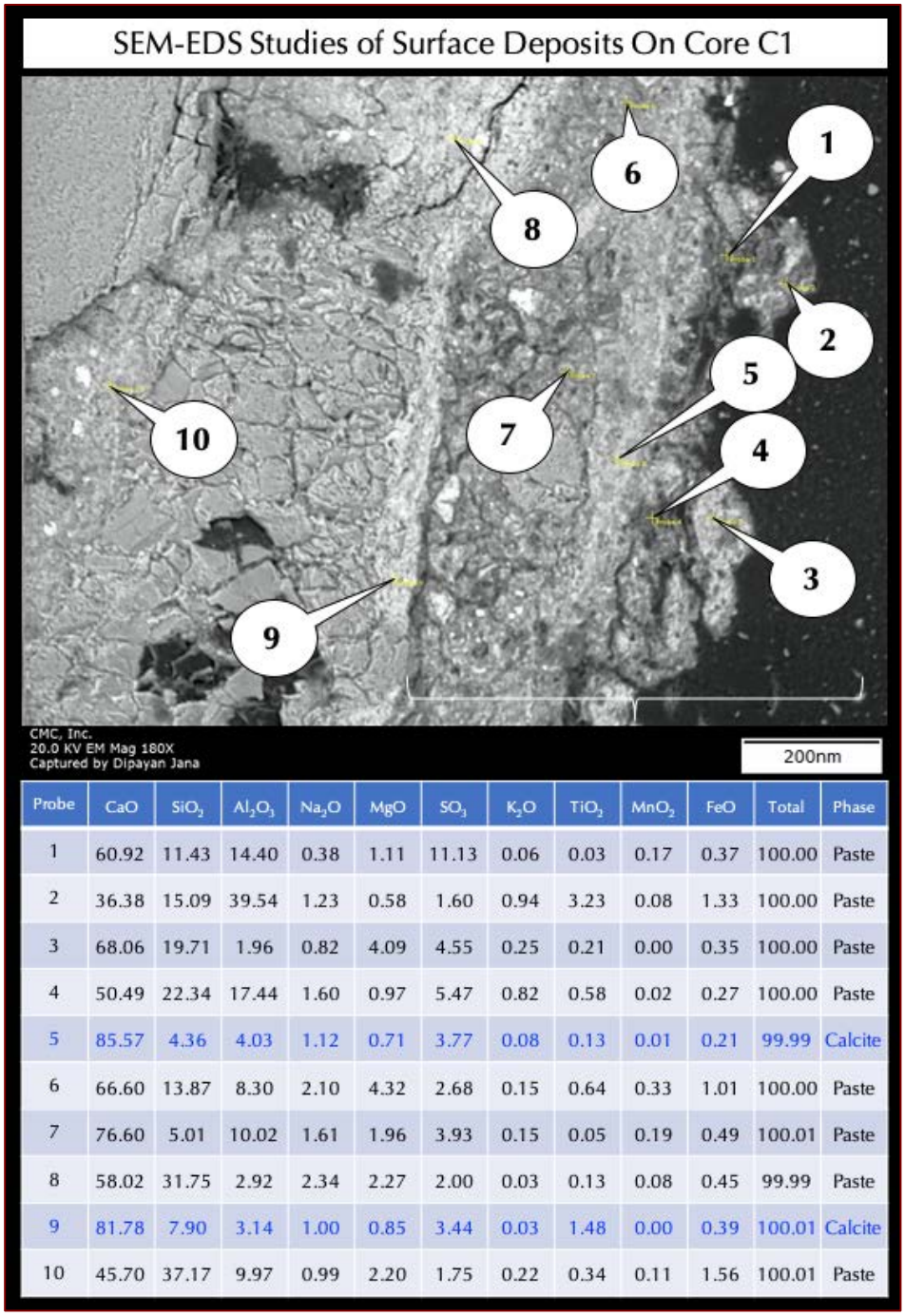

Probe	CaO	SiO_2	Al_2O_3	Na_2O	MgO	SO_3	K_2O	TiO_2	MnO_2	FeO	Total	Phase
1	60.92	11.43	14.40	0.38	1.11	11.13	0.06	0.03	0.17	0.37	100.00	Paste
2	36.38	15.09	39.54	1.23	0.58	1.60	0.94	3.23	0.08	1.33	100.00	Paste
3	68.06	19.71	1.96	0.82	4.09	4.55	0.25	0.21	0.00	0.35	100.00	Paste
4	50.49	22.34	17.44	1.60	0.97	5.47	0.82	0.58	0.02	0.27	100.00	Paste
5	85.57	4.36	4.03	1.12	0.71	3.77	0.08	0.13	0.01	0.21	99.99	Calcite
6	66.60	13.87	8.30	2.10	4.32	2.68	0.15	0.64	0.33	1.01	100.00	Paste
7	76.60	5.01	10.02	1.61	1.96	3.93	0.15	0.05	0.19	0.49	100.01	Paste
8	58.02	31.75	2.92	2.34	2.27	2.00	0.03	0.13	0.08	0.45	99.99	Paste
9	81.78	7.90	3.14	1.00	0.85	3.44	0.03	1.48	0.00	0.39	100.01	Calcite
10	45.70	37.17	9.97	0.99	2.20	1.75	0.22	0.34	0.11	1.56	100.01	Paste

Figure 55: Secondary electron image (top), and X-ray microanalyses at the tips of callouts in Probes 1 through 10 detecting compositional variations of surface deposit on the top of Core C1.

Compositions of surface deposit as well as of the near-surface paste region of concrete are presented (bottom) as oxide variations of all detected peaks normalized to 100% except carbon (from epoxy) and gold (from coating).

Interstitial phases in surface deposit are marked as 'paste' in the compositional analyses, which show typical lime, alumina, silica, magnesia and variable sulfate concentrations in the deposit, which are not noticeably different from the composition of paste in the near-surface region of concrete (e.g., in Probe #9) indicating no noticeable difference in the surface deposit to impart any chemical deterioration of near-surface paste in concrete.

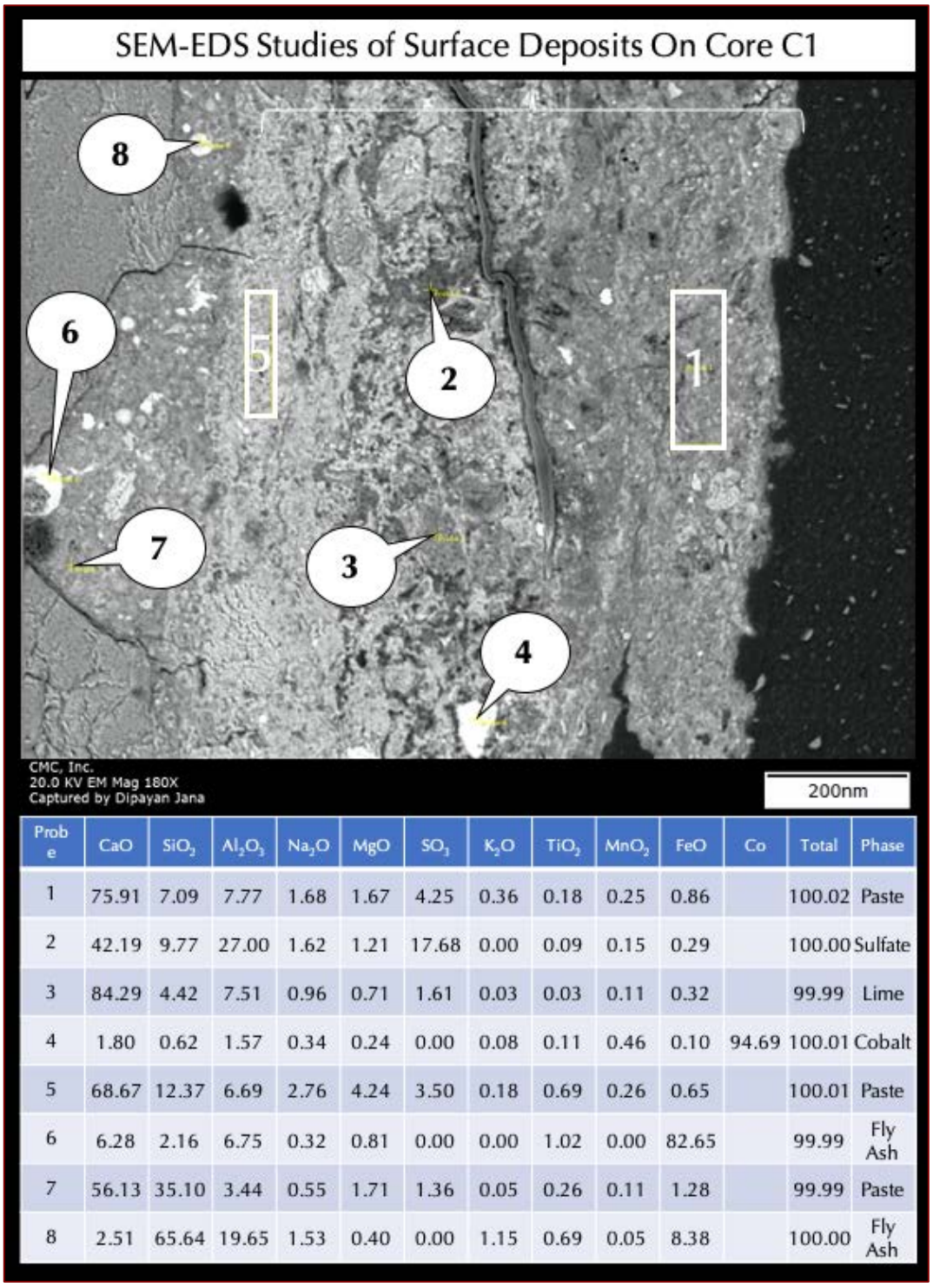

Probe	CaO	SiO_2	Al_2O_3	Na_2O	MgO	SO_3	K_2O	TiO_2	MnO_2	FeO	Co	Total	Phase
1	75.91	7.09	7.77	1.68	1.67	4.25	0.36	0.18	0.25	0.86		100.02	Paste
2	42.19	9.77	27.00	1.62	1.21	17.68	0.00	0.09	0.15	0.29		100.00	Sulfate
3	84.29	4.42	7.51	0.96	0.71	1.61	0.03	0.03	0.11	0.32		99.99	Lime
4	1.80	0.62	1.57	0.34	0.24	0.00	0.08	0.11	0.46	0.10	94.69	100.01	Cobalt
5	68.67	12.37	6.69	2.76	4.24	3.50	0.18	0.69	0.26	0.65		100.01	Paste
6	6.28	2.16	6.75	0.32	0.81	0.00	0.00	1.02	0.00	82.65		99.99	Fly Ash
7	56.13	35.10	3.44	0.55	1.71	1.36	0.05	0.26	0.11	1.28		99.99	Paste
8	2.51	65.64	19.65	1.53	0.40	0.00	1.15	0.69	0.05	8.38		100.00	Fly Ash

Figure 56: Secondary electron image (top), and X-ray microanalyses at the tips of callouts and in boxed areas in Probes 1 through 8 detecting compositional variations of surface deposit on the top of Core C1.

Compositions of surface deposit as well as of the near-surface paste region of concrete are presented (bottom) as oxide variations of all detected peaks normalized to 100% except carbon (from epoxy) and gold (from coating).

Interstitial phases in surface deposit are marked as 'paste' in the compositional analyses, which show typical lime, alumina, silica, magnesia and variable sulfate concentrations in the deposit, which are not noticeably different from the composition of paste in the near-surface region of concrete (e.g., in Probe #6 to 8) indicating no noticeable difference in the surface deposit to impart any chemical deterioration of near-surface paste in concrete.

THIN SECTION OF INCINERATOR ASH

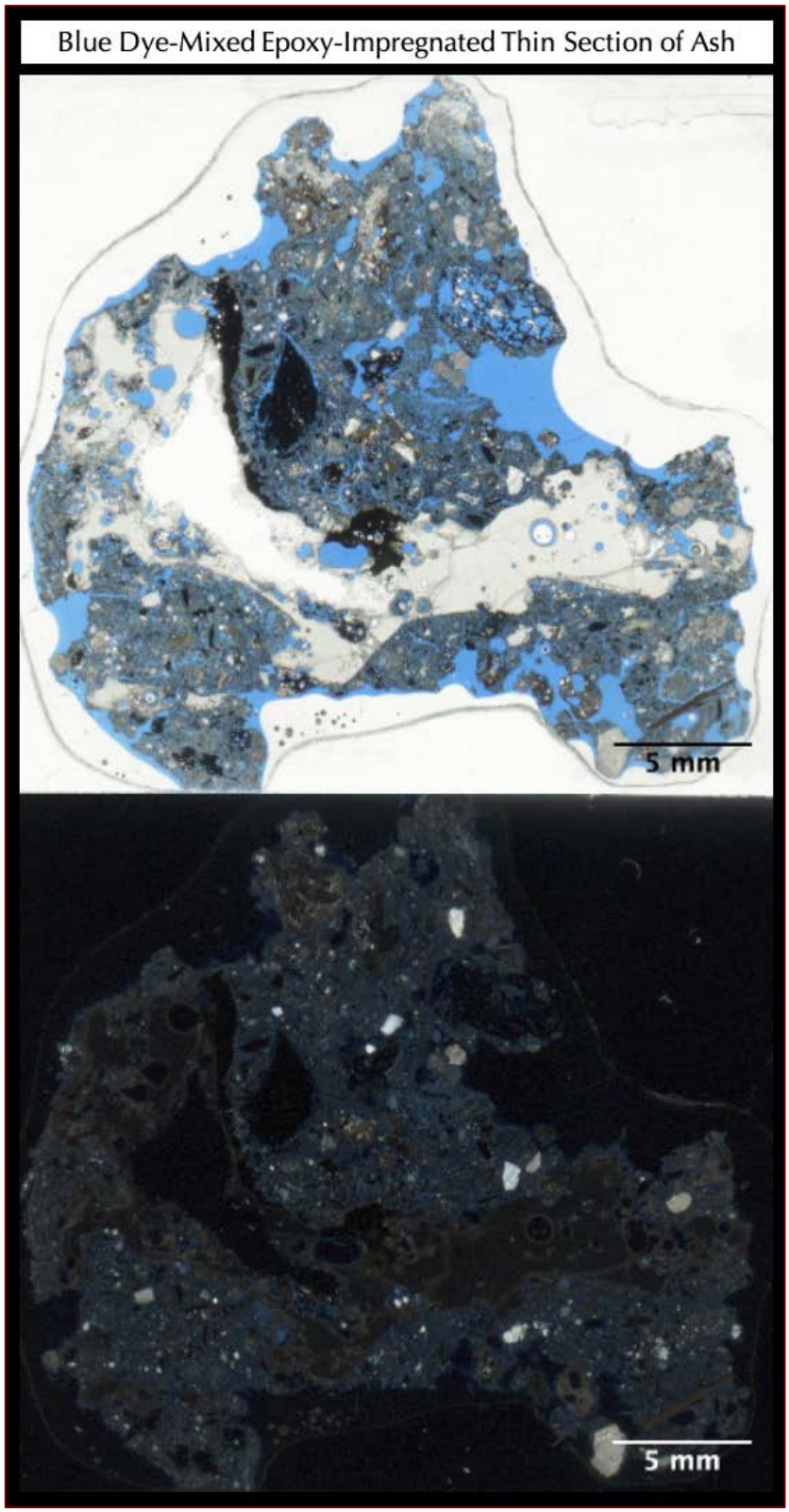

Figure 57: Blue dye-mixed epoxy-encapsulated thin section of an oven-dried mass of the incinerator ash sample showing a large chunk of glass fragment in the ash and many fine-grained crushed quartz, glass, dark opaque metal or oxide variants of metal , organic matter, and ultrafine dusts that are examined in detail in the next series of photomicrographs.

Top and bottom photos were taken by using one or two perpendicular polarizing filters, respectively, placed on the thin section of ash during scanning on a flatbed film scanner. Top photo shows plane polarized image to highlight the porous nature of ash and its fragments, whereas bottom photo shows cross polarized light view where the fine angular quartz particles and overall glassy nature of majority of the constituents of ash are seen.

MICROGRAPHS OF THIN SECTION OF INCINERATOR ASH

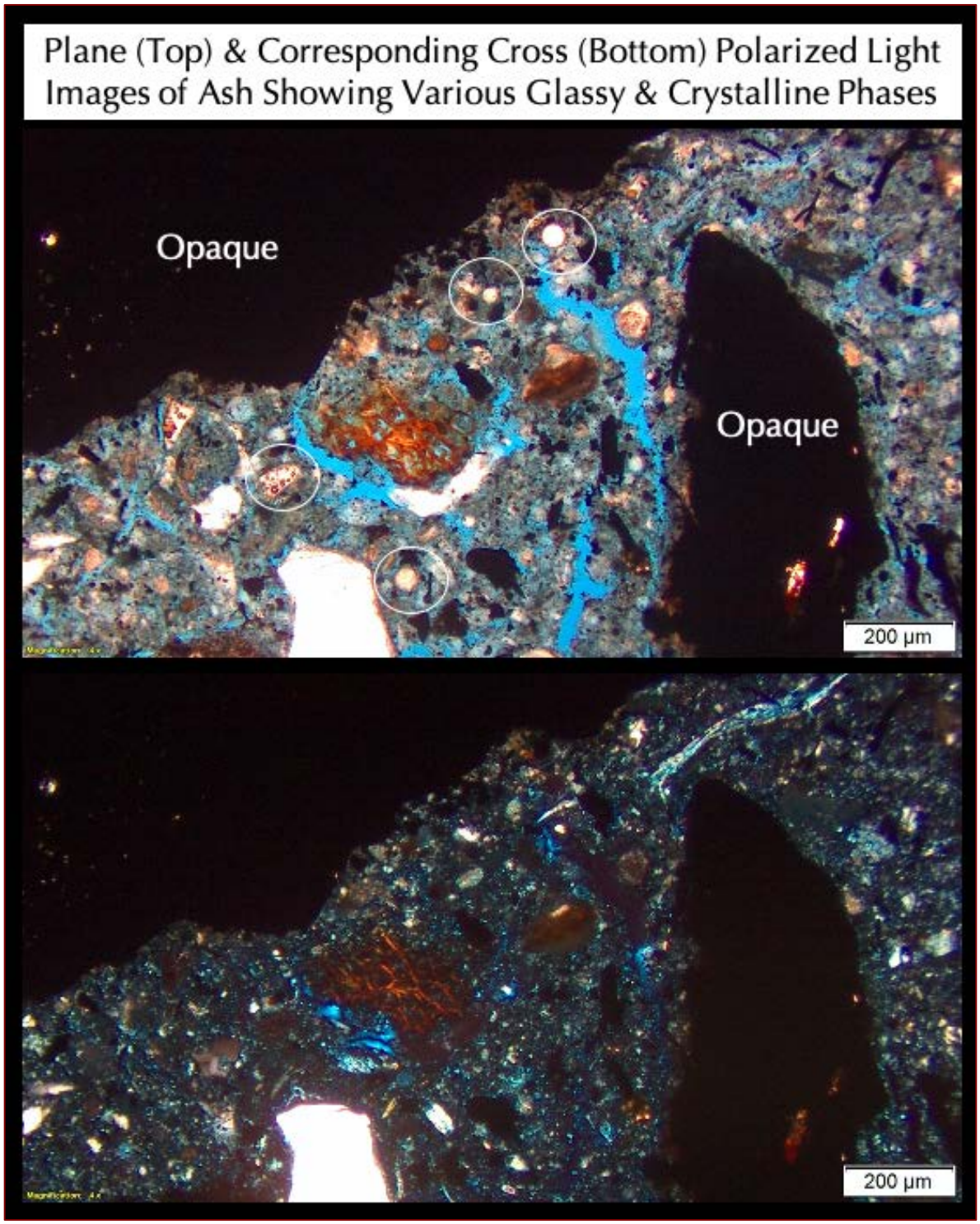

Figure 58: Micrographs of thin section of ash showing: (a) dark opaque metal and metal oxide particles, (b) spherical fly ash particles, some of which are circled, (c) medium to dark brown and clear shard-like glassy fragments of slag, (d) fine angular quartz particles, (e) ultrafine-grained carbonated lime, (f) occasional synthetic fibers, (g) dark organic matter, and (h) miscellaneous undetectable ultrafine particles that are too fine to be detected at the present magnification of the image.

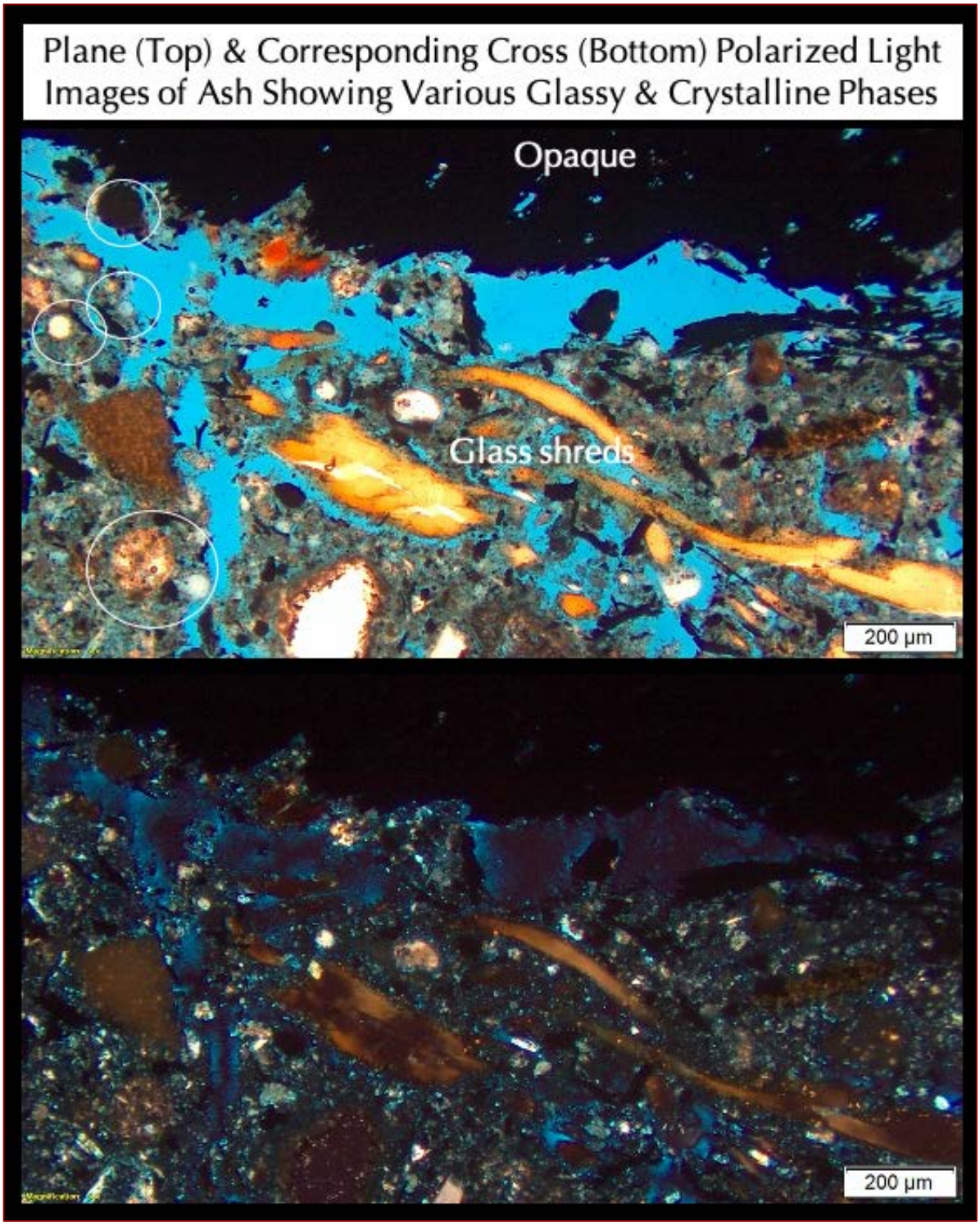

Figure 59: Micrographs of thin section of ash showing: (a) dark opaque metal and metal oxide particles, (b) spherical fly ash particles some of which are circled, (c) medium to dark brown and clear shard-like glassy fragments of slag, (d) fine angular quartz particles, (e) ultrafine-grained carbonated lime, (f) occasional synthetic fibers, (g) dark organic matter, and (h) miscellaneous undetectable ultrafine particles that are too fine to be detected at the present magnification of the image.

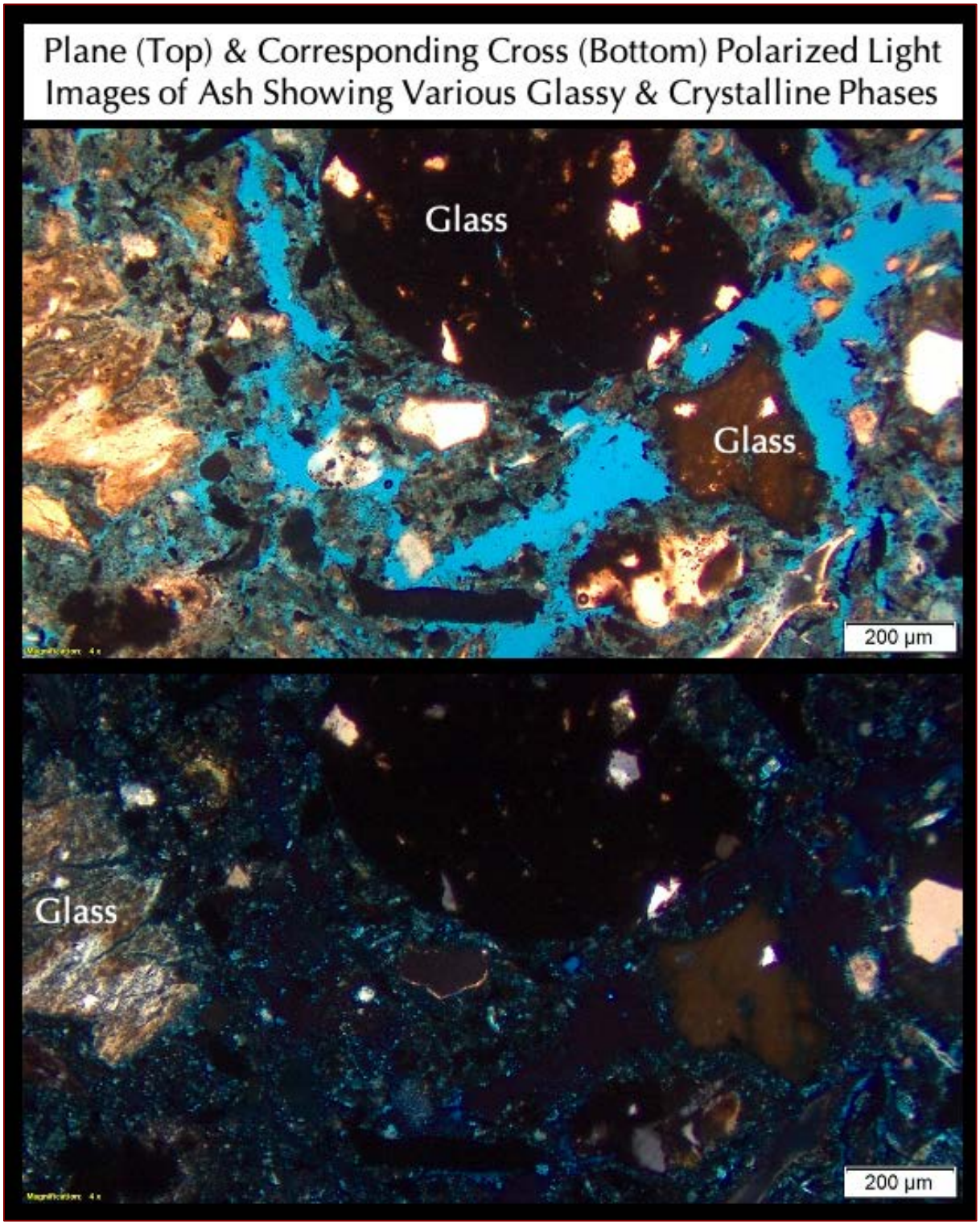

Figure 60: Micrographs of thin section of ash showing: (a) dark opaque metal and metal oxide particles, (b) spherical fly ash particles, (c) medium to dark brown and clear shard-like glassy fragments of slag, (d) fine angular quartz particles, (e) ultrafine-grained carbonated lime, (f) occasional synthetic fibers, (g) dark organic matter, and (h) miscellaneous undetectable ultrafine particles that are too fine to be detected at the present magnification of the image.

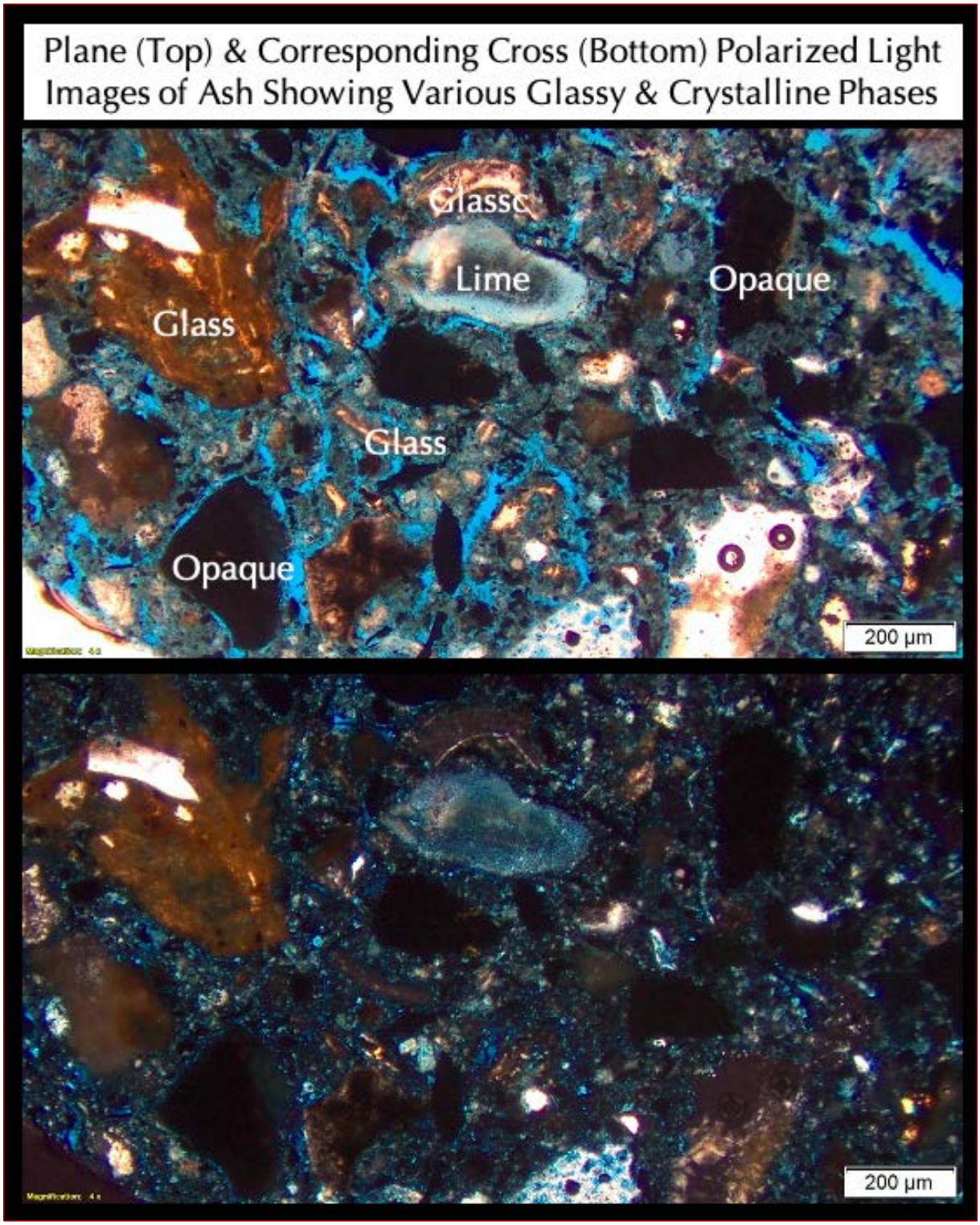

Figure 61: Micrographs of thin section of ash showing: (a) dark opaque metal and metal oxide particles, (b) spherical fly ash particles, (c) medium to dark brown and clear shard-like glassy fragments of slag, (d) fine angular quartz particles, (e) ultrafine-grained carbonated lime, (f) occasional synthetic fibers, (g) dark organic matter, and (h) miscellaneous undetectable ultrafine particles that are too fine to be detected at the present magnification of the image.

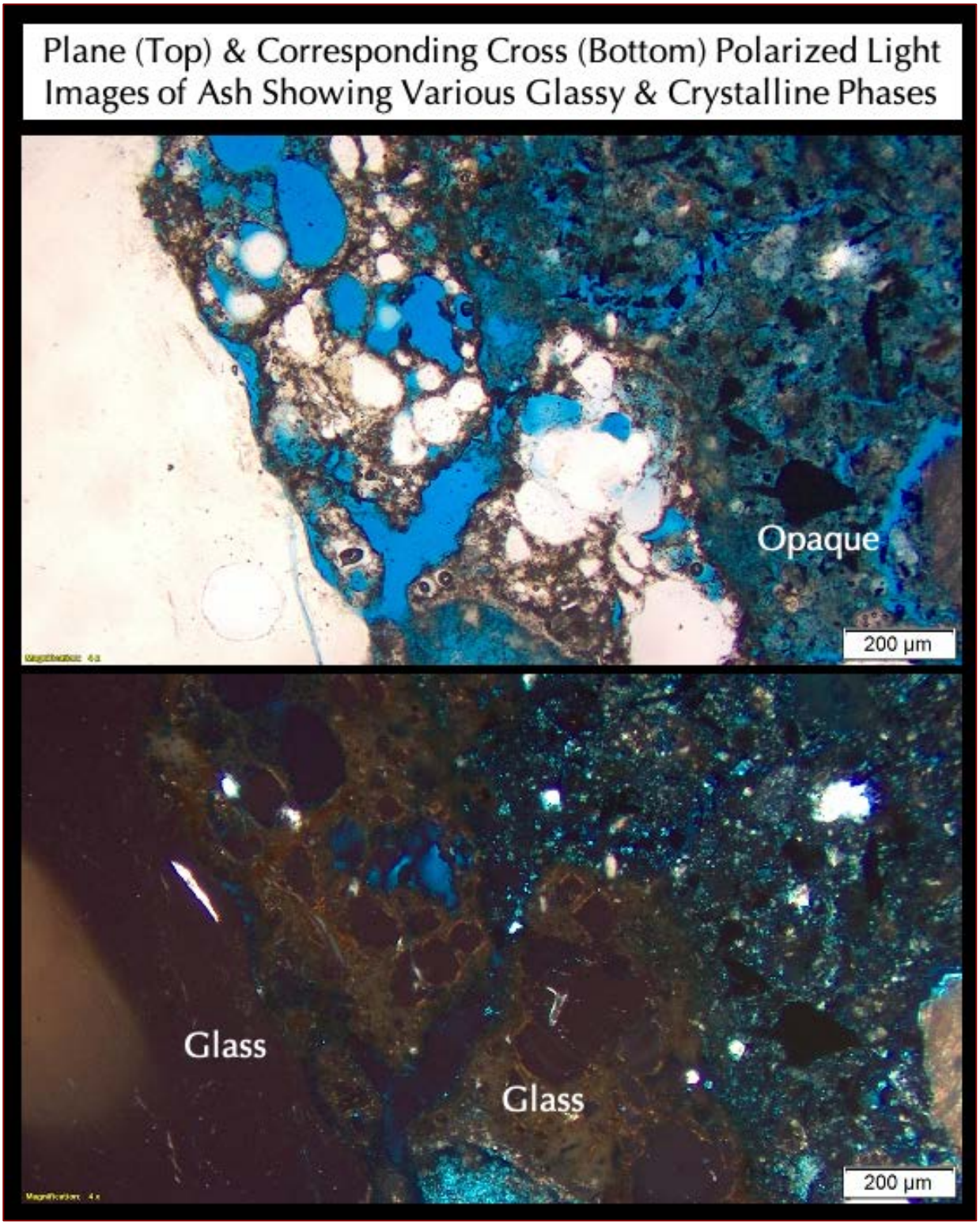

Figure 62: Micrographs of thin section of ash showing: (a) dark opaque metal and metal oxide particles, (b) spherical fly ash particles, (c) medium to dark brown and clear shard-like glassy fragments of slag, (d) fine angular quartz particles, (e) ultrafine-grained carbonated lime, (f) occasional synthetic fibers, (g) dark organic matter, and (h) miscellaneous undetectable ultrafine particles that are too fine to be detected at the present magnification of the image. Notice a large chunk of vesicular glass fragment.

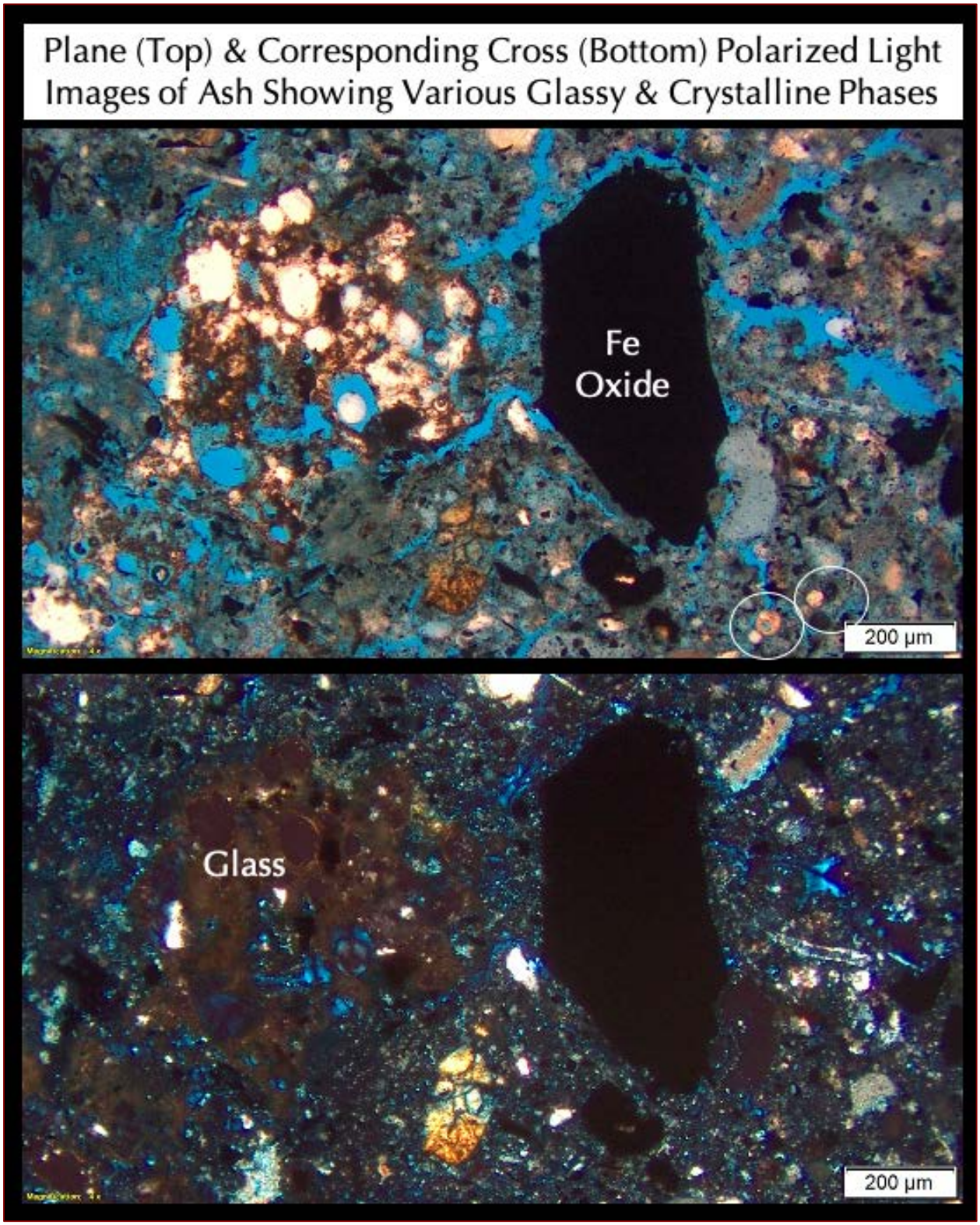

Figure 63: Micrographs of thin section of ash showing: (a) dark opaque metal and metal oxide particles, (b) spherical fly ash particles some of which are circled, (c) medium to dark brown and clear shard-like glassy fragments of slag, (d) fine angular quartz particles, (e) ultrafine-grained carbonated lime, (f) occasional synthetic fibers, (g) dark organic matter, and (h) miscellaneous undetectable ultrafine particles that are too fine to be detected at the present magnification of the image. Notice a vesicular glass fragment in the middle.

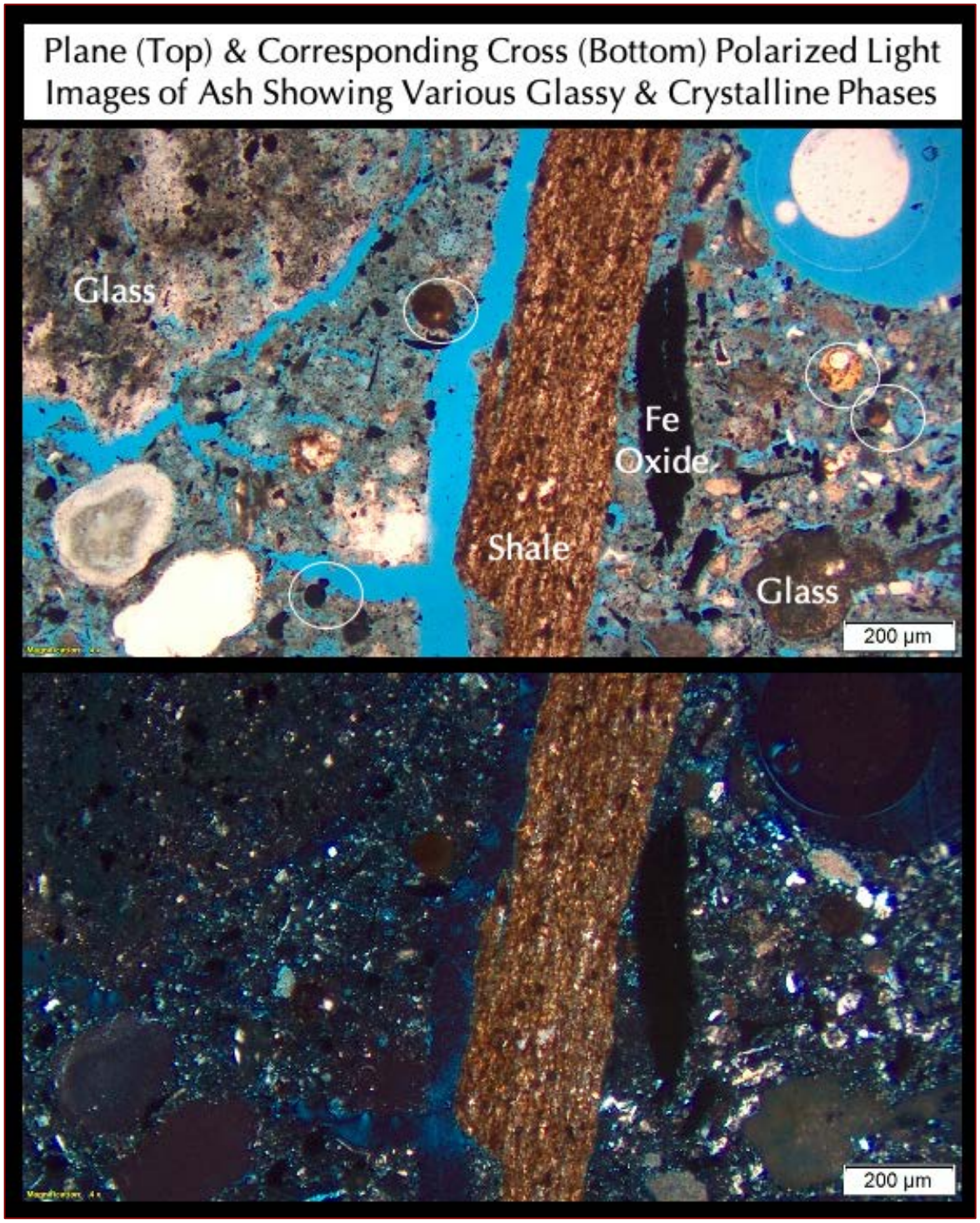

Figure 64: Micrographs of thin section of ash showing: (a) dark opaque metal and metal oxide particles, (b) spherical fly ash particles some of which are circled, (c) medium to dark brown and clear shard-like glassy fragments of slag, (d) fine angular quartz particles, (e) ultrafine-grained carbonated lime, (f) occasional synthetic fibers, (g) dark organic matter, (h) a shale fragment in the middle, and (i) miscellaneous undetectable ultrafine particles that are too fine to be detected at the present magnification of the image.

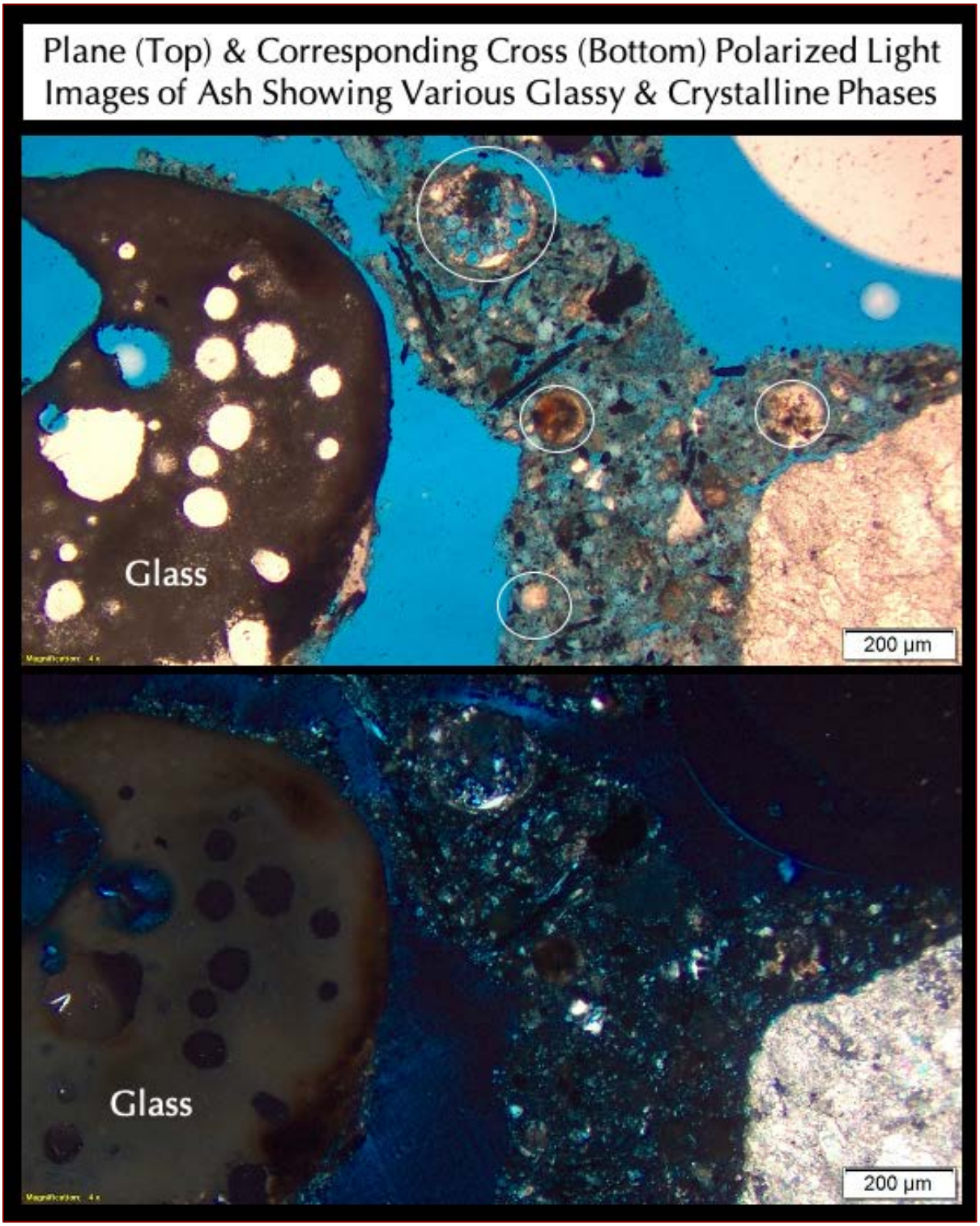

Figure 65: Micrographs of thin section of ash showing: (a) dark opaque metal and metal oxide particles, (b) spherical fly ash particles some of which are circled, (c) medium to dark brown and clear shard-like glassy fragments of slag, (d) fine angular quartz particles, (e) ultrafine-grained carbonated lime, (f) occasional synthetic fibers, (g) dark organic matter, and (h) miscellaneous undetectable ultrafine particles that are too fine to be detected at the present magnification of the image. Notice a vesicular glass fragment at left.

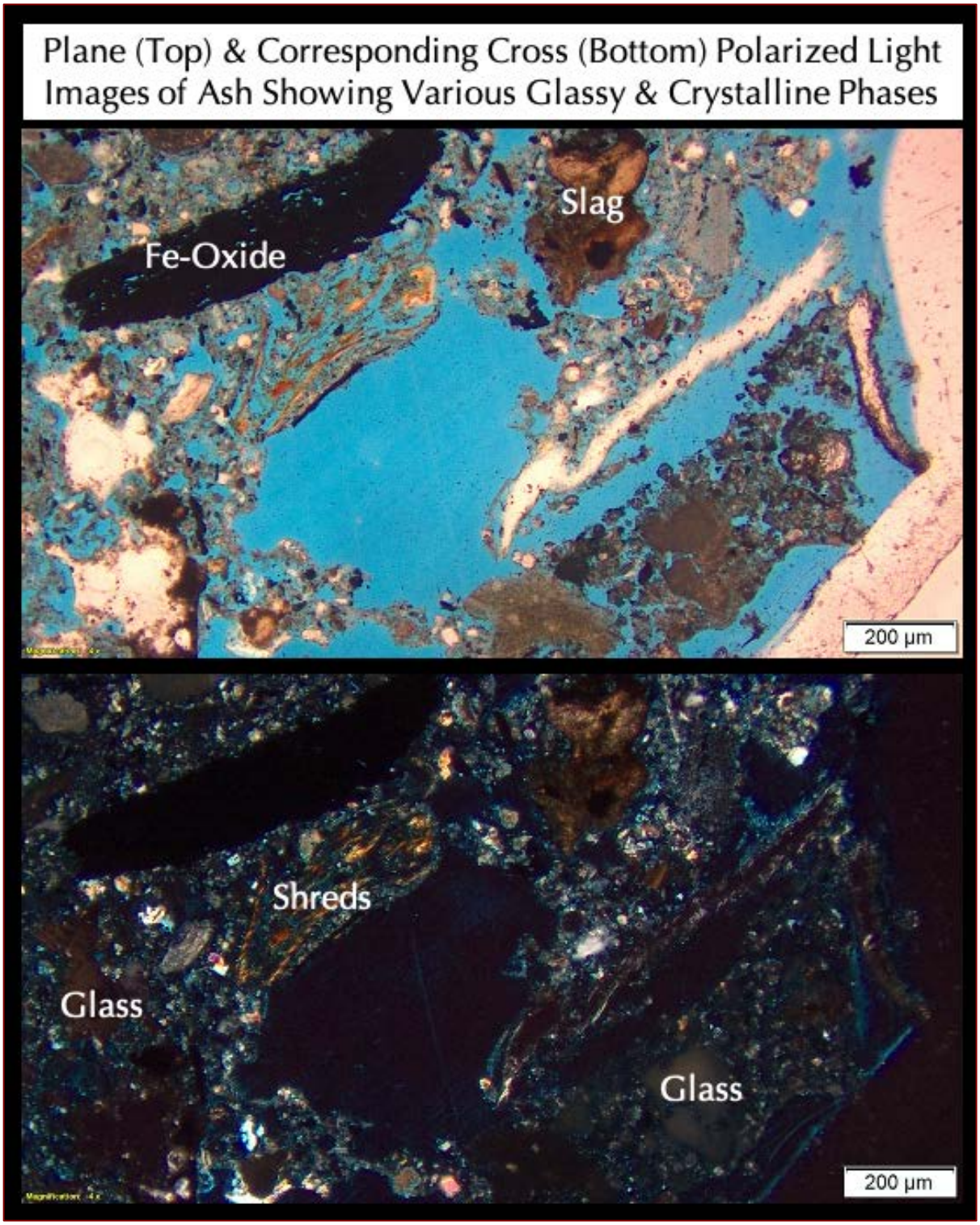

Figure 66: Micrographs of thin section of ash showing: (a) dark opaque metal and metal oxide particles, (b) spherical fly ash particles, (c) medium to dark brown and clear shard-like glassy fragments of slag, (d) fine angular quartz particles, (e) ultrafine-grained carbonated lime, (f) occasional synthetic fibers, (g) dark organic matter, and (h) miscellaneous undetectable ultrafine particles that are too fine to be detected at the present magnification of the image.

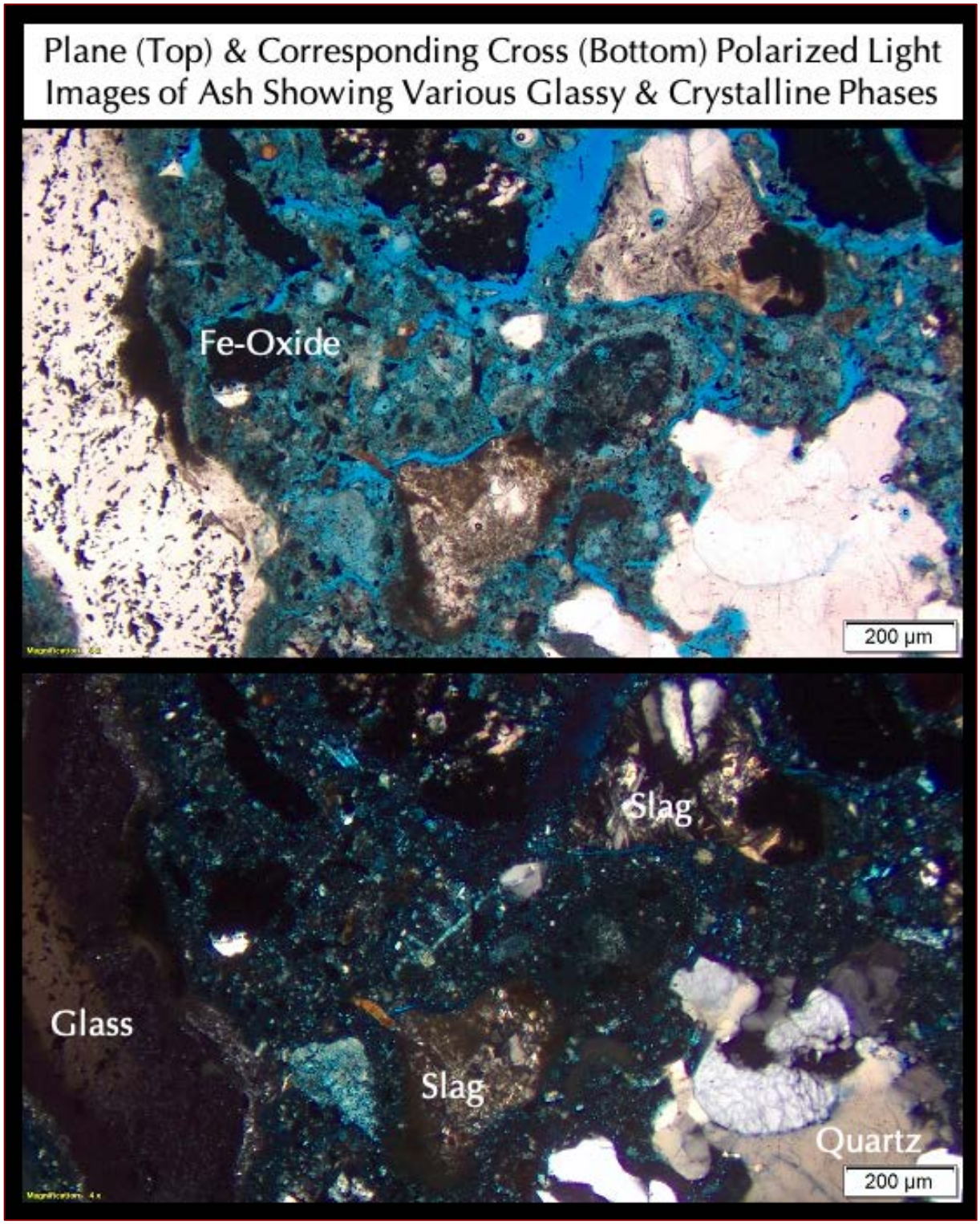

Figure 67: Micrographs of thin section of ash showing: (a) dark opaque metal and metal oxide particles, (b) spherical fly ash particles, (c) medium to dark brown and clear shard-like glassy fragments of slag, (d) fine angular quartz particles, (e) ultrafine-grained carbonated lime, (f) occasional synthetic fibers, (g) dark organic matter, and (h) miscellaneous undetectable ultrafine particles that are too fine to be detected at the present magnification of the image. Notice a glass fragment at left.

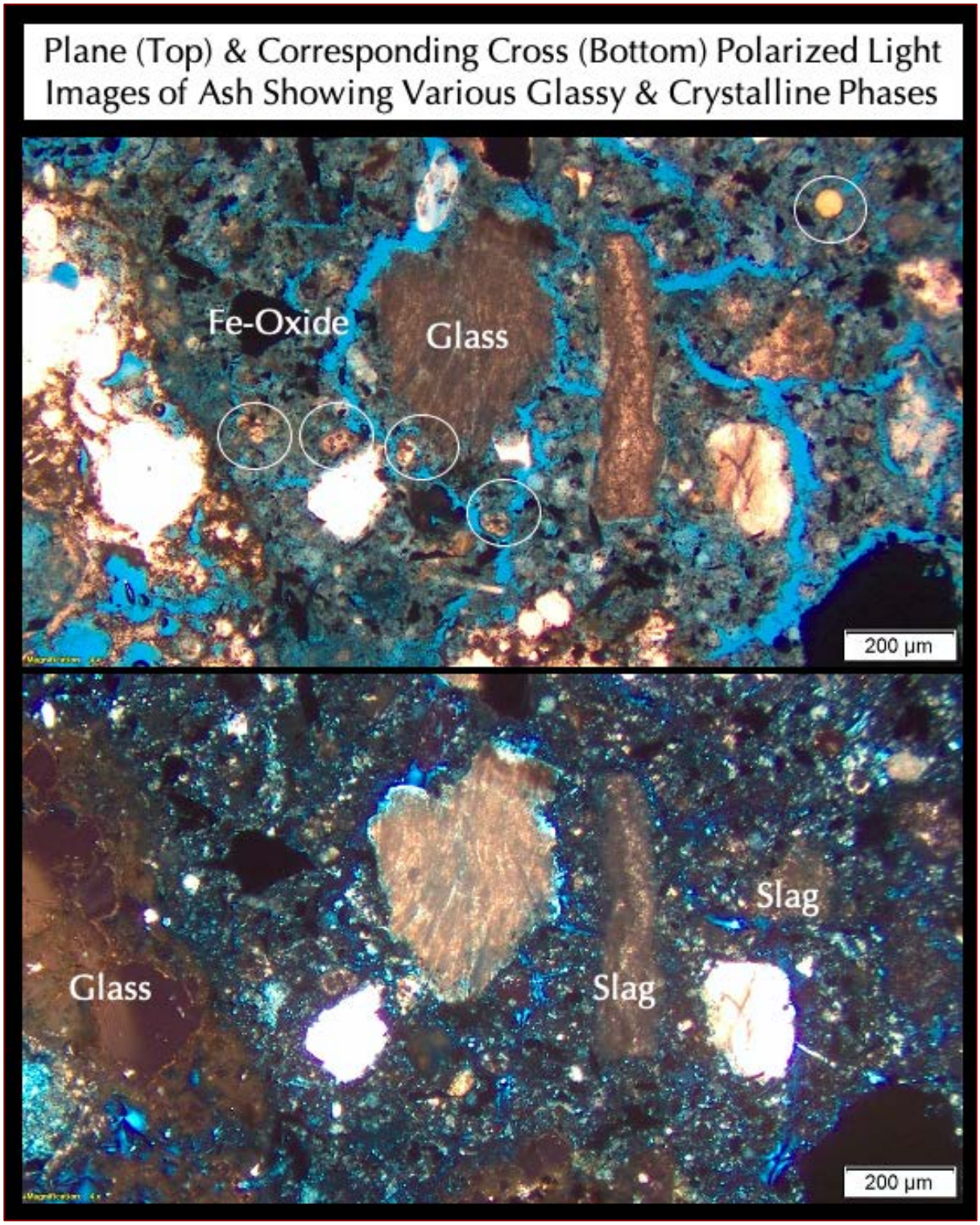

Figure 68: Micrographs of thin section of ash showing: (a) dark opaque metal and metal oxide particles, (b) spherical fly ash particles some of which are circled, (c) medium to dark brown and clear shard-like glassy fragments of slag, (d) fine angular quartz particles, (e) ultrafine-grained carbonated lime, (f) occasional synthetic fibers, (g) dark organic matter, and (h) miscellaneous undetectable ultrafine particles that are too fine to be detected at the present magnification of the image. Notice a vesicular glass fragment at left.

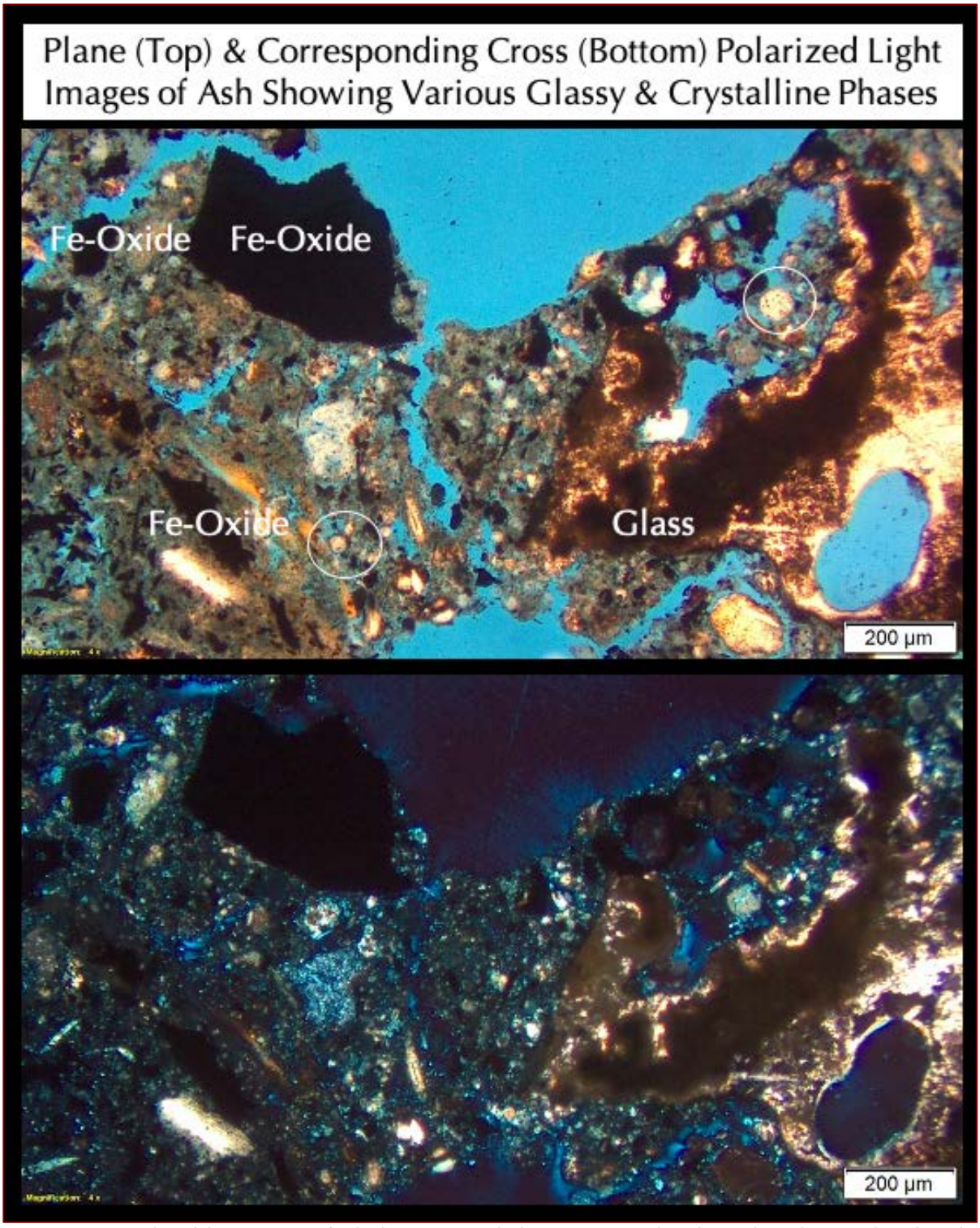

Figure 69: Micrographs of thin section of ash showing: (a) dark opaque metal and metal oxide particles, (b) spherical fly ash particles some of which are circled, (c) medium to dark brown and clear shard-like glassy fragments of slag, (d) fine angular quartz particles, (e) ultrafine-grained carbonated lime, (f) occasional synthetic fibers, (g) dark organic matter, and (h) miscellaneous undetectable ultrafine particles that are too fine to be detected at the present magnification of the image.

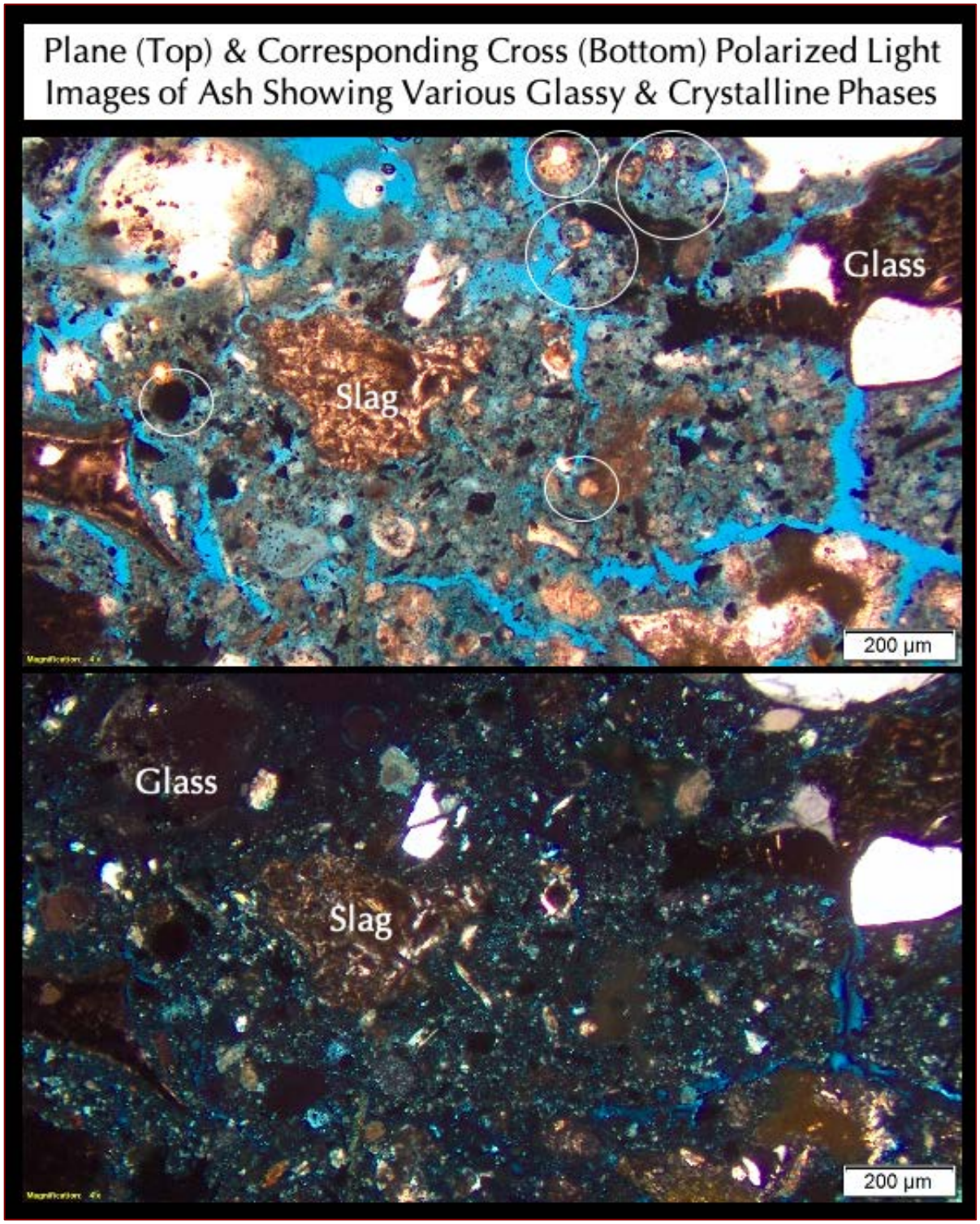

Figure 70: Micrographs of thin section of ash showing: (a) dark opaque metal and metal oxide particles, (b) spherical fly ash particles some of which are circled, (c) medium to dark brown and clear shard-like glassy fragments of slag, (d) fine angular quartz particles, (e) ultrafine-grained carbonated lime, (f) occasional synthetic fibers, (g) dark organic matter, and (h) miscellaneous undetectable ultrafine particles that are too fine to be detected at the present magnification of the image.

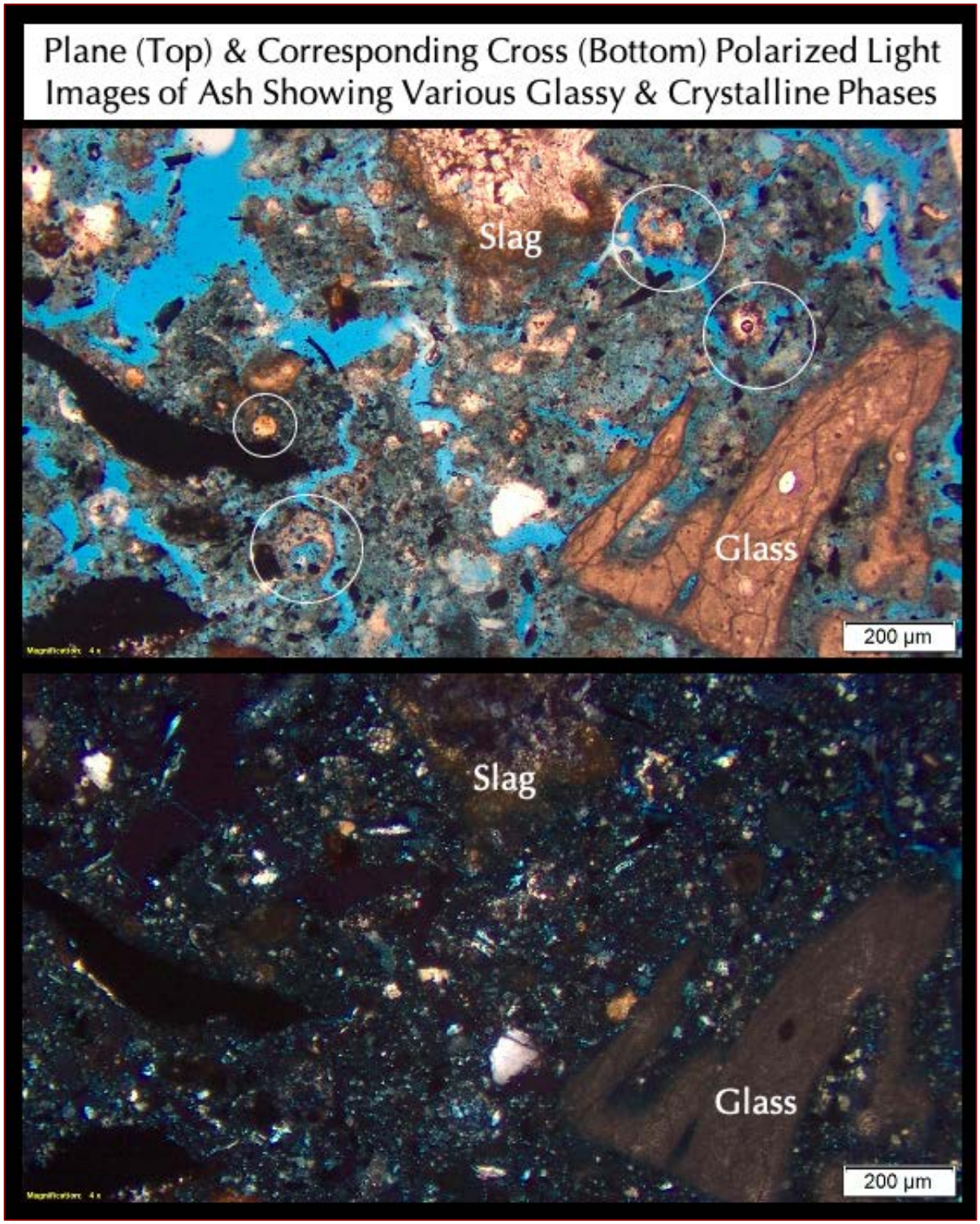

Figure 71: Micrographs of thin section of ash showing: (a) dark opaque metal and metal oxide particles, (b) spherical fly ash particles some of which are circled, (c) medium to dark brown and clear shard-like glassy fragments of slag, (d) fine angular quartz particles, (e) ultrafine-grained carbonated lime, (f) occasional synthetic fibers, (g) dark organic matter, and (h) miscellaneous undetectable ultrafine particles that are too fine to be detected at the present magnification of the image.

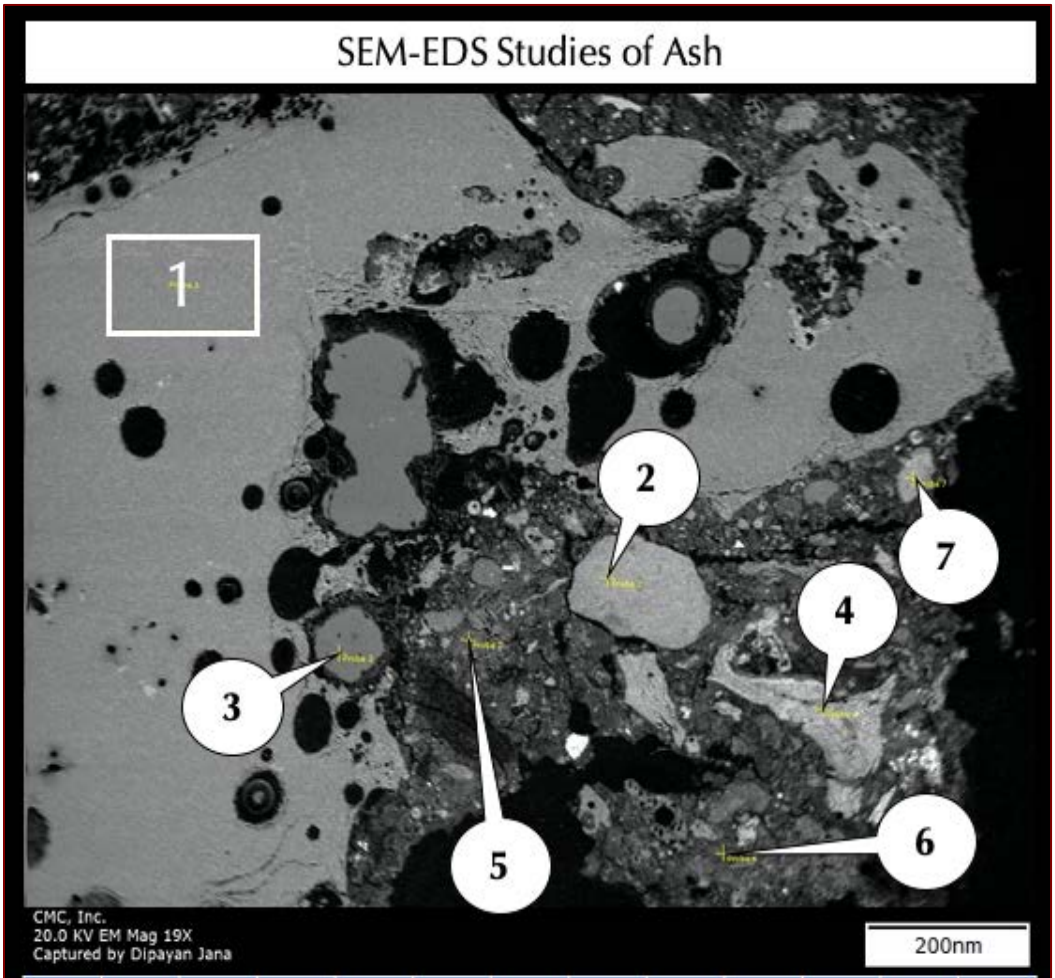

Probe	CaO	SiO_2	Al_2O_3	Na_2O	MgO	SO_3	K_2O	TiO_2	MnO_2	FeO	Total	Phase
1	9.82	78.18	1.27	9.81	0.09	0.00	0.16	0.05	0.23	0.41	100.02	Na-Silicate Glass
2	61.85	1.27	0.00	0.00	36.18	0.00	0.06	0.03	0.28	0.33	100.00	Dolomite
3	5.59	78.34	0.89	10.22	3.99	0.00	0.76	0.00	0.07	0.14	100.00	Na-Silicate Glass
4	21.89	38.87	13.03	13.21	2.06	0.00	1.48	8.53	0.10	0.83	100.00	Slag
5	0.49	53.93	24.76	1.53	8.32	0.00	6.71	0.44	0.08	3.73	99.99	Grain
6	68.56	15.69	6.04	2.81	4.49	0.00	0.23	0.44	0.49	1.25	100.00	Grain
7	28.58	60.07	0.88	7.45	1.61	0.00	0.27	0.15	0.05	0.93	99.99	Slag

Figure 72: Secondary electron image (top), and X-ray microanalyses at the tips of callouts and in boxed area in Probes 1 through 7 detecting compositional variations of various particles in the incinerator ash.

A large glass fragment shows sodium-lime-silicate composition of the glass.

Also detected are dolomite, slag, and miscellaneous other silicate grains, none of which are potentially deleterious to the concrete surface.

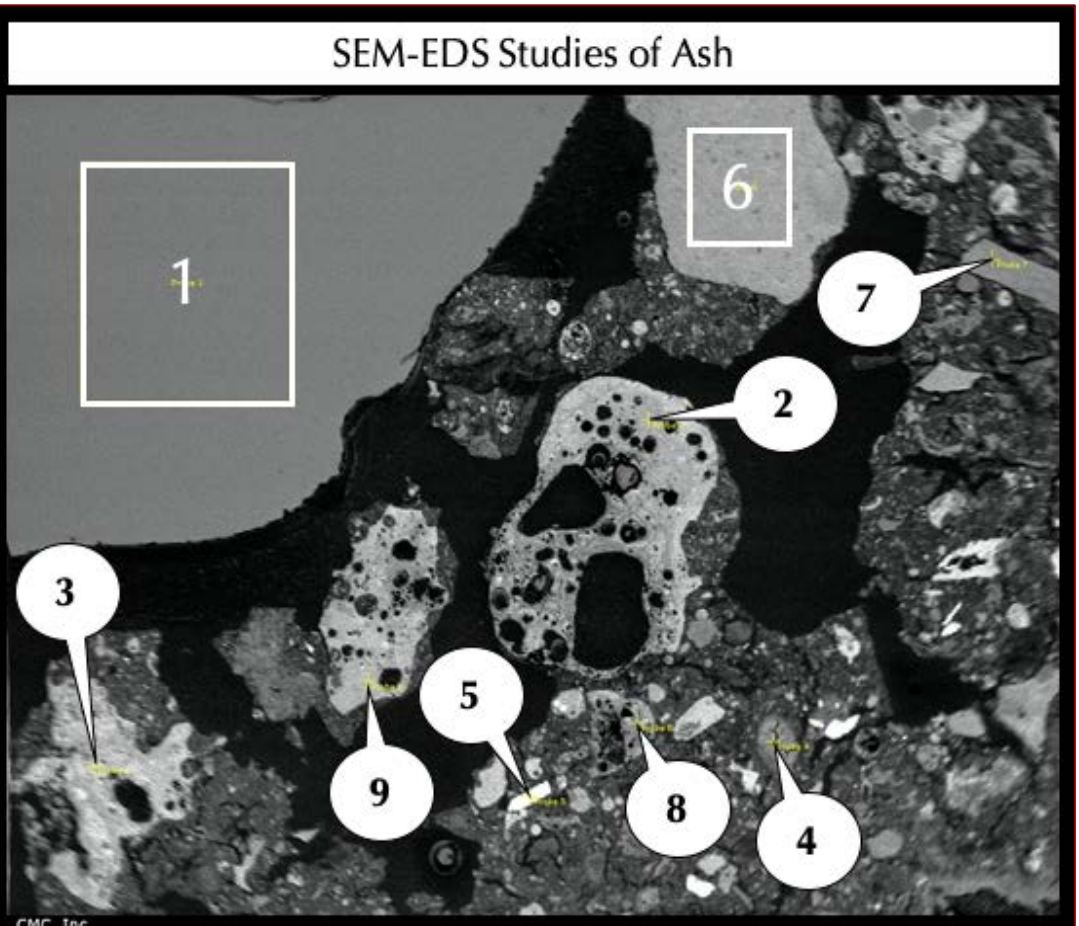

Probe	CaO	SiO_2	Al_2O_3	Na_2O	MgO	SO_3	K_2O	TiO_2	MnO_2	FeO	Total	Phase
1	5.55	78.20	0.96	10.32	3.93	0.00	0.78	0.02	0.08	0.15	99.99	Silicate Glass
2	29.21	34.05	24.37	1.78	2.36	0.00	0.93	6.61	0.14	0.53	99.98	Fly Ash
3	29.88	53.66	4.93	5.41	0.78	0.00	0.83	3.74	0.00	0.76	99.99	Silicate Glass
4	55.11	0.34	21.87	0.03	0.10	21.83	0.00	0.07	0.27	0.38	100.00	Ca-Al-Sulfate
5	45.41	12.22	7.58	1.66	5.24	18.34	0.18	1.31	0.50	7.56	100.00	Ca-S (Oldhamite?)
6	95.10	2.56	0.16	0.33	1.50	0.00	0.00	0.06	0.21	0.08	100.00	Limestone
7	0.25	66.71	19.09	1.49	2.50	0.00	3.59	1.20	0.10	5.08	100.01	Silicate
8	0.14	97.64	0.61	0.51	0.20	0.00	0.48	0.10	0.00	0.32	100.00	Si-Glass
9	23.89	41.34	21.68	2.58	4.05	0.00	0.88	1.32	0.27	4.00	100.01	Fly Ash

Figure 73: Secondary electron image (top), and X-ray microanalyses at the tips of callouts and in boxed areas in Probes 1 through 9 detecting compositional variations of various particles in the incinerator ash.

A large glass fragment shows sodium-lime-silicate composition of the glass.

Also detected are fly ash, slag, and miscellaneous other silicate grains, none of which are potentially deleterious to the concrete surface.

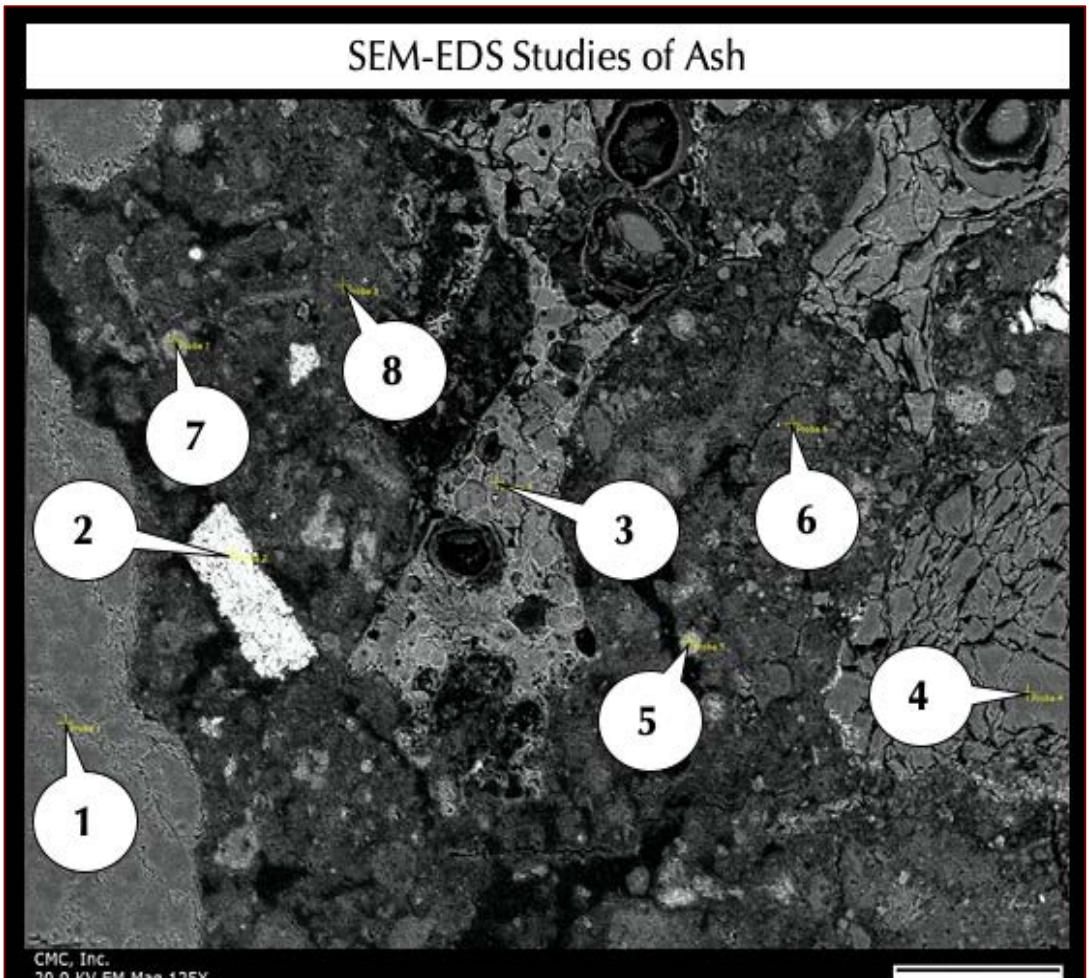

Probe	CaO	SiO_2	Al_2O_3	Na_2O	MgO	SO_3	K_2O	TiO_2	MnO_2	FeO	Cl	Total	Phase
1	0.00	99.92	0.00	0.06	0.02	0.00	0.00	0.00	0.00	0.01		100.01	Quartz
2	0.11	0.95	0.00	0.28	0.10	0.00	0.00	0.00	0.71	97.85		100.00	Fe-Oxide
3	1.19	67.15	15.54	4.65	1.74	0.00	6.66	0.46	0.06	2.54		99.99	Silicate Glass
4	0.00	99.80	0.00	0.10	0.00	0.00	0.00	0.04	0.00	0.05		99.99	Quartz
5	60.87	17.26	1.24	5.94	12.21	1.19	0.07	0.20	0.62	0.41		100.01	Ca-Silicate
6	83.33	9.90	0.49	2.32	2.18	0.00	0.05	0.26	0.48	1.00		100.01	Lime
7	35.15	37.26	23.07	1.60	0.73	0.00	0.00	1.22	0.34	0.62		99.99	Fly Ash
8	43.45	1.13	20.26	0.06	0.47	15.95	0.14	0.00	0.68	1.55	16.30	99.99	Ca-Al-Sulfate

Figure 74: Secondary electron image (top), and X-ray microanalyses at the tips of callouts in Probes 1 through 8 detecting compositional variations of various particles in the incinerator ash.

A large quartz and some glass fragments respectively show silica-rich composition in Probe #1 and sodium-alumina-silicate composition of the glass in Probe #3.

Also detected are iron oxide, fly ash, lime, lime-silicate, lime-alumina-sulfate (not ettringite), and miscellaneous other grains none of which are potentially deleterious to the concrete surface.

pH AND WATER-SOLUBLE ANIONS IN INCINERATOR ASH FROM ION CHROMATOGRAPHY

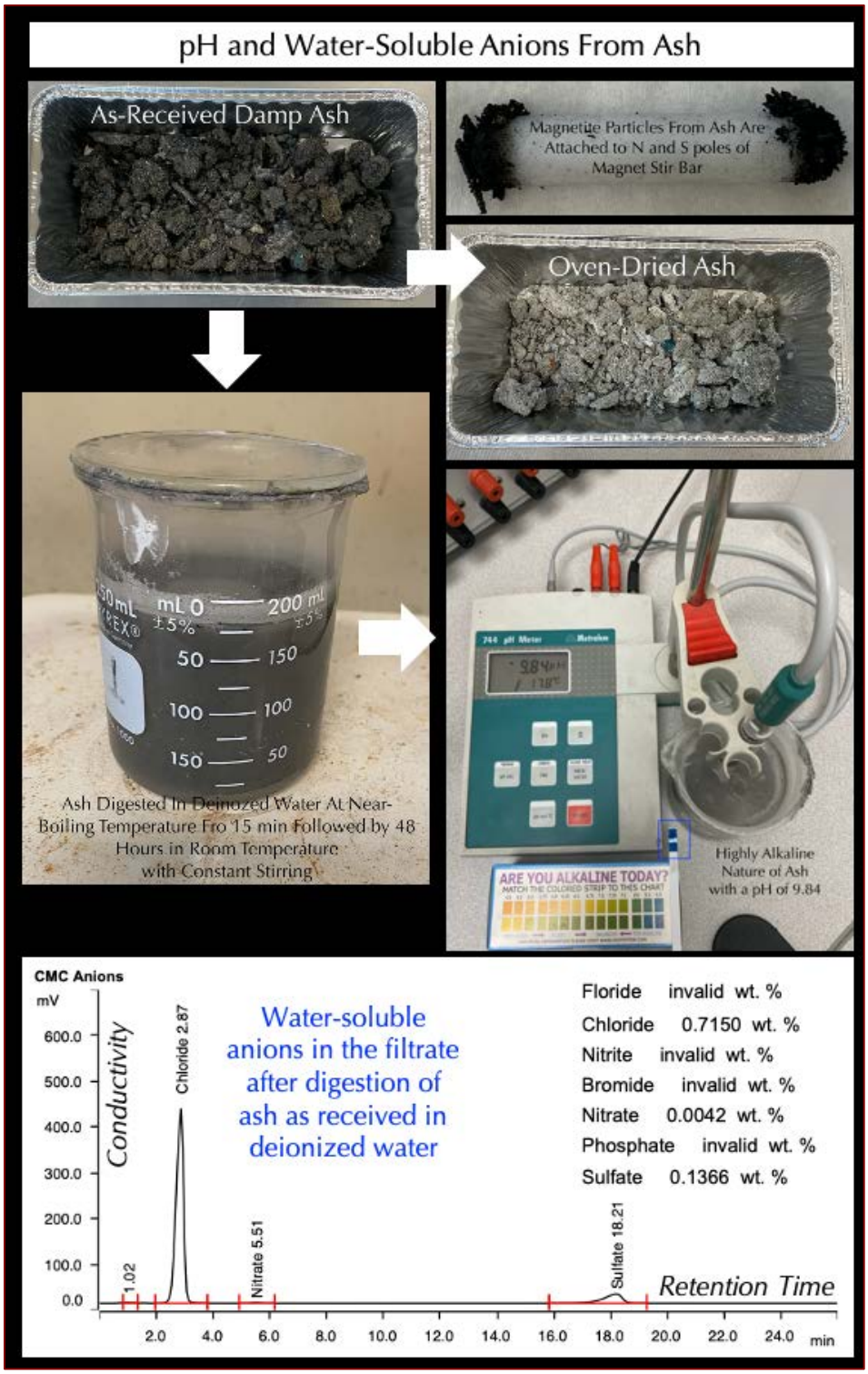

Figure 75: Tests of pH (alkalinity) in a pH strip and Metrohm 744 pH meter showing high alkalinity of ash, which in pH meter is measured to be 9.84. Middle left photo shows digestion of ash in deionized water for anion chromatography. Magnetic bar used for stirring the ash in water showed abundant magnetite particles (top right photo) in the ash. Water-soluble anions show detectable levels of chloride (0.715 weight percent) and sulfate (0.136 percent) ions.

CHEMICAL AND MINERALOGICAL COMPOSITIONS OF INCINERATOR ASH FROM XRF AND XRD

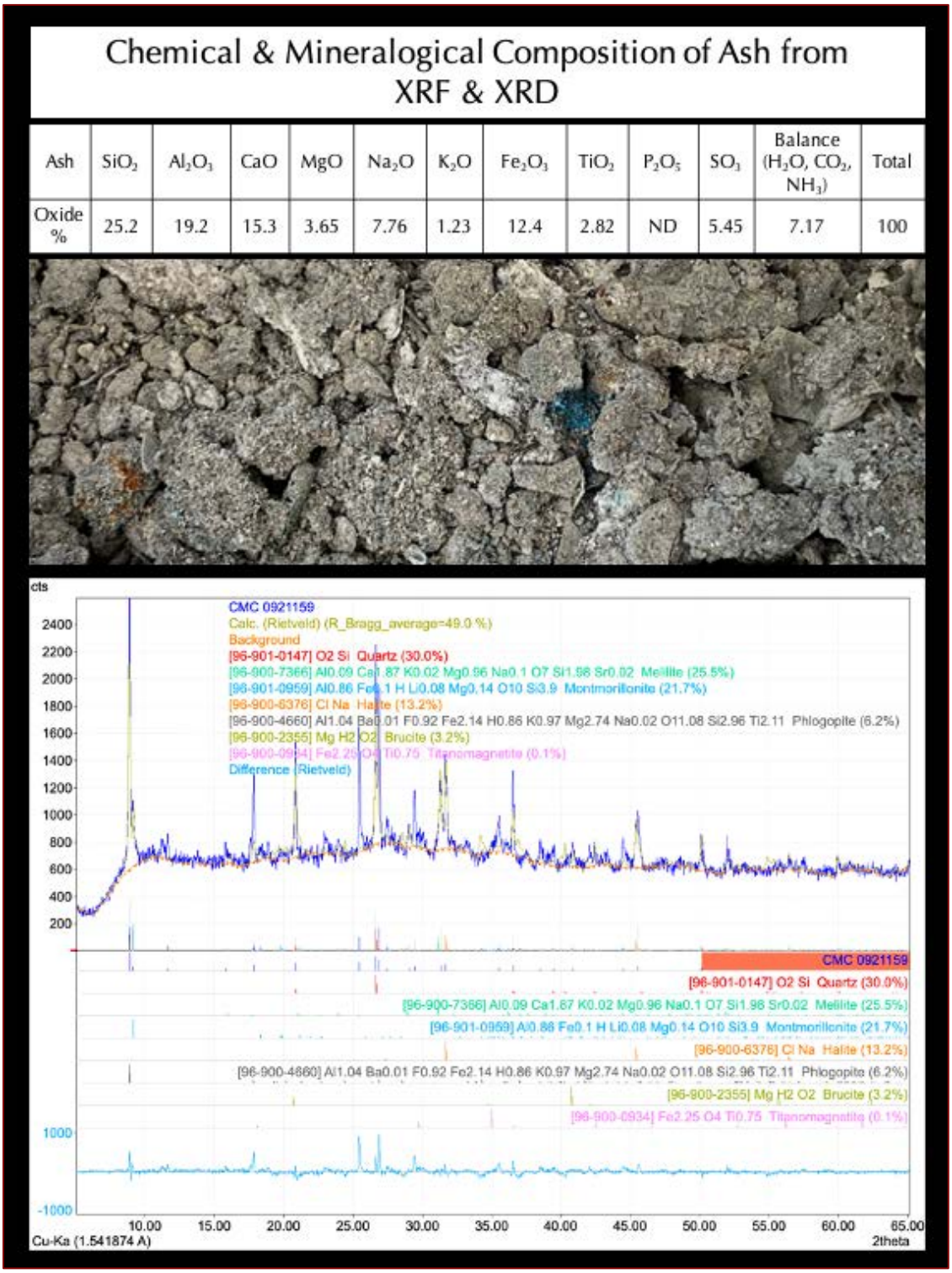

Figure 76: Chemical and mineralogical compositions of incinerator ash determined from an oven-dried mass, pulverized down to 45 microns or less in particle size with a lab pulverizer, then pressed to a 32-mm diameter pellet with a 25-ton hydraulic press for use in an X-ray fluorescence spectrometer for oxide chemical composition and then to an X-ray diffractometer for determining mineralogical compositions. Results show more or less similar silica-alumina-lime compositions all within 15 to 25 percent, subordinate magnesia-sodium-iron oxide

compositions within 3 to 12 percent, 5.45 percent sulfate, and 7.2 percent balance. XRD results show quartz from its ubiquitous presence in the concrete sand, melilite from slag, phlogopite and montmorillonite clay, halite (source of chloride in IC result), brucite, titanomagnetite (which showed magnetic adherence to the stirring bar), and an amorphous phase which did not produce any diffraction peak but indicated its presence from a low angle hump in the diffraction pattern. Glass is positively detected in optical microscopy and its sodium-lime-silicate composition was subsequently confirmed from SEM-EDS studies.

THERMAL ANALYSES OF INCINERATOR ASH

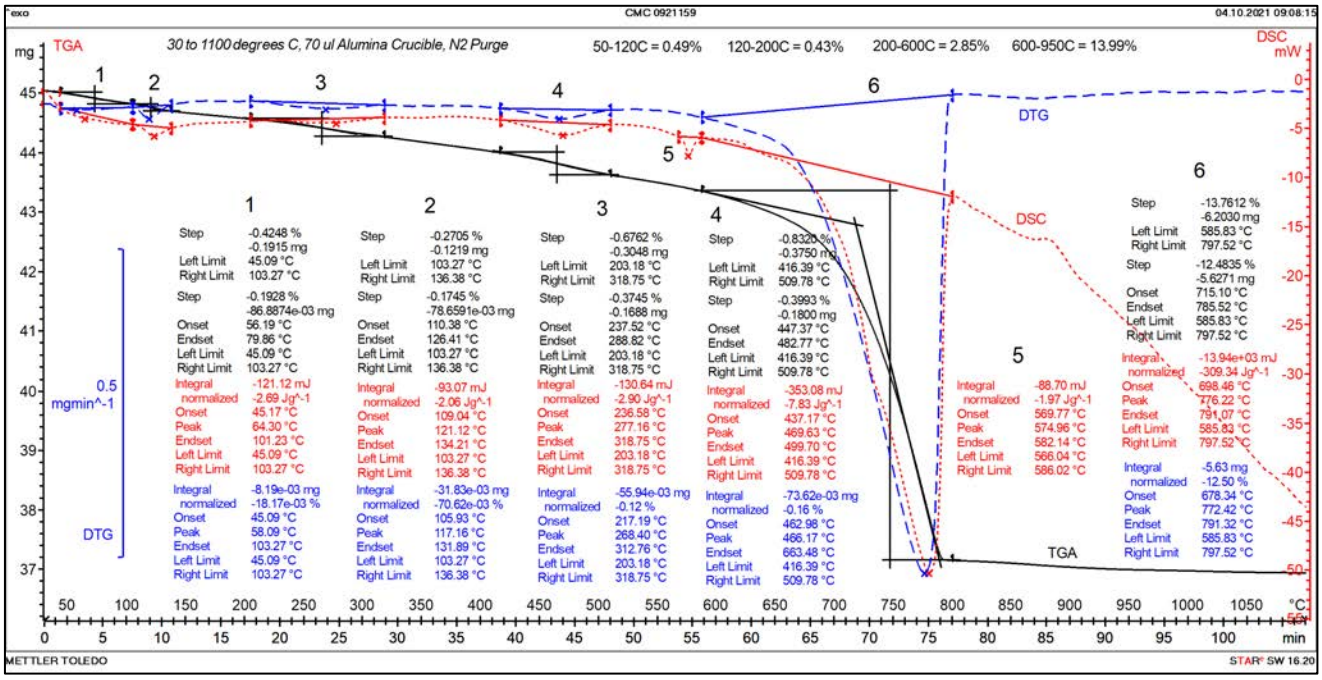

Figure 77: TGA (in bold black), DSC (in dotted red), and DTG (in dashed blue) curves of incinerator ash showing losses in weight due to decompositions (loss of water and carbon dioxide) of various phases during controlled heating in a Mettler-Toledo's simultaneous TGA/DSC 1 unit from 30ºC to 1100ºC in a ceramic crucible (alumina 70µl, no lid) at a heating rate of 10ºC/min in a nitrogen purge at a rate of 75 mL/min. Dehydration and decarbonation reactions are marked as endothermic peaks in the DTG curve, whereas alpha to beta-form polymorphic transition of quartz is marked at the characteristic temperature of 575ºC in the DSC curve. Mass losses from loss of free water (up to 120ºC), structural water (200 to 600ºC), and carbonation (600 to 950 ºC), respectively are also indicated. Notice the detection of brucite (peak #3 at 268 degrees C) from hydration of a magnesian component in the binder, which is also found in the XRD studies. Other endothermic peaks are from decompositions of hydrates, sulfate, carbonate, and halite phases in ash. Low temperature endothermic peaks at 58 and 117 degrees C (Peak 1 and 2, respectively) are from loss of free and structural water from hydrate phases. Endothermic peak at 772.42 degrees C (Peak #6) correspond to decarbonation of carbonate phases in ash.

COMPOSITION OF CONCRETE SLAB

Coarse Aggregates

Coarse aggregates in both concrete cores are compositionally similar #57 crushed limestone having nominal maximum sizes of 1 in. (25 mm) consisting of fine-grained micritic limestone, with occasional bands rich in detrital quartz grains. Particles are medium to dark gray, angular, dense, hard, equidimensional to a few elongated, well-graded, and well-distributed. There is no evidence of any potentially deleterious reactions of crushed limestone coarse aggregate particles found in either core.

Fine Aggregates

Fine aggregates are natural siliceous sands having major amount of variably strained quartz and subordinate amounts of quartzite, feldspar, quartz siltstone, microcrystalline chert, sandstone, siltstone, etc. A few argillaceous components are present, comprised mostly of shale, argillaceous, and ferruginous siltstone particles. Sand particles are $^{3}/_{8}$ in. (9.5 mm) in nominal size, variably dense, subangular to well-rounded, variably colored, equidimensional to elongated, uncracked, uncoated, and unaltered. Particles are well-graded and well-distributed. There is no evidence of any unsoundness or potential alkali-aggregate reactions of most of the sand particles.

Paste

Paste is very dense at the top 5 mm in Core C1 due to trowel finishing-induced densification of paste that has removed some mix water out of the paste to reduce water-cementitious materials ratio at the trowel-finished densified surface region compared to the interior as well as remove air out of the surface from such finishing. As a result, paste at the surface region is noticeably denser and darker than the interior. Freshly fractured surfaces have subvitreous lusters and subconchoidal textures. Residual and relict Portland cement particles are present and estimated to constitute 8 to 10 percent of the paste volumes in the interior but 12 to 16 percent in the top 5 mm of densified surface region. Besides Portland cement, fine, spherical clear to light to dark brown to black glassy particles of fly ash as well as many irregular-shaped dark opaque particles from fly ash are scattered all over the paste. Hydration of Portland cement and pozzolanic reaction of fly ash are normal in the interior and restricted at the densified surface region in Core C1, which is anticipated. The textural and compositional features of the paste are indicative of paste having similar estimated cementitious materials contents that are equivalent to $7^{1}/_{2}$ to 8 bags of Portland cement per cubic yard of which 15 to 20 percent is estimated to be fly ash, and similar water-cementitious materials ratios in the interior bodies estimated to be 0.40 to 0.44 except the top 5 mm of finishing-induced densified surface region in Core C1 where *w/cm* is estimated to be 0.35 to 0.40. Aggregate-paste bonds are tight, except in some areas of air-void clustering from excessive air entrainment in Core C1, where such clustering has weakened the bond to affect the overall compressive strength of concrete.

Properties and Compositions of Aggregates	Cores C1 and C4
Coarse Aggregates	
Types	Crushed Limestone
Nominal maximum size (in.)	1 inch (25 mm)
Rock Types	Fine-grained micritic limestone some with bands of detrital quartz grains
Angularity, Density, Hardness, Color, Texture, Sphericity	Particles are medium to dark gray, angular, dense, hard, equidimensional to a few elongated
Cracking, Alteration, Coating	Uncracked, unaltered, and uncoated
Grading & Distribution	Well-graded and Well-distributed
Soundness	Sound
Alkali-Aggregate Reactivity	None
Fine Aggregates	
Types	Natural siliceous sand
Nominal maximum size (in.)	$^{3}/_{8}$ in. (9.5 mm)
Rock Types	Natural siliceous sand having a major amount of variably strained quartz and subordinate amounts of quartzite, feldspar, quartz siltstone, microcrystalline chert (sometimes with dolomite rhombs or chalcedonic fibers), sandstone, etc. A few argillaceous components are present comprised mostly of shale, argillaceous, and ferruginous siltstone particles
Cracking, Alteration, Coating	Variably colored, rounded to subangular, dense, hard, equidimensional to elongated
Grading & Distribution	Well-graded and Well-distributed
Soundness	Sound
Alkali-Aggregate Reactivity	None

Table 2: Properties of coarse and fine aggregates in concrete in Cores C1 and C4.

Properties and Compositions of Paste	Cores C1 and C4
Color, Hardness, Porosity, Luster	Denser, darker gray, and harder at the top 5 mm of densified surface region in Core C1, but overall dense, hard in the interior; subvitreous lusters and subconchoidal textures
Residual Portland Cement Particles	Normal, 8 to 10 percent of the paste volumes in the interior but 12 to 16 percent in the top 5 mm of densified surface region
Calcium hydroxide from cement hydration	Normal, 10 to 14 percent by paste volume in the interior
Pozzolans, Slag, etc.	Fine, spherical clear to light to dark brown to black glassy particles of fly ash
Water-cementitious materials ratio (*w/cm*), estimated	0.40 to 0.44 except the top 5 mm of densified surface region in Core C1 where *w/cm* is estimated to be 0.35 to 0.40

Properties and Compositions of Paste	Cores C1 and C4
Cementitious Materials Contents (bags per cubic yard)	$7^1/_2$ to 8
Secondary Deposits	None in the interior except some carbonated paste in C1 at the surface
Depth of Carbonation, mm	Shallow patchy carbonation at the top 5 mm in Core C1, but none in Core C4
Microcracking	None except some in the porous surface deposits in both cores
Aggregate-paste Bond	Tight
Bleeding, Tempering	None
Chemical deterioration	None

Table 3: Proportions and composition of hardened cement paste.

Air

In Core C1, air occurs as: (a) numerous fine, discrete, spherical and near-spherical voids of sizes 1 mm or less, which are characteristic of intentionally introduced entrained air, and (b) a few coarse, near-spherical and irregularly-shaped voids, which are accidentally formed entrapped air. The concrete in Core C1 is excessively air-entrained in the body having as high as 7 to 8 percent air, but has no air at the top 5 mm due to trowel finishing-induced densification of paste at the surface region where finishing operations have washed air out of the surface. Figures 16 through 23 show excessive air entrainment in the body as well as loss of air at the top densified trowel-finished surface region of slab.

In Core C4, air occurs as a meager amount of very coarse spherical voids that are indicative of potential addition of an air-entraining agent. Concrete in Core C4 is marginally air-entrained having an estimated air content of 3 to 4 percent, which are mostly present in the interior body and contributed mostly from the coarse air bubbles. Figures 24 through 31 show marginal air entrainment of mostly coarse air bubbles in Core C4.

Core ID	Air Entrainment	Estimated Air Content (%)	Air-Void Spacing Factor ($in.^2/in.3$)	Air-Void System For Freeze-Thaw Durability	Effect of Air On Trowel Finishing
C1	Excessively air-entrained	7 to 8%	At least 600 in^2/in^3; abundant very fine air bubbles mostly less than 0.5 mm in size	Excellent	Incipient delamination at a depth of 5 mm from finished surface
C4	Marginally air-entrained	3 to 4%	Less than 300 in^2/in^3; minor amount of coarse air bubbles mostly greater than 0.5 mm in size	Poor	Delaminated surface

SURFACE CONTAMINANTS

Remains of so-called surface contaminants detected on the rough top surfaces of Cores C1 and C4 were examined in detail in Figures 36 through 41 for Core C1, and Figures 46 through 51 for Core C4 in optical microscopy, which were then followed by more detailed compositional analyses of surface deposits in SEM-EDS studies for Core C1 in Figures 55 and 56.

In all these photos, surface deposit shows the presence of: (a) very fine-grained deposits of organic matter, (b) ferruginous materials, (c) ultrafine crushed quartz, (d) limestone dusts, (e) spherical fly ash, (f) porous, ultrafine-grained carbonated lime, (g) shrinkage microcracks and overall porous nature of deposit, (h) occasional synthetic fibers, and (i) angular shard-like glassy particles of slag. None of these constituents on the surface deposit are potentially harmful to concrete, hence the concrete surface region immediately beneath the deposit shows no surface alteration (leaching, erosion, carbonation, etc.). For most cases, a sharp boundary is present between the porous fragile surface deposit and the underlying dense concrete surface.

INCINERATOR ASH

The incinerator ash, as received was (a) damp with abundant moisture, (b) emitted a strong ammonia odor, and (c) dark gray in color. Insertion of a pH strip immediately turned the strip to dark blue color indicating a strong alkaline nature.

A portion of the ash sample as received was digested in deionized water, first at near-boiling condition for 15 minutes followed by continuous digestion for 48 hours by stirring with a magnetic stir bar to remove all leachable constituents to the water. A significant amount of fine acicular magnetite grains were found adhered to the N and S poles of magnetic bar (Figure 75). A second pH test on the water-digested ash with a pH meter showed 9.48 pH confirming its alkaline nature.

The digested mass was then filtered to remove the filtrate for further examinations for water-soluble anions by ion chromatography. Results show detectable levels of chloride (0.715 weight percent) and sulfate (0.136 percent) ions in the filtrate.

An oven-dried mass of the ash was pulverized to finer than 45 micron particle size with a laboratory pulverizer for chemical and mineralogical analyses of ash by XRF and XRD, respectively. A 32-mm pressed pellet of pulverized ash was prepared in a 25-ton hydraulic press, which was then first used in an XRF unit for chemical (oxide) compositional analysis, followed by in an XRD unit for detailed mineralogical compositions. Results showed more or less similar silica-alumina-lime compositions all within 15 to 25 percent, subordinate magnesia-sodium-iron oxide compositions within 3 to 12 percent, 5.45 percent sulfate, and 7.2 percent balance. XRD results (Figure 76) show quartz from its ubiquitous presence in the concrete sand, melilite from slag, phlogopite and montmorillonite

clay, halite (source of chloride in IC result), brucite, titanomagnetite (which showed magnetic adherence to the stirring bar), and an amorphous phase which did not produce any diffraction peak, but indicated its presence from a low angle hump in the diffraction pattern. Glass is positively detected in optical microscopy and its sodium-lime-silicate composition was subsequently confirmed from SEM-EDS studies.

Detailed mineralogical, textural, and compositional analyses of ash are present in optical micrographs on thin section of ash in Figures 58 through 71. Optical microscopy showed (a) dark opaque metal and metal oxide particles, (b) spherical fly ash particles some of which are circled, (c) medium to dark brown and clear shard-like glassy fragments of slag, (d) fine angular quartz particles, (e) ultrafine-grained carbonated lime, (f) occasional synthetic fibers, (g) dark organic matter, (h) shale fragments, and (i) miscellaneous undetectable ultrafine particles that are too fine to be detected at the magnification of optical microscope.

SEM-EDS studies of ash in Figures 72 to 74 showed sodium-lime-silicate glass, slag, fly ash, quartz, dolomite, and miscellaneous other silicate grains none of which are potentially deleterious to the concrete surface.

Figure 77 shows results of thermal analysis of ash where dehydration and decarbonation reactions are marked as endothermic peaks in the DTG curve, whereas alpha to beta-form polymorphic transition of quartz is marked at the characteristic temperature of 575ºC in the DSC curve. Mass losses from loss of free water (up to 120ºC), adsorbed water (120 to 200ºC), structural water (200 to 600ºC), and carbonation (600 to 950 ºC) are measured to be 0.49%, 0.43%, 2.85%, and 13.99%, respectively. Brucite is detected from an endothermic peak at 268 degrees C from hydration of a magnesian component, which is also found in the XRD studies. Other endothermic peaks are from decompositions of various hydrates, sulfate, carbonate, and halite phases in ash. Endothermic peak at 772.42 degrees C correspond to decarbonation of carbonate phases in ash.

DISCUSSION

DELAMINATION OF TROWEL-FINISHED CONCRETE SLAB FROM AIR ENTRAINMENT

Delamination of trowel-finished surface of concrete slab is determined to be due incorporation of air entrainment in the concrete mix, which is strictly prohibited in the industry for an indoor slab intended receive a hard trowel finish. Core C1 showed spectacular development of near-surface *incipient delamination* as short, elongated isolated separations or tears at a depth of 5 mm from the very top surface which marked the boundary between the densified trowel-finished surface region at the top of the incipient delamination having very low to no air and very low *w/cm* due to loss of air and mix water by trowel-finishing operations, and, the interior air-entrained body where air contents and *w/cm* are higher than that beneath the trowel-densified surface. Concrete in Core C1 is excessively air-entrained having an estimated air content of 7 to 8 percent, whereas concrete in Core C4 is marginally air-entrained having many coarse air bubbles with an estimated air content of 3 to 4 percent. Contrary to incipient delamination in the excessively air-entrained concrete in Core C1, concrete in Core C4 showed the main body of

slab after the loss of the original finished surface and hence only the portion present beneath the delaminated surface. Incorporation of air-entraining agent has caused the delamination, especially in areas that have received the hard trowel-finish, and were subsequently exposed to traffic.

Based on detailed examinations of the remains of surface deposits on the top ends of both cores, as well as the ash sample received, the observed delamination of the slab is judged to be unrelated to the potentially deleterious nature of the ash or surface contaminant, if any, but solely due to the use of an air-entraining mix in a slab intended to receive a hard towel-finish which has delaminated specifically in areas that have been exposed to traffic.

LACK OF DELETERIOUS ACTIONS OF SURFACE CONTAMINANT ON CONCRETE

Detailed optical and scanning electron microscopy of the very top surface regions of both cores show no evidence of any chemical alteration or leaching of paste from the alleged exposure of the ash contaminant.

A detailed examination of the ash sample showed its highly alkaline nature, a strong ammonia odor but the non-evaporable constituents are similar in chemical and mineralogical compositions to the concrete itself, e.g., in having silica, alumina, lime, iron, magnesia compositions with quartz, melilite (from slag), clay, dolomite, calcite, magnetite phases and major amounts of sodium lime, alumina silicate glasses from slag and fly ash, and other residues from the burning process.

POTENTIAL ROLE OF AMMONIA IN INCINERATOR ASH ON CONCRETE

Apparently, the strong ammonia odor detected in the moist ash sample caused no detectable chemical effect on the concrete surface of two cores examined. The very top surface regions of both cores show dense paste with no indication of any alteration, leaching, or other chemical erosions from alleged exposure to surface contaminants having such odor.

REFERENCES

ASTM C 856 "Standard Practice for Petrographic Examination of Hardened Concrete," Vol. 4.02, ASTM International, West Conshohocken, PA, 2019.

ASTM C 1723, "Standard Guide for Examination of Hardened Concrete Using Scanning Electron Microscopy," In Annual Book of ASTM Standards, Section Four Construction, Vol. 04.02; ASTM Subcommittee C 9.65, 2017.

Jana, D., "Sample Preparation Techniques in Petrographic Examinations of Construction Materials: A State-of-the-art Review," Proceedings of the 28th Conference on Cement Microscopy, International Cement Microcopy Association, Denver, Colorado, pp. 23-70, 2006.

Jana, D., Petrography – A Powerful Tool for Quality Assurance and Failure Investigation of Construction Materials, International Seminar on Non-Destructive Testing (NDT), India Chapter of American Concrete Institute and ACI (USA), 2006, pp. 117-131.

Jana, D., Concrete, Construction or Salt – Which Causes Scaling? Part I: Importance of air-void system in concrete, Concrete International, American Concrete Institute, November 2004a, pp. 31-38.

Jana, D., Concrete, Construction or Salt – Which Causes Scaling? Part II: Importance of finishing practices, Concrete International, American Concrete Institute, December 2004b, pp. 51-56.

Jana, D., Petrography and Concrete Repair – A Link is Needed, Point of View Publication in Concrete International, American Concrete Institute, pp. 37-39, January 2005a.

Jana, D., Erlin, B., and Pistilli, M., A Closer Look at Entrained Air in Concrete, Concrete International, American Concrete Institute, June 2005b, pp. 31-38.

Jana, D., and Erlin, B., Delamination: A sometime curse of entrained air, Concrete Construction, January 2005, pp. 101-107.

Jana, D., Delamination – A State-of-the-Art Review, Proceedings of the 29th Conference on Cement Microscopy, ICMA, Quebec City, Canada, 2007, pp. 135-167.

✪ ✪ ✪ END OF TEXT ✪ ✪ ✪

END OF REPORT[1]

[1] The CMC logo is made using a lapped polished section of a 1930's concrete from an underground tunnel in the U.S. Capitol.